HYDROLOGICAL BEHAVIOR OF TWO MID-SIZED MOUNTAINOUS CATCHMENTS UNDER THE INFLUENCE OF CLIMATE CHANGE

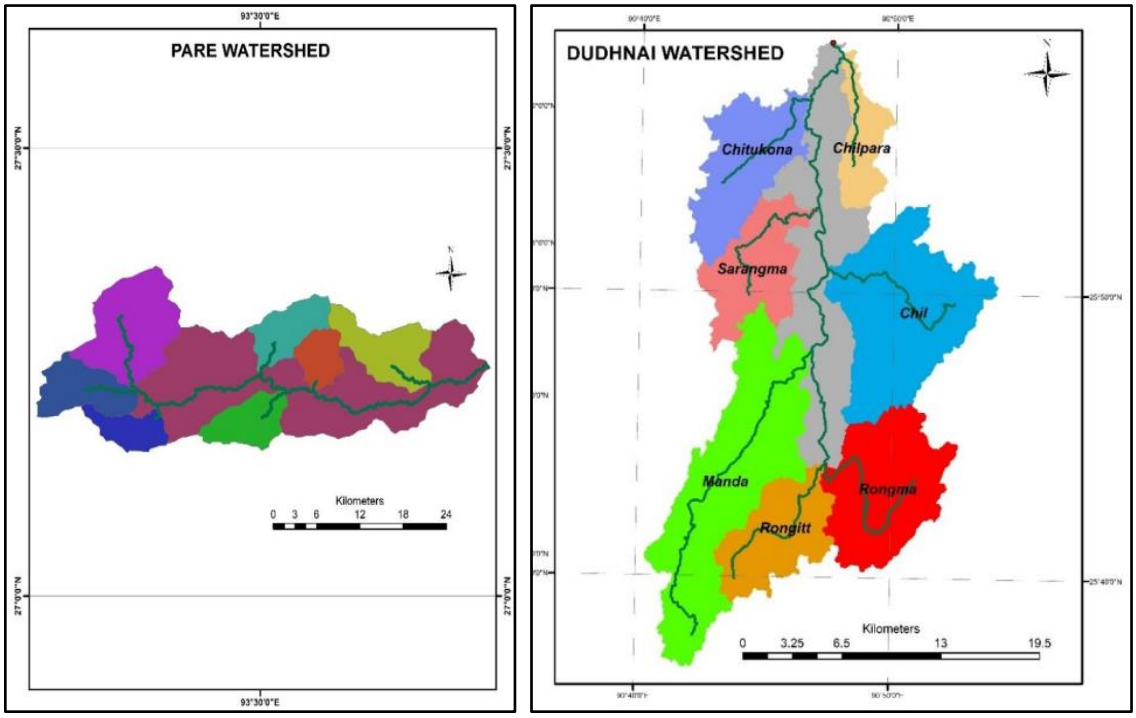

आपो हिष्टा मयोभुवः

NATIONAL INSTITUTE OF HYDROLOGY
NORTH EASTERN REGIONAL CENTRE
Dispur, Guwahati- 781006

2022

Summary of the Project

Title	**:**	Hydrological behavior of two mid-sized mountainous catchments under the influence of climate change
Type	**:**	Internal
Start	**:**	July 2019
Complete	**:**	June 2022
Duration	**:**	3 years (36 months)
PI and Co-PI	**:**	PI : Waikhom Rahul Singh, Scientist- B Co-PI : Dr. A. K. Lohani, Scientist- G Dr. A. Bandyopadhyay, Professor Dr. Swapnali Barman, Scientist- C Dr. Nitesh Patidar, Scientist- B

PREFACE

Hydrological modelling mainly deals with the estimation of discharge at a single or multiple sites of a watershed. The necessity of accurate and reliable hydrological model is increasingly being felt with increasing demands on water resources due to economic development and demographic expansion and also due to climate change. Impact of climate change on discharge is increasingly becoming important particularly in mountainous regions. Mountainous watersheds are more vulnerable to climate change due to its topography and high energy inputs. A hydrological modelling in mountainous watersheds with meteorological forcings of future could be benefitted to plan proper land and water management.

Dudhnai River is one of the north flowing tributaries of the mighty river Brahmaputra. The river originates in the hilly regions of Meghalaya plateau, flows through the hilly state of Meghalaya for majority of its path, and meets with the Krishnai River before joining the river Brahmaputra. The Dudhnai river basin partly lies in the Garo Hills (approximately 83 %) district of Meghalaya and partly in the Goalpara district of Assam (approximately 17 %). Dudhnai river form a flood plain in the Assam region which are frequently inundated due to flash floods and siltation of erosive materials brought during the flash flood. The Dudhnai watershed has an area of 483.76 km^2. Pare watershed draining an area of 775.37 km^2, located at Papumpare district of Arunachal Pradesh, India, was selected as another research area. The area lies between latitudes 27° 09’ 36” N and 27° 22’ 08” N and longitudes 93° 13’ 15” E and 93° 47’ 07” E with an elevation range from 260 to 2,894 m above mean sea level. Pare River, a sub-tributary to Dikrong River, dissected the watershed.

The report has been prepared by Waikhom Rahul Singh (Sc. ‘B’) and Dr. Swapnali Barman (Sc. ‘C’) of NIH-NERC Guwahati; Dr. A. K. Lohani (Sc. ‘G’) and Dr. Nitesh Patidar (Sc. ‘B’) of NIH Roorkee and Dr. A. Bandyopadhyay (Professor) of NERIST under the work programme for 2019-22.

(Jaivir Tyagi)
Director

ACKNOWLEDGEMENT

I would like to express my deep sense of gratitude to **Dr. Jaivir Tyagi**, Director, National Institute of Hydrology, Roorkee for his immense help, kind support and encouragement towards the successful completion of the project.

I wish to record my deep gratitude to **Dr. Sharad Kumar Jain**, former Director, National Institute of Hydrology, Roorkee for his encouragement in taking up this project and his valuable comments.

I also express my sincere thanks to **Dr. A.K. Lohani**, Scientist 'G' and Coordinator of North Eastern Regional Centre, Guwahati for his insightful comments in carrying out my work.

I am also thankful to **Dr. S. V. Vijaya Kumar**, Scientist 'G' and Head of North Eastern Regional Centre, Guwahati for his encouragement in carrying out my work.

I am also very grateful to **Dr. A. Bandyopadhyay**, Professor and **Dr. A. Bhadra**, Professor for enriching me with ideas and also their criticism which shaped the final outcome of this study.

I am also very much thankful to all the **RCC members and invitees** in the last three years for their valuable comments.

My sincere thanks to **Dr. Swapnali Barman**, Scientist 'C', NIH-NERC, Guwahati for her immense help in various stages of the project. I am also thankful to **Dr. N. Patidar**, Scientist 'B'; **Dr. S.K. Sharma**, Scientist 'C' and **Mr. G. Tirkey**, Scientist 'B' of National Institute of Hydrology for their suggestions during the project work.

I am grateful to Central Water Commission (**CWC)** and North Eastern Electric Power Corporation Limited (**NEEPCO**) for providing the necessary data required for the study.

(Waikhom Rahul Singh)
Scientist-B

ABSTRACT

The study is envisaged on the hydrological behavior of two mid-sized mountainous catchments in the eastern Himalayan region of India. The morphometric analysis of the Dudhnai and Pare Rivers, the hydrological modelling of the two watersheds using the Soil and Water Assessment Tool (SWAT), the analysis of the effects of climate change on discharge, and finally the estimation of return floods in the Dudhnai watershed for return periods of 25, 50, 100, and 200 years are all part of this study. Pare Watershed, which has an area of 775.37 km^2, is entirely within the mountain ranges of the state of Arunachal Pradesh, whereas the Dudhnai watershed, which has an area of 483.76 km^2, has about 20% of its area within the Assam's flood plains and the remaining 70% within the hilly terrain of Meghalaya. The current study's objective was to ascertain the effects of climate change on discharge in two medium-sized watersheds located in a mountainous area of north-eastern India. The study's meteorological and geographic data were from publicly available sources. The North Eastern Electric Power Corporation Limited (NEEPCO) and Central Water Commission (CWC)-discharge data for the Pare and Dudhnai watersheds, respectively, were obtained. To reflect the hydrological behaviors of the two watersheds, the hydrological model SWAT was chosen. The SWAT model was calibrated and validated using measured daily discharge data. The SWAT model was then simulated for the historical period (1976-2005), near future period (2019-2045), mid future period (2046-2072), and far future period (2073-2099) in the Pare watershed after the model had been calibrated for the appropriate watersheds. Similar simulations were conducted using the calibrated SWAT model in the Dudhnai watershed for the historical period (1976–2005), the near future (2024–2048), the mid future (2049–2073), and the distant future (2073–2099). (2074-2099). During these times, the resulting discharge and its constituent parts were examined. Future streamflow scenarios were provided and their percentage differences from the historical/baseline period were examined. The northern portion of the Dudhnai watershed contains flood areas where return floods from various return periods have been predicted. The results were then analyzed and discussed. The most vulnerable sub-watersheds to soil erosion, according to morphometric study, are Chil sub-watershed (Dudhnai) and SW25 (Pare), which required interventions to soil and water conservation measures on a priority basis. Only the RCP 8.5 scenario for the climate model NorESM1-M's near future period in the Pare watershed predicted a decrease in the study area's average yearly precipitation of around 7.5 percent from the historical period. The only climatic scenario for the Dudhnai watershed that projected a decline in average annual precipitation in the study area of less than 0.5 percent

from historical levels was RCP 4.5 for the near future timeframe. Temperature and precipitation were both expected to rise near the end of the century in general, and under the RCP 8.5 scenario they were expected to rise more than under the RCP 4.5 scenario. The amount of precipitation increased together with a decrease in wet episodes in the studied areas, which indicated the possibility of future extreme storms. The SWAT model was able to accurately depict the Pare and Dudhnai watersheds despite the uncertainties that may be present in hilly areas and from poor hydro-meteorological networks. SWAT model fared somewhat better in Pare watershed when compared to the Dudhnai watershed. The SWAT model that was created slightly exceeded the actual discharge in the Dudhnai watershed while slightly underestimating it in the Pare watershed. The SWAT model built in both watersheds was found to be adequate for its intended use since the indicators used to measure the uncertainty of SWAT forecast discharge (p-factor and r-factor) were within the approved permissible ranges for discharge prediction. The most sensitive parameters impacting stream discharge in both watersheds were channel hydraulic conductivity, curve number for antecedent moisture condition II, and bank storage's recession constant. Only NorESM1-M in the Pare watershed predicted decreasing streamflow conditions under RCP 8.5 projection scenarios, with a fall of about 10.7 percent. While only CNRM-CM5 and NorESM1-M models in the Dudhnai watershed have revealed decreases in discharge with magnitudes of -2.3 percent and -1.1 percent, respectively, in the near future period under RCP 4.5 and RCP 8.5 scenarios. In both watersheds, during the monsoon season, considerable favourable increase in discharge were seen in the future estimates. While the majority of the negative developments happened between November and March. This meant that high flow would grow even higher and low flow would become leaner in the future, amplifying the nature of flow. The percentage increase in surface runoff was predicted to occur among the streamflow components at a faster rate than the lateral and baseflow components. This could result in significant soil loss from the upstream of the watershed and major flooding in the low-lying areas downstream. The return floods in the Dudhnai watershed are not expected to vary much in the future, according to comparisons of the maximum series of observed, RCP 4.5, and RCCP 8.5 maximum series. Although future predictions for precipitation and streamflow both indicated increases, their pattern is still significant. Both watersheds were anticipated to experience extended dry periods with significant flooding potential within a short period of wet days, despite rising precipitation and streamflow. We came to the conclusion that the state of the watersheds is extremely sensitive to extreme events in the future based on reports from various news sources of springs disappearing in both watersheds and the findings from this study. In light of this, we advise

interested parties, including water resource departments, agriculture departments, and irrigation departments, to jointly approach watershed management in a scientific manner, create structures for collecting water in appropriate locations, and encourage afforestation.

TABLE OF CONTENT

LIST OF FIGURES

LIST OF TABLES

CHAPTER I
INTRODUCTION

1.1 General

The availability of natural resources such as water and soil have a significant impact on a region's social, economic, and environmental well-being. Potential for water resource development is mostly determined by its geographical location, climatic zones, and terrain. A mountainous region situated in the tropical region paves ways for rapid development of water resources. Various hydrological models have been developed to appraise the management of water and natural resources. The amount of land and water available per person is steadily declining due to population growth. Only 4% of the world's fresh water is distributed to India, which is home to 16% of global population. The first step in ensuring water sustainability in the future is to study how climate change will affect available water resources. One approach for understanding the hydrological behavior of the watershed is watershed-hydrological modelling.

A hydrological or hydro model attempt to replicate a watershed's response to precipitation. It is developed by forcing dynamic meteorology into a static watershed. When the modelling period is short or anthropogenic activities that change the watershed's land use are little, the static characteristics of the watershed can be taken into account as valid. By adjusting the meteorological forcings after the model has been calibrated, it can be used to anticipate both past and future scenarios. A variety of models and techniques to simulate streamflow have been developed in the past, including the physically based Richards' equation (Richards 1931); box modelling approaches (Laio et al. 2001; Brocca et al. 2008); Soil and Water Integrated Model, SWIM (Krysanova et al. 2005); Community Land Model, CLM3 (Vertenstein et al. 2004); Soil and Water NOAH Land Surface Model, Variable Infiltration Capacity, VIC Model (Liang et al. 1994); Decision Support System for Agrotechnology Transfer Crop Model, DSSAT (Ritchie and Otter 1985); Soil and Water Assessment Tool, SWAT Model (Neitsch et al. 2001); Regional Hydro-Ecological Simulation System, RHESSys (Band et al. 1991).

Climate modelling is the primary tool for predicting how the atmosphere, land, and ocean systems will react to changing atmospheric composition in the future. The General Circulation Models (GCMs), which use mathematical equations to explain the atmospheric process, are the most effective instrument for studying the effects of climate change at the regional level. The

Coupled Model Inter-Comparison Phase 5 (CMIP 5) provides daily data from more than 40 global climate models (GCMs) with various spatial resolutions (Rupp et al. 2013). The data from these models are constrained by the fifth assessment report (AR5) of the Intergovernmental Panel on Climate Change (IPCC), which provides current estimates of atmospheric conditions.

A river's flow pattern and drainage systems are dynamic in nature, changing over time and space as a result of a variety of factors including the region's geology, structural elements, geomorphology, vegetation, and soils (Rekha et al. 2011). The characteristics of the watershed and the hydrological processes that took place there should be known to the decision-makers. The watershed characteristics, which may be properly investigated by morphometric analysis, have an impact on the hydrological processes within a watershed.

1.2 Problem Statement

Even though the eastern Himalayan region is largely covered in a lush evergreen forest and has good seasonal snow cover at higher elevations, there have only been a few research on hydrological simulation. Hydrological systems in the eastern Himalayas are particularly susceptible to climate change, variability, and extremes, both seasonally and over longer time scales. Future flow regimes and soil moisture regimes could be significantly impacted by changes in temperature and precipitation. According to Rupakumar et al. (1992), the north-eastern region of India has experienced a decrease in summer monsoon rainfall. Singh et al. (2021) observed a decreasing trend in annual precipitation over the Pare watershed from 1981 to 2019, even though this was not statistically significant at the 0.05 level. This study's primary objective is to forecast future streamflow in the geographically distinct watersheds of Pare and Dudhnai. Both these watersheds are situated in mountains and they are subjected to higher energy inputs and are more vulnerable to climate change. Also, being pristine watersheds where human interventions are minimum, any changes in hydrological behavior are expected to cause by climate change.

In addition to this, one of the most persistent problems in both the Pare and Dudhnai basins is the significant erosion that occurs during periods of intense rainfall and that results in landslides. The development of a watershed representation model is thought required in order to parameterize watershed features and better understand hydrological behaviour in light of the aforementioned reasoning. Because of this, SWAT, a tool for assessing soil and water, was

chosen to conduct hydrological modelling in the Pare watershed. The Dudhnai watershed features a floodplain that occasionally floods. Watersheds must be prioritised for any intervention effort from the perspective of watershed management.

1.3 Objectives

Keeping the above-mentioned facts in view, the present study has been taken up with the following objectives:

1. To determine the morphometric parameters of Pare and Dudhnai river basins using Digital Elevation Model (DEM)
2. To simulate water yields using SWAT model for different climate change scenarios
3. To map inundation levels of Dudhnai river basin using HEC-RAS

1.4 Research Questions

1. How climate change will affect future precipitation and temperature over the Pare and Dudhnai watersheds?
2. Which sub-watersheds are needed to be prioritized for controlling soil erosion in the Pare and Dudhnai watersheds?
3. How climate change will impact future water resources for both the watershed?

CHAPTER II
REVIEW OF LITERATURE

In this chapter, various literature examined to attain the objectives of this study are discussed.

2.1 Morphometric Analysis

Initiation of morphometric studies began in the middle of the 20th century using a traditional approach based on manual assessments of topographic maps (Horton 1945; Strahler 1952, 1964; Schumm 1956). Decision-makers need to be aware of the features of the watershed and the hydrological processes that took place there. A watershed's properties, which may be properly evaluated through morphometric analysis, have an impact on how the hydrological processes within it work.

The mathematical analysis of the earth's surface that describes its topographic reliefs is known as morphometry (Clarke 1966). According to Rastogi and Sharma (1976), a number of hydrologic phenomena are associated with the physiographic features of watersheds. A thorough assessment of the hydrologic response, including surface runoff generation, infiltration capacity, and even groundwater potential, is provided through morphometric analysis. In ungauged watersheds where information on hydrology, geology, geomorphology, and soil is limited, morphometric analysis may be a good alternative. It can be used to forecast other basin features such as travel time, time to peak, and severity of erosional processes (Romshoo et al. 2012; Puno and Puno 2019).

Evaluation of a drainage basin, analysis of flood frequency, management of natural resources, their conservation, and yet erosion control might all benefit greatly from morphometric analysis (Tukura et al. 2021). The information obtained from morphometric study of watersheds could be an important tool for managing water resources, preventing soil erosion, mapping landslide susceptibility, assessing groundwater potential, and prioritizing watersheds (Jena and Dandabat 2019).

The traditional method of assessing river morphometrics is a very labor-intensive task that takes a lot of time. However, with the development of geospatial and computational technology, it is now much easier to undertake more exact and precise assessments. When topographic maps are not accessible, morphometric parameters of a watershed may be determined using satellite terrain data, such as a digital elevation model (DEM). Scientific

literatures which used DEMs for morphometric analysis in recent years are Nag (1998); Korup et al. (2005); Lindsay and Evans (2008); Wang et al. (2010) and Jacques et al. (2014). In context to India, Chopra et al. (2005), Kale and Shejwalkar (2007), Rudraiah et al. (2008), Sreedevi et al. (2009), Patel and Sarkar (2010), Pareta and Pareta (2011), Altaf et al. (2013) and Magesh et al. (2013).

According to Pandey et al. (2007), sub-watershed prioritizing is a technique for ranking sub-watersheds according to the severity of soil erosion and the condition of the drainage areas. Prioritizing sub-watersheds may take into account a number of characteristics, including soil loss, land use and cover, morphometric data, socioeconomic status of the local population, etc. Numerous scientific publications have discussed the use of morphometry in the prioritization of watersheds. For example, Noorkaratnam et al. (2005) used the sediment yield index (SYI) model to position check dams and Said et al. (2018) used the Nagmati river watershed to implement soil and water conservation measures. To eliminate any potential uncertainty, Rahmati et al. (2019) created an automated GIS-based approach for prioritizing sub-watersheds. Nine sub-watersheds in the Piperiya watershed were prioritized for watershed management using morphometric analysis by Chandniha and Kansal (2014). The research by Syed et al. (2017) and Obeidat et al. (2018) apply morphometric analysis and watershed prioritization for flood risk assessment (2021). Based on morphometric characteristics, Borah and Deka (2020) selected 14 sub-watersheds of the Jamuna River in Assam and divided the watersheds into low, medium, and high priority zones in terms of managing land and water resources.

2.2 Hydrological Models

A variety of hydrological models have been built to look at the hydrological processes for various watershed investigations. By addressing particular hydrologic processes that are important in forested watersheds (such as precipitation interception from a forest canopy or melt from a snowpack), some models can accurately replicate forest hydrologic regimes, whereas others may not have the necessary hydrologic-process representation. Others are better suited to tiny watersheds or steep terrain. Some types work better in large watersheds or on flat ground. Precipitation-Runoff Modelling System was developed by Leavesley et al. (1983) to evaluate the impacts of various climatic and land use configurations on streamflow and overall watershed hydrology. It is a deterministic, distributed-parameter, physical process-based

modelling system.

Arp and Yin (1992) introduced the Forest Hydrology Model (ForHyM), a process-oriented computer model that addresses all major water fluxes through forests. A forest soil temperature model (FORSTEM) (Yin and Arp 1993) and a model for nitrogen cycling are two companion models (Oja *et al.* 1995). The ForHyM model is a lumped watershed model that runs on a monthly basis. A single vegetation layer and two soil layers are included in the model. To simulate the impacts of forest water dynamics on stand growth and development, the ForHyM model was updated at the University of British Columbia (the Forest Water Dynamics model, ForWaDy) and combined with the FORCEE and FORECAST forest ecosystem (growth) models (Kimmins *et al.* 1999). The lack of channel-routing simulation in ForHyM and ForWaDy is a disadvantage of these models, limiting their use to forest stands or small watersheds.

The Hydrologic Modeling System (HEC-HMS), developed by the US Army Corps of Engineers (USACE 2000), simulates precipitation runoff processes. Only one soil layer and one vegetation layer are used in the model, which runs at a sub-daily time step. The US Environmental Protection Agency (EPA) developed the Hydrologic Simulation Program-Fortran (HSPF13) to simulate a variety of surface and subsurface hydrologic and water quality processes in watersheds (Bicknell et al. 2001). The HSPF hydrologic model, which uses lumped parameters, can simulate all essential natural hydrological processes on pervious and impervious land surfaces, in streams, and in well-mixed impoundments.

Incorporating water and biogeochemical cycle and transport at small (first-order streams) to medium (fourth- and fifth-order streams) sizes over topographically varied terrain is the Regional Hydro-Ecological Simulation System (RHESSys), a GIS-based modelling platform. It may mimic connected water-carbon-nutrient cycling and the ensuing growth of the vegetation canopy over a variety of terrain types (Band et al. 1993). In order to organise stream routing, RHESSys divides hydrologically distinct units into patches, hillslopes, climate zones, and watersheds.

The Distributed Hydrology Soil Vegetation Model (DHSVM), developed by Wigmosta et al. in 1994, aims to capture the effects of topography and vegetation on water fluxes through the landscape. The DHSVM is a totally distributed hydrologic model that divides the model domain (often the watershed or group of watersheds under consideration) into small computational grid pieces using the spatial resolution of an underlying digital elevation model

(DEM). It is frequently utilised at sub-daily time scales and high spatial resolutions of 10 to 100 m for watersheds up to 10,000 km2 for multi-year simulations (best results are obtained at hourly time increments).

SWAT is a watershed-scale model created to investigate how watershed management practises affect the yields of agricultural chemicals, water, and sediment (Gassman et al. 2007). Watersheds are divided into sub-watersheds, which are then divided into SWAT's HRUs. Among the meteorological factors needed by SWAT are daily precipitation, maximum/minimum air temperatures, sun radiation, wind speed, and relative humidity. These variables could originate from the model itself or come from the observed data. SWAT is made simpler to set up by using GIS-based interfaces, which also provide an easy way to transform digital data (land use, topography, and soils) into model inputs. The model has been applied to a variety of watersheds, small and large.

Wang et al. (2011) developed the Coupled Routing and Excess STorage (CREST) model, which uses cell-to-cell simulation to mimic the fluctuation of atmospheric, land surface, and underground water fluxes and storages in both time and space. CREST can be applied both globally and locally. The CREST Model can be forced using a variety of gridded PET (Potential Evapotranspiration) and precipitation datasets, including satellite-based precipitation estimates, gridded rain gauge observations, weather radar, and quantitative precipitation forecasts from numerical weather prediction models.

2.3 Application of SWAT Model

King et al. (1999) looked at two methods for mimicking severe rain utilising various rain gauges over a large basin. They stated that they were able to establish a high degree of correlation between measured and simulated hydrographs by utilising a sub-daily routing strategy. Luo et al. examined SWAT2000's variability and transferability as well as the performance of the plant-soil-groundwater modules (2008). According to the study, SWAT performed poorly in yield estimations, soil-water estimation under dry soil-profile conditions, and LAI forecasts during the senescence stage. SWAT was used by Rostamian et al. (2008) to simulate runoff and sediment at the Beheshtabad and Vanak watersheds in central Iran. One of the programmes in the SWAT-CUP package that interfaces with SWAT is sequential uncertainty fitting (SUFI-2).

Jain et al. (2010) simulated runoff and sediment output for a Himalayan watershed using the SWAT Model. They asserted that the SWAT model successfully forecasted the runoff and sediment discharge from a Himalayan intermediate watershed. In the Gumera river basin upstream of Lake Tana in Ethiopia, Habte et al. (2013) looked at the applicability of the SWAT model for simulating streamflow and sediment load. The SWAT calibration and uncertainty programme (SWAT-CUP)'s Sequential Uncertainty Fitting (SUFI2) and fully automated Parameter Solution (ParaSol) calibration processes were utilised to calibrate the model parameters. Ning et al. (2015) investigated continuous HRUs with a discrete spatial position for SWAT in a small watershed of the Taihu River, China using Geographic Information System technology.

SWAT was employed by Upadhyay et al. (2019) to forecast runoff in Rajasthan's Sirohi district's Pindwara watershed, which spans 1,428 square kilometres. The established model anticipated a total annual runoff of 277.57 mm, consisting of 174.96 mm of surface runoff, 15.55 mm of lateral flow, and 87.06 mm of baseflow. The NSE and R2 values for the model were 0.402 and 0.465, respectively. The model needed calibration and validation before being employed at a watershed size because it was shown to be unsuitable for direct field application.

The SWAT hydrological model was used by Guug et al. (2020) to determine how much water was present in the Sherigu watershed. The developed hydrological model performed well with Nash-Sutcliffe and a correlation coefficient greater than 0.7. Surface runoff and baseflow accounted for roughly 9 and 5 percent of the entire water balance, respectively, while percolation into unconfined and confined aquifers as soil and groundwater storages accounted for an additional 14 percent of the total outflow. The results also showed that shallow aquifer storage was high, leading to an overly high potential for groundwater extraction during the dry season.

Marahatta et al. (2021) used SWAT to describe the hydrological behaviour of a mountainous watershed in central Nepal. The study looked at the spatial distribution of streamflow in the watershed and the applicability of the SWAT model in a complicated and data-poor mountainous watershed. The study's results demonstrate the model's excellent performance.

2.4 Climate Change Impacts on Streamflow

The Working Group on Coupled Modelling, one of 20 global climate modelling groups,

collaborated to create CMIP5 as a component of the World Climate Research Programme (WCRP) (WGCM). Representative Concentration Pathways (RCPs), which are based on assumptions about economic activity, energy supplies, population growth, and other socioeconomic factors, include starting values and anticipated emissions up to the year 2100. Radiative forcing is the term for the extra energy that the earth system absorbs as a result of the stronger greenhouse effect (W m^{-2}). Each RCP specifies a particular emissions trajectory, and the resulting radiative forcing serves as a gauge of the influence on the energy balance of the earth-atmosphere system (measured in W m^{-2}). The best tool currently available for analysing significant changes in the earth's climate is GCM climate output (Houghton et al. 2001; Moss et al. 2010).

Risbey and Entekhabi (1996) looked into the streamflow response to temperature and precipitation changes in the Sacramento basin and its applicability to climate impact studies. They found that mean seasonal temperature had no effect on streamflow volume in the basin, despite precipitation being very responsive to it. Sharma et al. (2000) examined the hydrologic sensitivity of the basin to projected land-use and future climate change scenarios using water balance and distributed deterministic modelling. Zierl and Bugmann (2005) investigated how climate change affected the hydrological processes in Alpine catchments. On five case studies in the European Alps that represented different climatic zones, they employed RHESSys.

Using the SWAT model, Jha *et al.* (2006) evaluated the implications of anticipated future climate change on the hydrology of the upper Mississippi river basin. They compared the effects of nine 30-year sensitivity trials (1968 to 1997) and six climate change scenarios to a baseline. In response to climate change estimates generated by the CISRO-RegCM2, CCC, CCSR, CISRO-Mk2, GFDL, and HadCM3 GCM simulations, SWAT anticipated mean annual streamflow changes of 51, 10, 2, -6, 38, and 27 percent. The effects of long-term potential future climate change on average mean monthly streamflow from the five spatially scattered USGS gauging stations in the UPRW (Upper Pearl River Watershed) were examined using SWAT by Parajuli (2010). Basheer *et al.* (2015) investigated the effects of climate change on streamflow in the Dinder River Basin (DRB) and inferred their relative potential consequences on the ecosystem habitats of the Dinder National Park (DNP) in Sudan. They projected climate change conditions over the research area in the 2020s, 2050s, and 2080s using two global circulation models (GCMs) from the Coupled Model Intercomparison Project Phase 5 and two

statistical downscaling methodologies paired with a hydrological model -SWAT.

By analysing the SWAT, Bhatta et al. (2019) calculated the effect of climate change on streamflow in the Tamor River Basin. An ensemble of CMIP5 and four Regional Climate Models (RCMs) were used to create future climate scenarios for the 2030s, 2060s, and 2080s under the Representative Concentration Pathways (RCP 4.5 and RCP 8.5) scenarios. The SWAT model was used to forecast the basin's future streamflow after the climate data had been bias-corrected using the linear scaling method (LSM). RCP 8.5 scenarios forecast an increase in annual average maximum temperature (+4 °C) and lowest temperature (+5.5 °C) by the end of the twenty-first century as well as a decline in precipitation (-4.5 percent).

Neves et al. (2020) prepared input data for the climate simulation using a stochastic generator PGECLIMA R after calibrating and validating the hydrological model SMAP for the study site. Five hypothetical futures were developed, with scenarios A, B, C, and D based on the fifth IPCC report and scenario E based on regional climatic data patterns. Scenario D, which includes a 4.8°C rise in air temperature and a 10% decrease in rainfall, resulted in the worst water situation in the basin.

Quansah et al. (2021) evaluated the anticipated hydrologic responses and changes in streamflow resulting from future climate change in the Alabama River Basin for the 2045s (2030-2060) and 2075s (2060-2090). (ARB). They employed regional climate models from CNRM-CM5, CESM1- BGC.1, and HADGEM2-AO.1 for the CMIP5's Representative Concentration Pathway (RCP) 4.5. The historical climate data used to build the model were analysed for trends and levels of variability using Mann-Kendall and Theil Sen's slope, and the effects of climate change were assessed using SWAT. They came to the conclusion that the results were influenced by inherent uncertainties in the used downscaled GCM data.

CHAPTER III
MATERIALS AND METHODOLOGY

In this chapter, location of the study areas, data and various methodologies adopted in the present study are described. The chapter starts with describing the study area and followed by description on the data used in the current research. Then, methods, processes and models used to attain the three objectives are described.

3.1 Study Areas

3.1.1 Dudhnai watershed

Dudhnai River is one of the north flowing tributaries of the mighty river Brahmaputra. The river originates in the hilly regions of Meghalaya plateau, flows through the hilly state of Meghalaya for majority of its path, and meets with the Krishnai River before joining the river Brahmaputra. The Dudhnai river basin partly lies in the Garo Hills (approximately 83 %) district of Meghalaya and partly in the Goalpara district of Assam (approximately 17 %). Dudhnai river form a flood plain in the Assam region which are frequently inundated due to flash floods and siltation of erosive materials brought during the flash flood. The study area (shown in Fig. 3.1) has an area of 483.76 km^2, out of which approximately 20% lies in flood plain region and the rest lies in the hilly terrain. The watershed is characterized by undulated topography in the upland regions with elevation ranges from 47 m to 688 m as given by the Shuttle Radar Topographic Mission (SRTM) DEM. The study area falls under humid sub-tropical climate with intense pre-monsoon and monsoon rainfall from May to October. This high rainfall causes lot of erosion problems in the southern hilly region and siltation problems in the northern plain areas. The average annual temperature ranges between 19 °C and 30 °C. Agriculture (jhum or shifting cultivation at the hill slopes and traditional rice cultivation at the lower plain region) and forest are the main livelihood of the people inhabited in the basin. The people in the basin cultivate rice as their principal crop. However, tea plantations are also carried out in higher land areas. Other crops grown in the basin are sugarcane, mustard, pulses, cashewnut and jute. The soil in the hilly region of this basin is laterites and loamy in nature. In the northern plain areas, the soils are mostly new alluvium formed by the deposition of silt due to floods. Because of this reason and also due to heavy rainfall in the basin, the soils are slightly acidic in nature, and the texture of the soil is mostly sandy loam to silt loam.

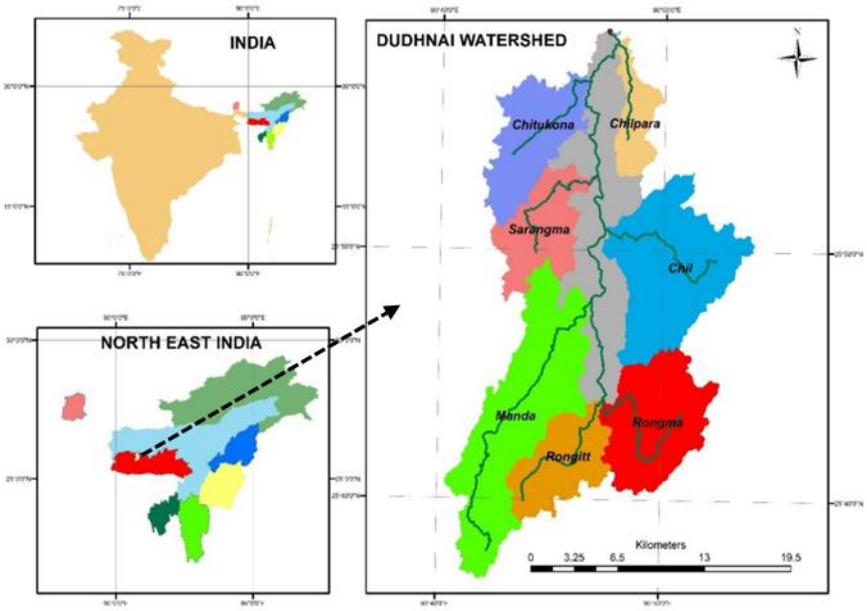

Fig. 3.1 Dudhnai watershed

3.1.2 Pare watershed

Pare watershed (Fig. 3.1), draining an area of 775.37 km^2, located at Papumpare district of Arunachal Pradesh, India, was selected as another research area. The area lies between latitudes 27° 09’ 36” N and 27° 22’ 08” N and longitudes 93° 13’ 15” E and 93° 47’ 07” E with an elevation range from 260 to 2,894 m above mean sea level (MSL). Pare River, a sub-tributary to Dikrong River, dissected the watershed. North Eastern Electric Power Corporation (NEEPCO) Limited has a gaging site at Hoj, just upstream of its outlet point of hydro power generation. The gaging site at Hoj was selected as the outlet point which lies at 93° 47’ 7.92” E, 27° 15’ 18.24” N, with an elevation of 260 m above MSL. The length of the Pare River is about 72 km within the watershed boundary. The watershed features highly undulated terrain with elevation ranging from 260 m to 2894 m above mean sea level. The watershed is a well dissected drainage basin, elongated in east-west direction with very fine drainage texture. The watershed is dominated by channel erosion over overland flow erosion. The annual average rainfall in the watershed is about 2731 mm (Singh *et al.* 2021) with monsoon season starting from June and last till September. The study area also received abundant amount of rainfall in pre-monsoon season (March-April-May). The soils in the study area are rich in organic matter and highly acidic in nature due to excessive leaching. The study area is a mountainous forested watershed where the villagers do jhum cultivation by deforesting small portion of forest in the hillslopes. Major crops/plants grown in the area are paddy, maize, mustard, chilly, large cardamon and orange. The locals love fishing from the Pare River and are dependent on this

river and many localized springs for domestic water supply. Few villagers irrigate their fields through collection of spring water into a tank. Doni and Gajurel (2020) reported diversified species of wild edible plants traditionally used by tribal people (Galo tribe) in Arunachal Pradesh for floods, nutrients, medicines and other purposes. The locals in the study area harvest a variety of forest produce and used them on daily basis.

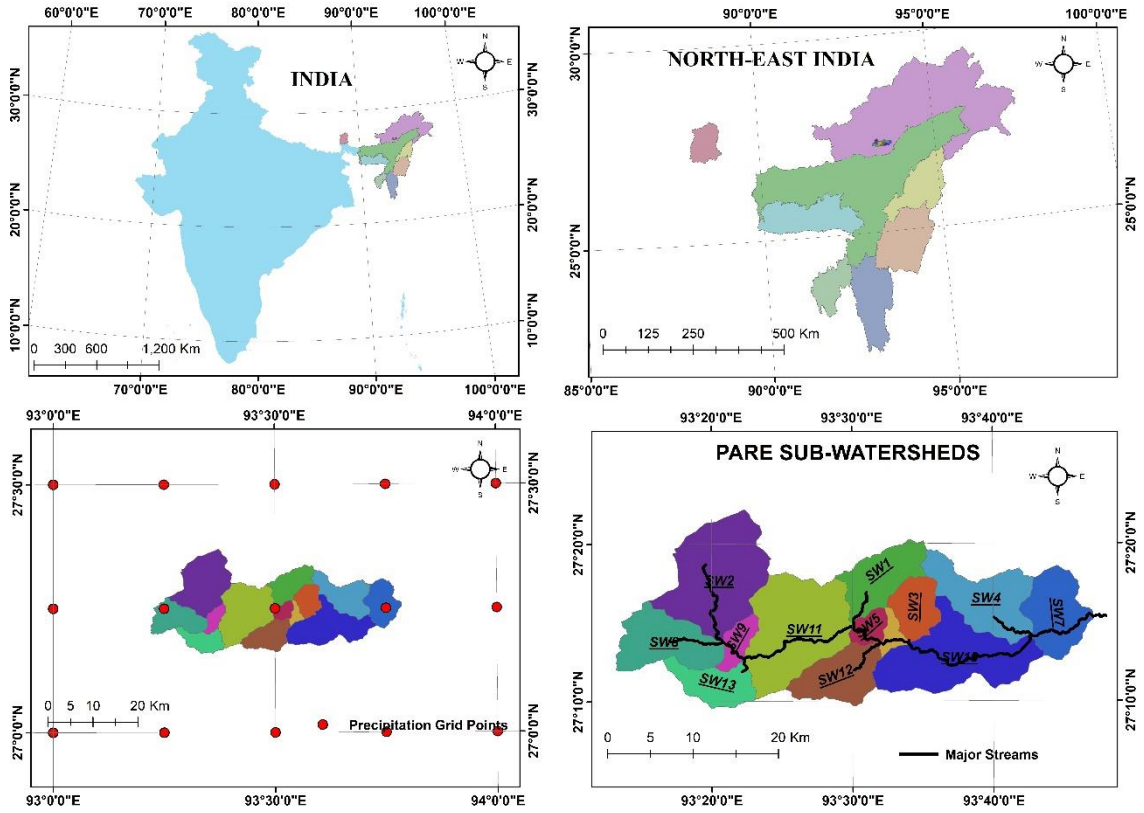

Fig. 3.2 Pare watershed

3.2 Data Used

3.2.1 Hydro-meteorological data

Weather data are one of the primary requirements for carrying out any hydrological modelling. Weather data such as precipitation, maximum and minimum temperatures, relative humidity, wind velocity, and solar radiation are required to simulate hydrological processes in SWAT. Daily discharge data at Hoj for Pare watershed was obtained from NEEPCO and daily discharge data at Dudhnai for Dudhnai watershed was obtained from Central Water Commission (CWC). Time period of the data collected were given in detail in Table 3.1. Daily gridded precipitation and temperature data were obtained from IMD website. Other data such as relative humidity, wind velocity, and solar radiation are simulated in SWAT using weather generator which was also provided by IMD for the entire India. Table 3.1 shows the various

hydro-meteorological data along with time periods.

Table 3.1 Hydro-meteorological data

Sl. No.	Type of data	Period			Source
		From	To	For watershed	
1.	Precipitation (Daily, gridded, 0.25º spatial resolution)	1989 2003	2005 2019	Pare Dudhnai	https://www.imdpune.gov.in/Clim_Pred_LRF_New/Grided_Data_Download.html
2.	Maximum and Minimum Temperature (Daily, gridded, 0.5º spatial resolution)	1989 2003	2005 2019	Pare Dudhnai	
3.	Weather Generator				https://swat.tamu.edu/data/india-dataset/
4.	Discharge (Daily, station)	1991	1997	Pare	NEEPCO
		2003	2005	Pare	
		2005	2019	Dudhnai	CWC

3.2.1.1 Projected meteorological data

The NASA (National Aeronautics and Space Administration) Earth Exchange Global Daily Downscaled Projections (NEX-GDDP) dataset consisted of biased corrected downscaled climate scenarios for the globe that are derived from the General Circulation Model (GCM) runs conducted under the Coupled Model Inter-comparison Project Phase 5 (CMIP5) and across two out of the four greenhouse gas emission scenarios known as Representative Concentration Pathways (RCPs). Downscaled RCP 4.5 and RCP 8.5 forecasts from 21 models supplied under CMIP5 are included in the NEX-GDDP dataset. Daily maximum and minimum temperatures, as well as precipitation, are included in each climate estimate for the years 1950 to 2100. The NEX-GDDP dataset is created using the Bias-Correction Spatial Disaggregation (BCSD) approach, which is a statistical downscaling algorithm devised to solve the constraints of global general circulation model (GCM) outputs (Wood *et al.* 2004; Thrasher *et al.* 2012). A comprehensive documentation is available at https://cds.nccs.nasa.gov.

Bannister *et al.* (2017) evaluated a huge number of global climate models from CMIP5 and concluded that determining best overall (mean, maximum, and minimum temperature) GCM was difficult. They found that climate model CCSM4 performed better for maximum temperature. Wu *et al.* (2018) found the climate model CNRM-CM5 performed better for precipitation data. The climate model CCSM4 was also one of the preferred models analysing Indian summer monsoon (Jena *et al.* 2016). Among the 12 CMIP5 models studied by Panjwani *et al.* (2019), NorESM1-M was found suitable for maximum temperature in India. Again, CNRM-CM5 and MPI-ESM-LR climate models were found suitable for analysis in Upper

Narmada Basin of India (Pandey *et al.* 2019). Latif *et al.* (2018) evaluated 36 CMIP5 climate models for the Indo-Pakistan subcontinent for precipitation data, in which, CNRM-CM5 and CCSM4 were found to have relatively reliable future projections. NorESM1-M climate model was found preferred by Le and Bae (2013), Agyekum *et al.* (2018), Ahmed *et al.* (2018), Ahmed *et al.* (2019), Afshar *et al.* (2017), Zamani and Berndtsson (2019) and Homsi *et al.* (2020) in their respective studies. The climate model MPI-ESM-LR was among the top five preferred GCMs for analysing precipitation over the Lower Mekong basin in South East Asia (Ruan *et al.* 2018). It is come to the notice that the performance of the climate models varies for different regions as well as different variables e.g., temperature, minimum temperature, maximum temperature, etc. Also, Grose *et al.* (2014) pointed that determining best climate models should not be perceived as guideline for weighting or sub-setting the climate models. After throughout reviewing of the climate models, a subset of four models was chosen from the 21 models provided by NASA NEX- GDDP. The NASA NEX-GDDP dataset that were chosen is shown in Table 3.2. The selected RCMs will henceforth be referred to by their short names for the sake of simplicity. The NASA data portal has downscaled bias corrected datasets of the mentioned RCMs for download at https://www.nccs.nasa.gov/services/data_portal. The dataset has a spatial resolution of 0.25 degrees (approximately 25 km x 25 km).

Table 3.2 List of future climate models used in this study

Sl. No.	Model	RCPs	Date Range
1.	CCSM 4	• RCP 4.5 • RCP 8.5	• 1976-2005 (Historical): 30 years • 2019-2099 (Future)
2.	CNRM-CM5		
3.	MPI-ESM-LR		
4.	NorESM1-M		

In the very initial stage of this project, preliminary analysis of precipitation was conducted using historical data from IMD and future data from Coordinated Regional Downscaling Experiment (CORDEX) for the period of 2021–2050. The CORDEX data was generated from precipitation scenarios from the model RegCM4-4 driven by the model MPI-MMPI-ESM-MR belonging to the r1i1p1 ensemble family given by Indian Institute of Tropical Meteorology, Pune, India, available at https://esgfnode.llnl.gov/projects/esgf-llnl/. The data includes RCP4.5 and RCP 8.5 scenarios. The data were then bias corrected using observed precipitation data to reduce the uncertainties in the assessment studies.

3.2.2 Spatial data

Table 3.3 lists the spatial data used in this study. The Digital Elevation Model (DEM) of Shuttle Radar Topography Mission (SRTM) with 30 m spatial resolution was downloaded for both the study areas from the website: https://srtm.csi.cgiar.org/. Digital soil map provided by Food and Agriculture Organization (FAO) for the study area was downloaded from website: http://www.fao.org/soils-portal/data-hub/soil-maps-and-databases/other-global-soil-maps-and-databases/en/. The FAO digital soil map is available at 1:25000000 scale. The Land Use Land Cover (LULC) map for the study area was obtained from Oak Ridge National Laboratory Distributed Active Archive Center (ORNL DAAC). It provides three LULC maps (Roy *et al.* 2016) for the years- 1985, 1995 and 2005 and LULC of 2005 was used in the present study. The data has a spatial resolution of 100 metres and was derived from various satellite data. Four topographic maps having toposheet number 78K/9, 78K/10, 78K/13 and 78K/14 and a total of 8 toposheets with toposheet number: 83E_3, 83E_4, 83E_7, 83E_8, 83E_11, 83E_12, 83E_15, and 83E_16OI were downloaded from Survey of India for Dudhnai and Pare watersheds, respectively. The toposheets are of
the scale of 1:50,000. The sole purpose of using these toposheets was to decide the threshold of stream network generation in ArcGIS.

Table 3.3 Spatial data

Sl. No.	Type of data	Source
1.	DEM	SRTM, https://srtm.csi.cgiar.org/
2.	Soil Map	FAO, http://www.fao.org/soils-portal/data-hub/soil-maps-and-databases/other-global-soil-maps-and-databases/en/
3.	LULC	ORNL DAAC, https://daac.ornl.gov/cgi-bin/dsviewer.pl?ds_id=1336
4.	Toposheets	Survey of India (SOI) http://soinakshe.uk.gov.in/

3.3 Pre-processing of Data

3.3.1 Digital elevation model (DEM)

The DEM downloaded is in Geographic Coordinate System (GCS) and was projected to the Universal Transverse Mercator (UTM) Projected Coordinate System (PCS) zone 46 N, using ArcMap 10.1 (Fig. 3.3). Pare watershed was delineated using Hoj as the outlet point and Dudhnai watershed using the CWC gaging station at Dudhnai. The levation in the Pare

watershed ranges from 260 m to 2894 m above mean sea level (msl), while elevation in Dudhnai watershed ranges between 49 and 683 m above msl.

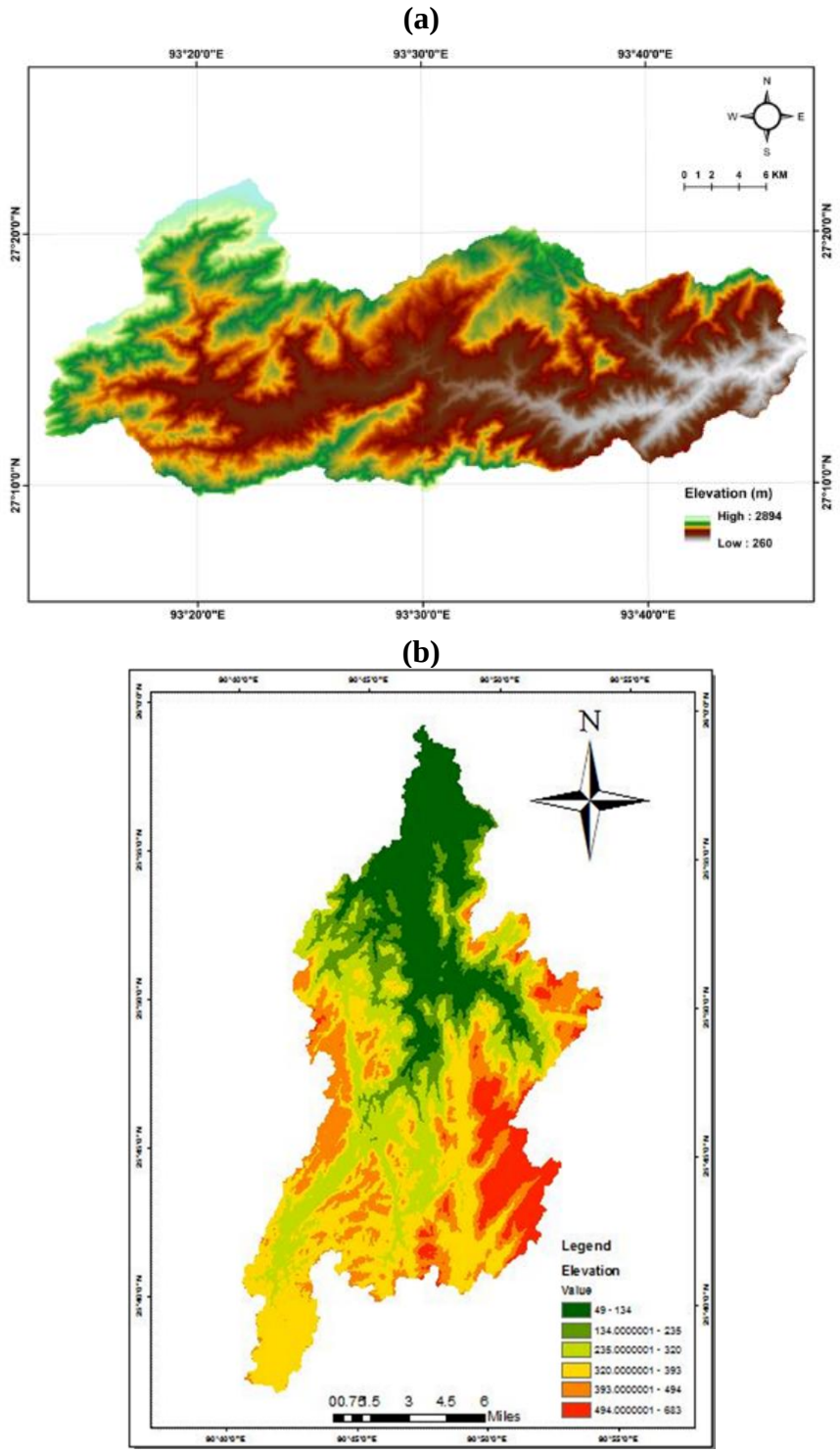

Fig. 3.3 DEM of (a) Pare watershed, and (b) Dudhnai watershed

3.3.2 Land use land cover (LULC) maps

The type of vegetation defines many components of the hydrological cycle. Land use land

cover (LULC) map for the entire India for the year 2005 from ORNL DAAC was clipped for the study areas. The data was reprojected to the UTM zone 46 N. Reclassifications of the LULC maps were performed to enable the model to link to the SWAT database codes, so that their properties can be used later during simulation. Fig. 3.4 shows the LULC maps of the study areas with SWAT code.

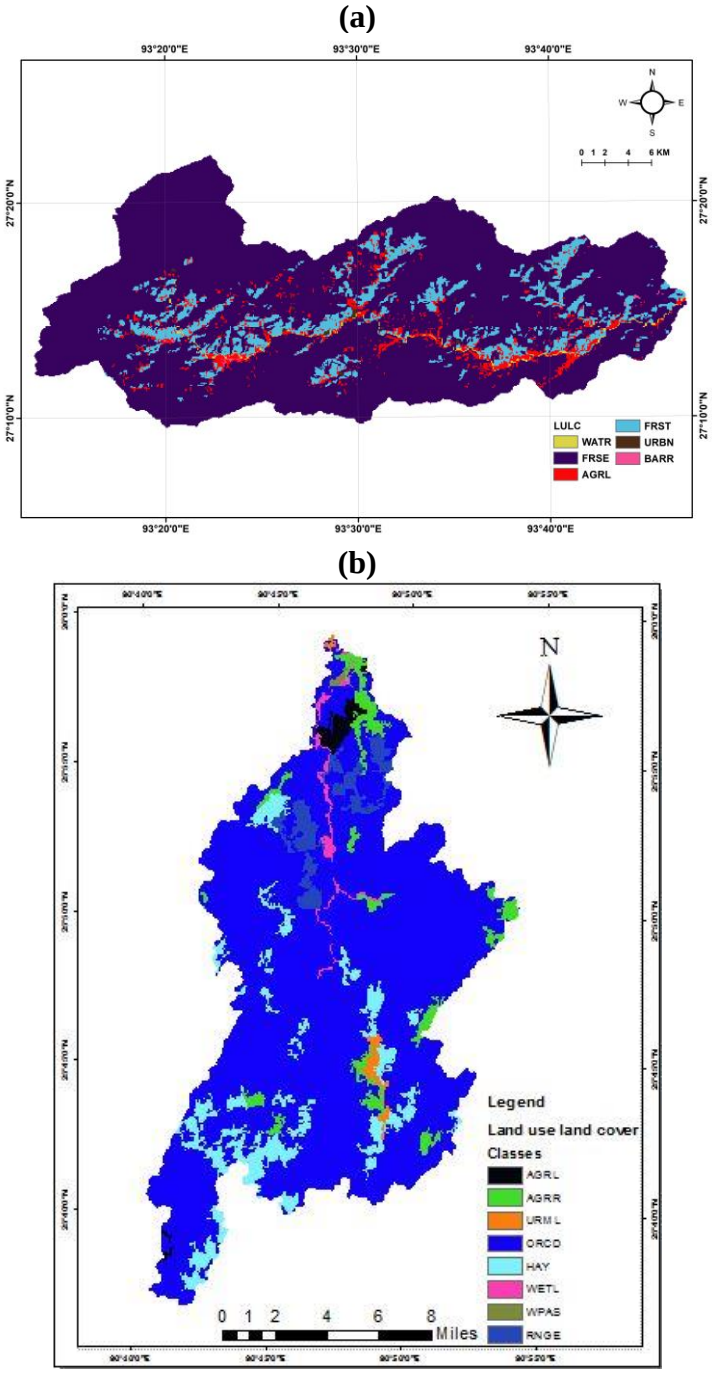

Fig. 3.4 LULC maps (a) Pare watershed and (b) Dudhnai watershed

Six types of LULC class (Fig. 3.4 (a)) were found in the Pare watershed. Forest land uses [evergreen (FRSE) and mixed (FRST)] cover the majority of the study region. Forest coverage

in the watershed is more than 94 percent. Other land uses such as cropland (AGRL) and residential areas (URBN) are situated along the river network. In the case of Dudhnai watershed, eight different LULC type were found (Fig. 3.4 (b)). Rangeland which is basically forest was found predominant in this watershed. This watershed has wetland and agriculture activities in its northern part. Necessary lookup tables were prepared for these two watersheds.

3.3.3 Soil maps

Properties of soil are highly important in the land surface schemes of climate and hydrological models due to its relation to evapotranspiration and consequently to the distribution of sensible and latent heat fluctuations (IPCC, 2013). The soil map for the study areas (Fig. 3.5) acquired from FAO was clipped to the study area. Necessary lookup table was prepared. In both the watersheds, there were only two types of soil.

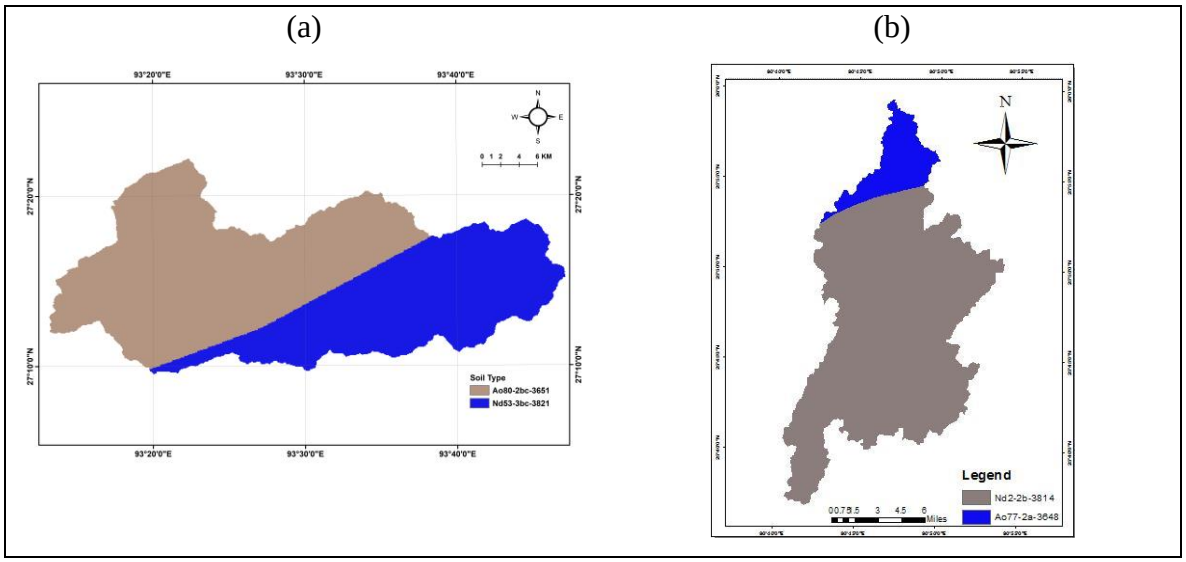

Fig. 3.5 Soil maps (a) Pare watershed and (b) Dudhnai watershed

3.3.4 Pre-processing of future precipitation and temperature dataset

The downloaded NEX-GDDP dataset consisted of precipitation, and maximum and minimum temperatures were in ASCII format. They were analyzed in Microsoft excel to get time series for each grid within the Pare watershed. Location file, precipitation and temperature data were prepared as text file (.txt) in the required format of the SWAT model. Again, the meteorological data for the four regional climate models (RCMs) were average each day to calculate meteorological data for the ensemble model.

3.4 Methodology

3.4.1 Morphometric analysis

In ArcGIS software, each toposheet was georeferenced after being converted to TIFF files. The toposheets obtained in this way also included legends, which could lead to matching problems during digitization. To solve this problem, distinct polygon shapefiles that perfectly matched the toposheet boundaries were digitally created. The whole research areas were then covered by clipping and merging the georeferenced toposheets into a single composite toposheet using the mosaic tool in ArcGIS. In order to access the watershed's stream network, the merged toposheets had finally been digitalized. Figure 3.6 depicts the methodology's overall flowchart for conducting morphometric analysis.

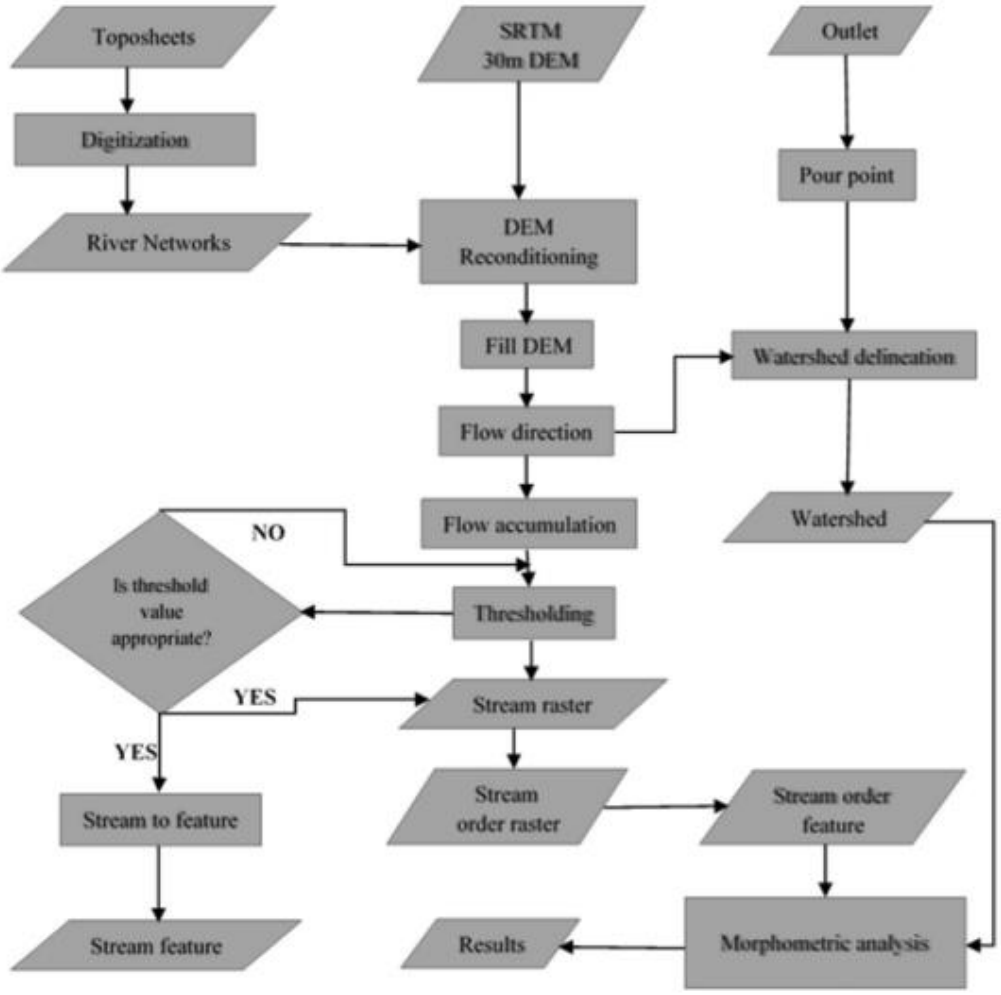

Fig. 3.6 Method for carrying out morphometric analysis

According to Ahmed et al. (2010), precise watershed delineation is necessary for watershed prioritization and management methods, which will lead to an accurate estimate of stream flow

routes and its contributing areas. The Dudhnai watershed's stream network creation via DEM demonstrated a large spatial variance from the ground reality, particularly in the proximity of the watershed's outlet. This may be explained by the flood plains' rather uniform relief. The original DEM was reconditioned, and the digitized stream networks from the toposheets were used to burn-in the DEM. The "Hydrology" tool of ArcGIS was then used to determine the watershed boundary, drainage network, and stream order network using the reconditioned DEM. The flow directions in the research areas were determined using the D8 (eight directions) flow direction technique. This technique allows water to flow from each raster cell to its eight adjacent neighbour cells. The algorithm determines the adjacent cell with the steepest downslope and assigns an integer code between 1 and 255 based on the flow directions. The Dudhnai watershed was divided into seven sub-watersheds: Rongma, Rongitt, Manda, Chil, Sarangma, Chitukona, and Chilapara, which cover the main tributaries of the Dudhnai River. The "cell threshold" value, which specifies the number of raster cells at which a stream grid should be created, is one of the most crucial steps in the delineation of a drainage network. The threshold value is inversely correlated with drainage density, meaning that a higher threshold value will lead to fewer streams. The Pare watershed has been separated into 25 sub-watersheds using the proper threshold.

ArcGIS was used to calculate the basin area, basin perimeter, basin length, main channel length, and length of stream order for each sub-watershed in Dudhnai and Pare. Then, to ascertain the linear, areal, and relief features of the watersheds and their sub-watersheds, Beg (2015) built an automated morphometric toolbox for ArcGIS written in Python. The scientific literature of Beg (2015) can be used to learn more specifics about the toolbox. The bare minimum information needed for this toolbox is a projected coordinate system watershed boundary, stream order shapefile, and digital elevation model (DEM). Table 3.4 provides an illustration of the morphometric characteristics determined by this toolbox, together with their equations and authors.

Table 3.4 Morphometric parameters and their formulae

Morphometric Parameter	Formula	Author
Number of stream orders (N_u)	$N_u = N1 + N2 + \cdots + Nn$	Horton (1945)
Length of stream orders (L_u)	$L_u = L1 + L2 + \cdots + Ln$	Horton (1945); Strahler (1964)
Bifurcation Ratio (R_b)	$R_b = {}^{N_u}/_{N_{u+1}}$	Schumm (1956); Strahler (1964)
Average bifurcation ratio (Rb_m)	$R_{b_m} = \frac{\frac{N1}{N2} + \frac{N2}{N3} + \cdots + \frac{Nn-1}{Nn}}{n-1}$	Strahler (1957)
Total Basin Area (A) (Km^2)	Projected area enclosed by watershed boundary	Schumm (1956)
Total Basin Surface Area (As) (km^2)	Integrated surface area enclosed by watershed boundary	
Total Basin perimeter (P) (Km)	Length of horizontal projection of watershed divide	Schumm (1956)
Basin Length (L_b) (Km)	Distance from outlet to farthest point on watershed boundary	Schumm (1956)
Main Channel Length (L_c) (Km)	Length of longest water course	
Fitness ratio (R_f)	$R_f = {}^{L_c}/_{P}$	Melton (1957)
Form factor (F_f)	$F_f = {}^{A}/_{{L_b}^2}$	Horton (1932)
Shape Factor (S_f)	$S_f = {}^{1}/_{F_f}$	Strahler (1964)
Relative perimeter (R_p)	$R_p = A/P$	Schumm (1956)
Length Area Relation (Lar)	$Lar = 1.4 \times A^{0.6}$	Hack (1957)
Rotundity coefficient (R_c)	$R_c = {L_b}^2 \times \pi/4A$	Strahler (1964); Zavoianu (1985)
Mean Basin Width (W_b)	$W_b = A/L_b$	Horton (1932)
Drainage Texture (D_t)	$D_t = {}^{N_u}/_{P}$	Horton (1945)
Compactness Coefficient (C_c)	$C_c = 0.282 \times P/\sqrt{A}$	Horton (1945)
Circularity ratio (R_c)	$R_c = 4\,\pi\,A\,/\,P^2$	Miller (1953)
Elongation ratio (R_e)	$R_e = \frac{D_c}{L_b} = 1.129 \times \frac{\sqrt{A}}{L_b}$	Schumm (1956)
Drainage density (D_d) (Km/km^2)	$D_d = \sum_{i=1}^{k} \sum_{i=0}^{N} {L_u}/_{A}$	Horton (1932); Strahler (1964)
Stream frequency (F) (number/Km)	$F = \sum_{i=1}^{k} {N_u}/_{A}$	Horton (1932)
Constant of channel maintenance (Ccm) (km^2/km)	$Ccm = {}^{1}/_{D_d}$	Schumm (1956); Strahler (1964)
Infiltration Number (Ifn)	$Ifn = F \times D_d$	Faniran (1968); Pareta and Pareta (2011)
Drainage Intensity (D_i)	$D_i = {}^{F}/_{D_d}$	Faniran (1968); Pareta and Pareta (2011)
Average Length of Overland Flow (L_g) (Km)	$L_g = 0.5 \times D_d$	Horton (1945)
Height of basin outlet (m)	DEM	
Maximum Height of basin (m)	DEM	
Total Basin Relief (H)	$H = Z - z$	Strahler (1952)
Relief Ratio	$Rhl = {}^{H}/_{L_b}$	Schumm (1956); Melton (1957)
Relative Relief Ratio	$Rhp = H \times {}^{100}/_{P}$	Melton (1957)
Gradient Ratio	$Rg = {}^{(Z-z)}/_{L_b}$	Pareta and Pareta (2011)
Ruggedness Number	$R_n = D_d \times ({}^{H}/_{1000})$	Strahler (1964)
Melton Ruggedness Number	$MRn = {}^{H}/_{0.5A}$	Melton (1965)
Terrain Undulation Index	$TUi = {}^{As}/_{A}$	Beg (2015)

This study's goal is to select watersheds based on their vulnerability to erosion and flooding. For the purpose of prioritizing watersheds, linear morphometric variables like mean bifurcation

ratio and average length of overland flow, areal morphometric variables like drainage density, drainage texture, stream frequency, form factor, elongation ratio, circularity ratio, and compactness coefficient, and relief morphometric variables like relief ratio and ruggedness number were chosen. Each parameter received a weighting based on how significant it was in relation to the danger of soil erosion. Greater importance of the characteristics in relation to the occurrence of soil erosion was indicated by higher weighting. While some morphometric parameters, such as form factor, compactness coefficient, circulatory ratio, and elongation ratio, have an inverse relationship with soil erodibility, others, like bifurcation ratio, drainage texture, drainage density, stream frequency, length of overland flow, relief ratio, and ruggedness number, have a direct relationship with soil erodibility.

Higher priorities (numerically small) are given to the sub-watersheds having higher soil erodibility and vice versa. Depending on the importance of each morphometric characteristic, a priority rank was given to each sub-watershed, ranging from 1 to 25 for the Pare watershed and 1 to 7 for the Dudhnai watershed. The compound rank for each sub-watershed is then calculated by summing all of the morphometric parameters for each priority rank and their associated weightages. Finally, the sub-watersheds have been rated and given a priority value depending on the magnitude of compound ranks. The most vulnerable sub-watershed, which requires soil conservation measures, has been given the highest priority of rank 1 based on the lowest numerical value of the compound rank. While the largest numerical value of compound rank has been given the lowest priority of rank 7 or 25 indicating the least vulnerable sub-watershed to soil erosion.

3.4.2 SWAT model

For the United States Department of Agriculture's Agricultural Research Service, Dr. Jeff Arnold developed the Soil and Water Assessment Tool (SWAT) (Arnold et al. 1998), a physically based, continuous-time, quasi-distributed, river basin-scale, long-term hydrologic model (USDA-ARS). The main objective of SWAT was to predict how land management practises will affect water, sediment, and agricultural chemical yields over time in complex watersheds with changing soils, land uses, and management conditions.

3.4.2.1 Theoretical considerations of SWAT

SWAT is capable of simulating a watershed in the absence of monitoring data and calculating the relative effects of various input data. The impacts of terrain, land use/cover, soil, and other

watershed characteristics on the hydrology are taken into account when dividing an area. Modeling is done using a spatially explicit discretization method and a parameterization strategy. The first step in discretization is to divide the entire watershed into a number of sub-basins depending on the topography and tributary drainage areas. These sub-basins are further separated into hydrologic response units (HRUs) based on soil, land use, and slope to increase the precision of flow forecasts and the physical description of the water balance. When different areas of the watershed are dominated by land uses or soils with characteristics that differ enough to effect hydrology, sub-basins are particularly helpful in simulations. By dividing the watershed into sub-basins, the user can use the watershed to refer to various geographically separate regions. A sub-HRUs basin's are a collection of land areas with varying soil types, land cover types, and management practises. Four storage volumes are used to calculate the water balance inside each HRU: snow, soil, shallow aquifer, and deep aquifer. The fundamental hydrological processes are surface runoff, infiltration, evaporation, plant water absorption, interflow, and percolation to shallow and deep aquifers. The water balance equation, which is denoted as follows, serves as the foundation for SWAT's hydrological cycle modelling.

$$SW_t = SW_0 + \sum_{i=1}^{t}(R_i - Q_i - ET_i - G_i - B_i) \quad (3.1)$$

Where, SW_t (mm) is the final soil water content, SW_0 (mm) is the initial soil water content on day i, t (days) is the time step, R_i (mm) is the amount of precipitation on day i, Q_i (mm) is the amount of surface runoff on day i, ET_i (mm) is the amount of evapotranspiration on day i, G_i (mm) is the amount of water entering the vadose zone from the soil profile on day i, and B_i (mm) s the amount of return flow on day i. To get the total runoff from the watershed, runoff is projected separately for each HRU and then averaged at the sub-basin level. As a result, the physical representation of the water balance is more precise and exact. Fig. 3.7 depicts the generic process flow SWAT used to represent the land portion of the hydrologic cycle.

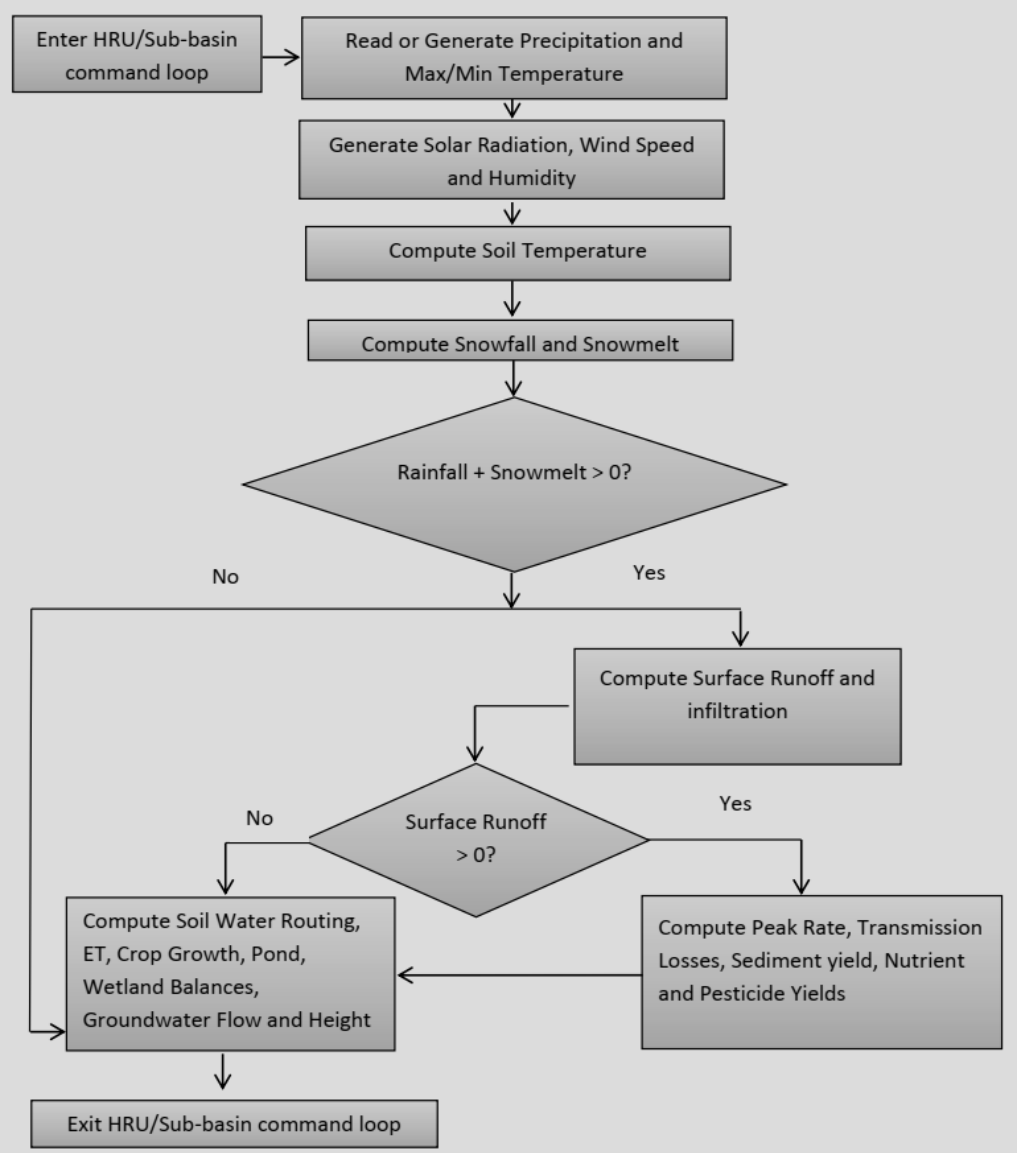

Fig. 3.7 HRU/Sub-basin command loop (Neitsch *et al.* 2005)

Using daily or sub-daily rainfall levels, SWAT models surface runoff volumes and peak runoff rates for each HRU. The Soil Conservation Service Curve Number (SCS-CN) technique, which considers excess precipitation, abstractions, and infiltration factor, is used in SWAT hydrologic modelling to determine surface runoff. The Green-Ampt excess rainfall method is another surface runoff calculation method in the SWAT model. King et al. (1999) found that neither approach had a clear advantage over the other in terms of producing findings that were acceptable. The Green-Ampt technique appears to have more limitations in predicting seasonal fluctuation than the SCS-CN method (King et al. 1999). Therefore, in this study, surface runoff was calculated using the SCS-CN method. The Curve Number is influenced by soil type, land use/cover, and prior moisture conditions. The four kinds of hydrologic soils can be summarised

as follows: Group A- deep sandy soil → heavy loss of moisture → low runoff potential; Group B- sandy loam soil → moderately high loss of moisture → low to moderate runoff potential; Group C- clay loam soil → moderate loss of moisture → moderate to high runoff potential; and Group D- heavy plastic clay, swelling soil → low loss of moisture → high runoff potential.

The hydrologic modelling of a watershed in the SWAT model can be divided into two categories. The first division is the hydrologic cycle's land phase, in which the hydrologic cycle regulates the quantity of water, sediment, nutrient, and pesticide loadings into each sub basin's main channel. The second segment of the hydrologic cycle is the water or routing phase, which describes the passage of water, sediments, and other materials through the watershed's channel network to the outlet. Fig. 3.8 depicts a schematic layout of water circulation paths in SWAT. In the following sections, we'll go through a quick rundown of the key procedures involved in the SWAT used in this study.

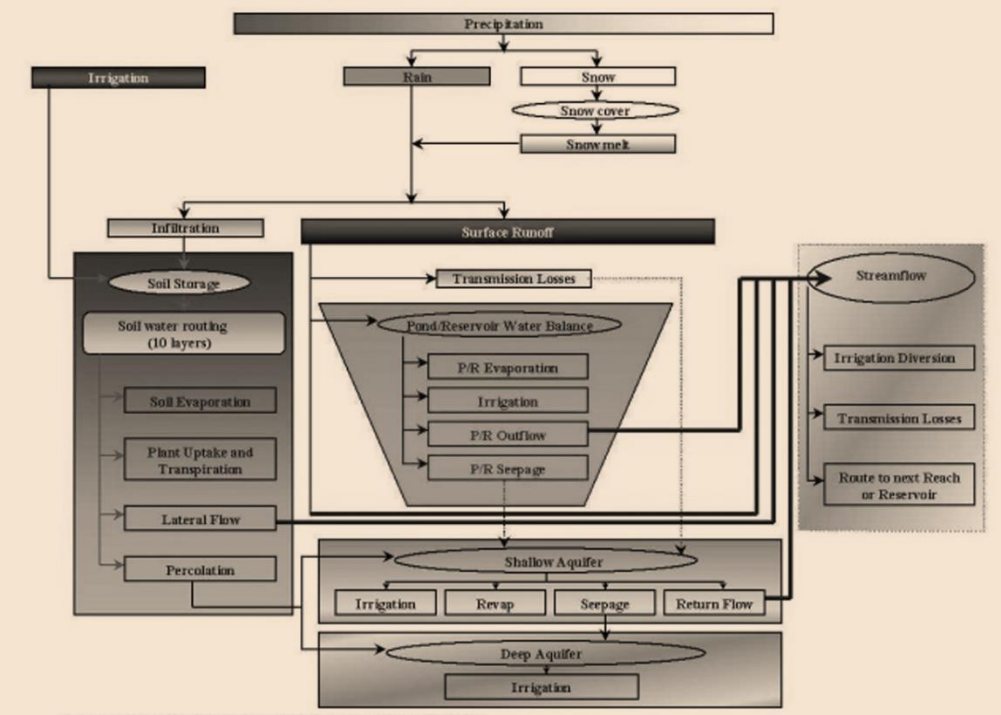

Fig. 3.8 Pathways of water movement in SWAT model (Neitsch *et al.* 2005)

Determination of surface runoff in SWAT

Two SWAT methodologies for determining surface runoff include the SCS curve number process (USDA SCS 1972) and the Green & Ampt infiltration method (Green and Ampt 1911). The SCS runoff equation is a prominent empirical model that dates back to the 1950s. It was

the culmination of more than two decades of research into rainfall-runoff interactions in tiny rural watersheds across the United States. The model was developed to provide a consistent foundation for calculating runoff volumes under a variety of land use and soil conditions (Rallison and Miller 1981). The SCS CN equation (USDA SCS 1972) is given as:

$$Q_{surf} = \frac{(R_{day} - I_a)^2}{(R_{say} - I_a + S)} \quad (3.2)$$

where Q_{surf} is the accumulated runoff or rainfall excess (mm H_2O), R_{day} is the rainfall depth for the day (mm H_2O), I_a is the initial abstractioas which includes surface storage, interception and infiltration prior to runoff (mm H_2O), and S is the retention parameter (mm H_2O). The retention parameter is affected spatially by changes in soils, land use, management, and slope, while it is affected temporally by changes in soil water content. The retention parameter's definition is as follows:

$$S = 25.4\left(\frac{1000}{CN} - 10\right) \quad (3.3)$$

where *CN* is the curve number for the day. The initial abstractions, I_a, is commonly approximated as 0.2S and equation 3.2 becomes:

$$Q_{surf} = \frac{(R_{day} - 0.2S)^2}{(R_{day} + 0.8S)} \quad (3.4)$$

Only when $R_{day} > I_a$, there will be runoff. The Green & Ampt equation was developed to predict infiltration assuming excess water at the surface at all times (Green and Ampt, 1911). The equation assumes that the soil profile is homogenous and antecedent moisture is uniformly distributed in the profile. The model assumes that as water seeps into the soil, the soil above the wetting front becomes completely saturated and the moisture content at the wetting front drops abruptly. The Green-Ampt method was added to SWAT to provide an alternative way for estimating surface runoff. For this strategy to work, the user must provide sub-daily precipitation data.

Determination of peak runoff rate in SWAT

The peak runoff rate is the maximum runoff flow rate that occurs during a specific rainfall event. The peak runoff rate is used to forecast sediment loss and is a measure of a storm's erosive intensity. SWAT calculates the peak runoff rate using a modified rational method. The rational method is widely used in the design of ditches, channels, and storm water control systems. The logical technique assumes that if a rainstorm of intensity *i* starts at time t = 0 and continues indefinitely, the rate of runoff will grow until the time of concentration, t = t_{conc},

when the entire subbasin area contributes to flow at the outlet. The rational formula is:

$$q_{peak} = \frac{C.i.Area}{3.6} \quad (3.5)$$

where q_{peak} is the peak runoff rate ($m^3\ s^{-1}$), *C* is the runoff coefficient, *i* is the rainfall intensity (mm/hr). *Area* is the subbasin area (km^2) and 3.6 is a unit conversion factor. The period of time between the start of a rainfall event until the entire subbasin area contributing to flow at the outlet is called the time of concentration. In other words, the time it takes for a drop of water to travel from the farthest point in the subbasin to the subbasin outflow is the time it takes a drop of water to travel from the farthest point in the subbasin to the subbasin outlet. The time of concentration is estimated by adding the overland flow time (the time it takes for water to travel from the farthest point in the subbasin to the channel) and the channel flow time (the time it takes for water to travel from the upstream channels to the outlet). The rational formula is modified and used in SWAT as:

$$q_{peak} = \frac{\alpha_{tc} \cdot Q_{surf} \cdot Area}{3.6\ t_{conc}} \quad (3.6)$$

where q_{peak} is the peak runoff rate ($m^3\ s^{-1}$), α_{tc} is the fraction of daily rainfall that occurs during the time of concentration, Q_{surf} is the surface runoff (mm H_2O), *Area* is the subbasin area (km^2), t_{conc} is the time of concentration for the subbasin (hr) and 3.6 is a unit conversion factor.

Determination of potential evapotranspiration

Thornthwaite (1948) first proposed the concept of potential evapotranspiration (PET) as part of a climatic classification scheme. PET, according to him, is the rate at which evapotranspiration occurs from a wide area uniformly covered with growing vegetation, with an infinite supply of soil water and no advection or heat storage effects. Penman (1956) characterised PET as "the amount of water transpired by a short green crop, totally shading the ground, of uniform height, and never short of water". Penman used grass as his reference crop, but later study (Jensen *et al.* 1990) suggests that alfalfa grown at a height of 30 to 50 cm might be a better option. PET has been estimated using a variety of approaches. The Penman-Monteith approach (Monteith 1965; Allen 1986; Allen *et al.* 1989), the Priestley-Taylor method (Priestley and Taylor 1972), and the Hargreaves method (Priestley and Taylor 1972) have all been incorporated into SWAT (Hargreaves *et al.* 1985). If the user decides to utilise a different potential evapotranspiration method, the model will read in daily PET values. The number of inputs required by the three PET methods featured in SWAT differ. Solar radiation,

air temperature, relative humidity, and wind speed are all requisite for the Penman-Monteith method to work. Solar radiation, air temperature, and relative humidity are all needed in the Priestley-Taylor method. Only air temperature is needed for the Hargreaves approach.

The Penman-Monteith equation combines components that account for energy needed to sustain evaporation, the strength of the mechanism required to remove the water vapor and aerodynamic and surface resistance terms. The Penman-Monteith equation is:

$$\lambda E = \frac{\Delta \cdot (H_{net} - G) + \rho_{air} \cdot c_p \cdot [e_z^0 - e_z]/r_a}{\Delta + \gamma \cdot (1 + {}^{r_c}/_{r_a})} \quad (3.7)$$

where λE is the latent heat flux density (MJ m^{-2} d^{-1}), E is the depth rate evaporation (mm d-), Δ is the slope of the saturation vapor pressure-temperature curve, de/dT (kPa ºC^{-1}), H_{net} is the net radiation (MJ m^{-2} d^{-1}), G is the heat flux density to the ground (MJ m^{-2} d^{-1}), ρ_{air} is the air density (kg m^{-3}), c_p is the specific heat at constant pressure (MJ kg^{-1} °C^{-1}), e_z^0 is the saturation vapor pressure of air at height z (kPa), e_z is the water vapor pressure of air at height z (kPa), γ is the psychromctric constant (kPa °C^{-1}), r_c is the plant canopy resistance (s m^{-1}), and r_a is the diffusion resistance of the air layer (aerodynamic resistance) (s m^{-1}). For well-watered plants under neutral atmospheric stability and assuming logarithmic wind profiles, the Penman-Monteith equation may be written (Jensen *et al.*, 1990):

$$\lambda E_t = \frac{\Delta \cdot (H_{net} - G) + \gamma \cdot K_1 \cdot (0.622\lambda \cdot {}^{\rho_{air}}/_{P} \cdot [e_z^0 - e_z]/r_a}{\Delta + \gamma \cdot (1 + {}^{r_c}/_{r_a})} \quad (3.8)$$

where λ is the latent heat of vaporization (MJ kg^{-1}), E_t is the maximum transpiration rate (mm d^{-1}), K_1 is a dimension coefficient needed to ensure the two terms in the numerator have the same units (for u_z in m s^{-1}, K_1 = 8.64 x 10^4), and P is the atmospheric pressure (kPa).

Determination of actual evapotranspiration

Actual evaporation must be computed once total potential evapotranspiration has been determined. Any rainfall absorbed by the plant canopy is first evaporated by SWAT. SWAT then uses an approach similar to Ritchie (1972) to compute the maximum amount of transpiration and the maximum amount of sublimation/soil evaporation. After that, the real amount of soil sublimation and evaporation is estimated. Sublimation will occur if there is snow in the HRU. Evaporation from the soil occurs only when there is no snow on the ground.

Stream flow routing

An open channel flow, such as that in a river or a partially full pipe, is defined as channel flow

with a free surface. To determine the rate and velocity of flow, SWAT employs Manning's equation. Using the variable storage routing method or the Muskingum routing method, water is channelled through the channel network. Both the variable storage and Muskingum routing methods are variations of the kinematic wave model. Manning's equation for uniform flow in a channel is used to calculate the rate and velocity of flow in a reach segment for a given time step:

$$q_{ch} = \frac{A_{ch} \cdot {R_{ch}}^{2/3} \cdot {slp_{ch}}^{1/2}}{n} \quad (3.9)$$

$$v_c = \frac{{R_{ch}}^{2/3} \cdot {slp_{ch}}^{1/2}}{n} \quad (3.10)$$

where q_{ch} is the rate of flow in the channel (m^3/s), A_{ch} is the cross-sectional area of flow in the channel (m^2), R_{ch} is the hydraulic radius for a given depth of flow (m), slp_{ch} is the slope along the channel length (m/m), n is Manning's coefficient for the channel, and v_c is the flow velocity (m/s). SWAT routes water as a volume. This present study adopts the variable storage routing method which was developed by Williams (1969). For a given reach segment, storage routing is based on the continuity equation:

$$V_{in} - V_{out} = \Delta V_{stored} \quad (3.11)$$

where V_{in} is the volume of inflow during the time step (m^3 H_2O), V_{out} is the volume of outflow during the time step (m^3 H_2O), and ΔV_{stored} is the change in volume of storage during the time step (m^3 H_2O). This equation can be written as:

$$\Delta t = \left(\frac{q_{in,1}+q_{in,2}}{2}\right) - \Delta t \cdot \left(\frac{q_{out,1}+q_{out,2}}{2}\right) = V_{stored,2} - V_{stored,1} \quad (3.12)$$

where Δt is the length of the time step (s), $q_{in,1}$ is the inflow rate at the beginning of the time step (m^3/s), $q_{in,2}$ is the inflow rate at the end of the time step (m^3/s), $q_{out,1}$ is the outflow rate at the beginning of the time step (m^3/s), $q_{out,2}$ is the outflow rate at the end of the time step (m^3/s), $V_{stored,1}$ is the storage volume at the beginning of the time step (m^3 H_2O), and $V_{stored,2}$ is the storage volume at the end of the time step (m^3 H_2O). Rearranging equation 3.12 so that all known variables arc on the left side of the equation,

$$q_{in,ave} + \frac{V_{stored,1}}{\Delta t} - \frac{q_{out,1}}{2} = \frac{V_{stored,2}}{\Delta t} + \frac{q_{out,2}}{2} \quad (3.13)$$

where $q_{in,ave}$ is the average inflow rate during the time step: $q_{in,ave} = \frac{q_{in,1}+q_{in,2}}{2}$. Travel time is computed by dividing the volume of water in the channel by the flow rate.

$$TT = \frac{V_{stored}}{q_{out}} = \frac{V_{stored,1}}{q_{out,1}} = \frac{V_{stored,2}}{q_{out,2}} \quad (3.14)$$

where TT is the travel time (s), V_{stored} is the storage volume (m^3 H_2O), and q_{out} is the discharge

rate (m^3/s). Substituting equation 3.14 in equation 3.13,

$$q_{in,ave} + \frac{V_{stored,1}}{\left(\frac{\Delta t}{TT}\right)\left(\frac{V_{stored,1}}{q_{out,1}}\right)} - \frac{q_{out,1}}{2} = \frac{V_{stored,2}}{\left(\frac{\Delta t}{TT}\right)\left(\frac{V_{stored,2}}{q_{out,2}}\right)} + \frac{q_{out,2}}{2} \quad (3.15)$$

Which is then simplifies to

$$q_{out,2} = \left(\frac{2\Delta t}{2TT+\Delta t}\right) q_{in,ave} + \left(1 - \frac{2\Delta t}{2TT+\Delta t}\right) q_{out,1} \quad (3.16)$$

This equation is similar to the coefficient method equation

$$q_{out,2} = SC \,.\, q_{in,ave} + (1 - SC).\ q_{out,1} \quad (3.17)$$

where *SC* is the storage coefficient. Equation 3.29 is the basis for the SCS convex routing method (SCS, 1964) and the Muskingum method (Brakensiek, 1967; Overton, 1966). From equation 3.28, the storage coefficient in equation 3.17 is defined as:

$$SC = \frac{2\Delta t}{2TT+\Delta t} \quad (3.18)$$

It can be shown that

$$(1 - SC)q_{out} = SC\frac{V_{stored}}{\Delta t} \quad (3.19)$$

Substituting equation 3.19 into 3.17,

$$q_{out,2} = SC\left(q_{in,ave} + \frac{V_{stored,1}}{\Delta t}\right) \quad (3.20)$$

To express all values in units of volume, both sides of the equation are multiplied by the time step which gives into:

$$V_{out,2} = SC\left(V_{in} + V_{stored,1}\right) \quad (3.21)$$

3.4.2.2 ArcSWAT interface for SWAT 2012

The ArcSWAT is an ArcGIS extension. This plugin produces streams, demarcates watersheds, and gets simulation input files ready by generating/writing the specialized files needed for SWAT modelling. The following data inputs are needed to run a SWAT simulation using the ArcSWAT interface: (1) a digital elevation model (DEM) layer, (2) a land use and land cover layer, (3) a soil data layer, and (4) climate information such as precipitation, maximum and minimum temperatures, solar radiation, relative humidity, and wind speed. ArcSWAT's user interface consists of six menu tabs. The menu titles and the primary tasks found within each menu are shown in Fig. 3.9. A successful run of the model requires that the menus be processed in order.

The first ArcSWAT menu allows users to set the project and the second menu defines the

basin's boundaries. SWAT defines the basin's boundaries and divides it into sub-basins using topographical data and other user inputs (e.g., the spatial location of the basin outlet and other user-defined outlets). The ArcSWAT application allows users to accept default sub-basin delineations while also allowing them to alter the subbasins. SWAT creates a geographic layer of the subbasin boundaries as part of the delineation procedure. The third menu of the ArcSWAT interface is used to further partition each sub-basin into SWAT hydrologic response units (HRUs) after the basin and sub-basins have been defined. They're based on land use, soils, and topographic data, as well as their distinctive combinations. Whether or not to use numerous HRUs in the modelling application is a decision that must be made. If several HRUs aren't used, the interface will default to the watershed's dominant land use and soil characteristic. To simulate multiple HRUs, a threshold level must be determined that accounts for the variability of land uses and soil in each sub-basin. The fourth menu accepts climatic input from the weather generator, either observed or simulated, and writes input files for later use by the SWAT. The fifth menu is optional, and it allows you to edit and modify SWAT input files. In the 6^{th} menu, simulation period, wide range of outputs can be selected.

3.4.2.3 Sensitivity Analysis in SWAT

There are a number of parameters linked with distinct processes in the SWAT model. Some of these parameters are forcing variables, while others are initial or boundary conditions. During model setup, a default value is assigned to each parameter based on the topography, soil type, land use, slope, and climate of the region. Based on knowledge of local hydrologic processes and interpretation of the pre-calibration versus simulated hydrograph, twelve parameters (Table 3.5) and fifteen parameters (Table 3.6) were chosen for sensitivity analysis in Pare and Dudhnai watersheds, respectively. In this study, sensitivity analysis and calibration were performed using SWAT Calibration Uncertainty Programs (SWAT-CUP) (Abbaspour 2011) and its Sequential Uncertainty Fitting (SUFI-2) algorithm (Abbaspour *et al.* 2004). Because of its ease of implementation and low number of model runs required to obtain acceptable prediction, the SUFI-2 algorithm has been frequently employed in the calibration of the SWAT model (Yang *et al.* 2008). The sensitivity of the parameters was determined using global sensitivity approach. It may see the effect of each parameter on the model output at the same time. Because the values of all the parameters were changing at the same time in the global sensitivity approach, a single simulation with 1000 runs was done to see how each parameter affected the objective function.

Menu 1: SWAT Project Setup

Menu 2: Watershed Delineator

- Input topographical information, stream network and area threshold;
- Determine locations of sub-basin outlets;
- Delineate watershed and determine watershed parameters

Menu 3: SWAT Hydrologic Response Unit Analysis

- Input land use and soil information;
- Indicate slope intervals for HRU development.

Menu 4: SWAT Write Input Tables

- Enter climate data;
- Write SWAT files.

Menu 5: Edit SWAT Input

- Edit databases if necessary (lulc, soil etc.);
- Add point source discharges if applicable;
- Make changes to input at the sub-basin level;
- Make changes to input at watershed level;
- Rewrite SWAT files as needed.

Menu 6: SWAT Simulation

- Select simulation period;
- Select output settings;
- Click SWAT Setup, then click Run.

Fig. 3.9 ArcSWAT menus (Karcher *et al.* 2013)

Table 3.5 Parameters considered for sensitivity analysis in Pare watershed

Sl. No.	Parameter	Description	Remark/Type of parameter
1.	CN2.mgt	CN number for moisture condition II	Management
2.	GW_DELAY.gw	Groundwater delay	Groundwater
3.	ALPHA_BF.gw	Baseflow recession constant	Groundwater
4.	GWQMN.gw	Threshold water's depth in shallow aquifer required for occurrence of return flow	Groundwater
5.	ESCO.hru	Compensation factor for soil evaporation	HRU
6.	SOL_AWC(..).sol	Available water capacity of soil layer	Soil
7.	SOL_K(..).sol	Soil's saturated hydraulic conductivity	Soil
8.	CH_N2.rte	Manning's roughness *n* of main channel	Main Channel
9.	CH_K2.rte	Channel hydraulic conductivity	Main Channel
10.	REVAPMN.gw	Threshold water's depth in shallow aquifer for occurrence of percolation to deep aquifer	Groundwater
11.	GW_REVAP.gw	Groundwater "revap" coefficient	Groundwater
12.	ALPHA_BNK.rte	Bank storage's recession constant	Main Channel

Table 3.6 Parameters considered for sensitivity analysis in Dudhnai watershed

Sl. No.	Name of the parameter	SWAT Notation
1	SCS runoff curve number	CN2.mgt
2	Baseflow alpha factor (days)	CH_K2.rte
3	Groundwater delay (days)	ALPHA_BNK.rte
4	Threshold depth of water in the shallow aquifer required for return flow to occur (mm)	CH_N2.rte
5	Soil evaporation compensation factor	SLSOIL.hru
6	Available water capacity of the soil layer	REVAPMN.gw
7	Saturated hydraulic conductivity	GW_REVAP.gw
8	Manning's "n" value for the main channel	GW_DELAY.gw
9	Effective hydraulic conductivity in main channel alluvium	SURLAG.bsn
10	Groundwater "revap" coefficient	SOL_AWC(..).sol
11	Threshold depth of water in the shallow aquifer for "revap" to occur (mm)	SOL_K(..).sol
12	Baseflow alpha factor for bank storage	ESCO.hru
13	Manning's "n" value for overland flow	OV_N.hru
14	Slope length for lateral subsurface flow	GWQMN.gw
15	Surface runoff lag time	ALPHA_BF.gw

3.4.2.4 Calibration of the SWAT model

The model's calibration was primarily focused on streamflow. On a daily timestep, the model was calibrated for seven years (1991–1997) in Pare watershed and for ten years (2005-2014) in Dudhnai watershed. Model calibration entailed changing the values of sensitive parameters to match field conditions within a set of permissible parameters. Two ways of altering the values of sensitive parameters were used in this investigation. A relative method in which the existing parameter value is multiplied by (1+ a provided value) and a replacement technique in which the old value of a parameter is replaced with a new parameter value. For parameters with geographical heterogeneity, such as CN2, the relative technique was used. The Nash-Sutcliffe Efficiency, NSE (Nash and Sutcliffe 1970) was used as the objective function for calibration. Subsequent iterations increase the NSE however, care was taken not to amplified the model uncertainties. Table 3.7 shows the minimum, maximum, and default values for the 12 model parameters calibrated in the Pare watershed. For Dudhnai watershed, minimum, maximum and method for calibrating 15 model parameters are illustrated in Table 3.8.

Table 3.7 Minimum, maximum, and default values of the model parameters in Pare watershed

Sl. No.	Parameter	Minimum	Maximum	Default
1.	CN2.mgt	-0.20	0.20	Spatially varied
2.	GW_DELAY.gw	5	450	31
3.	ALPHA_BF.gw	0	1	0.048
4.	GWQMN.gw	0	2000	1000
5.	ESCO.hru	0.70	0.99	0.95
6.	SOL_AWC(..).sol	-0.20	0.20	Spatially varied
7.	SOL_K(..).sol	-0.30	0.30	Spatially varied
8.	CH_N2.rte	0.05	0.30	0.014
9.	CH_K2.rte	0	150	0
10.	REVAPMN.gw	0	500	0
11.	GW_REVAP.gw	0.02	0.20	0.02
12.	ALPHA_BNK.rte	0	1	0.048

Table 3.8 Minimum, maximum and method of model parameters used in Dudhnai watershed

Sl. No.	Parameters	Minimum	Maximum	Method
1	CN2	-0.389109	0.003775	Relative
2	ALPHA_BF.gw	0.333951	1	Replace
3	GW_DELAY.gw	0	270.9827	Replace
4	GWQMN.gw	771.223755	2315.443	Replace
5	ESCO.hru	0.600612	0.860288	Replace
6	SOL_AWC(..).sol	-0.011751	0.365085	Relative
7	SOL_K(..).sol	-0.056626	0.430626	Relative
8	CH_N2.rte	0.148903	0.3	Replace
9	CH_K2.rte	29.585041	109.915	Replace
10	GW_REVAP.gw	0.068112	0.164488	Replace
11	REVAPMN.gw	126.977676	381.3557	Replace
12	ALPHA_BNK.rte	0.400613	1	Replace
13	OV_N.hru	0.129563	0.368937	Replace
14	SLSOIL.hru	22.092209	107.4078	Replace
15	SURLAG.bsn	0.05	2.719959	Replace

3.4.2.5 Validation of the SWAT model

Using observed daily and monthly streamflow time series at the watershed's outlet, the strength and reliability of the hydrologic prediction generated by the calibrated model were examined in this study. The catchment response was evaluated during the validation phase using the parameter values obtained at the end of the calibration process. The SWAT model was validated in SWAT-CUP utilising discharge data from 2003 to 2005 in Pare watershed and from 2015 to 2019 in Dudhnai watershed while keeping the same parameter range.

3.4.2.6 Uncertainty analysis

In SWAT-CUP, an uncertainty analysis was performed for the calibration and validation periods. To quantify all of the uncertainties associated with the SWAT model, the p-factor (percentage of observed data bracketed by the 95 percent prediction uncertainty band), also known as 95PPU (Percent Probability Uncertainty), was utilised. For 95PPU and determining the final cumulative distribution of the model outputs, the Latin hypercube sampling approach was used. These were calculated with a prediction limit of 97.5 percent and 2.5 level. SUFI-2 assumed a substantial parameter uncertainty during model parameter initialization and then reduced this uncertainty using the p-factor and r-factor performance statistics. The p-factor ranged from 0 to 1, with values around 1 indicating very high model performance and efficiency, whereas the r-factor is the average width of the 95PPU band divided by the standard deviation of the measured variable, and ranged from 0 to a finite number. (Abbaspour *et al.* 2018; Yang *et al.* 2008). The p-factor and the r-factor are closely related, implying that a desirable greater p-factor can only be obtained at the expense of a higher r-factor which is not an ideal scenario.

3.4.2.7 Streamflow response under projected climatic scenarios in SWAT

Climate change is likely to have an impact on the study area's hydrological cycle. Understanding the effects of climate change on hydrological processes is critical for developing the best long-term water management strategies and ensuring water security. The examination of the basin's hydrologic response to climate change in this study focuses on estimating the probable effects of temperature and precipitation variations on streamflow and soil moisture in the watershed. The most powerful tools now available for simulating the reaction of the global climate system to growing Green House Gases (GHG) concentrations in the atmosphere are the General Circulation Models (GCM). The calibrated parameter values were manually transferred from SWATCUP to ArcSWAT. The After appropriate calibration and validation, SWAT model was run for 35 climatic scenarios which included five historical scenarios (4 climate models and an ensemble) and five scenarios each for near, mid and far future periods under two RCPs. The impacts of future climate change to the future streamflow were studied and discussed.

3.4.2.8 Performance indicators of the models

Four statistics, including Nash-Sutcliffe efficiency (NSE), coefficient of determination (R^2), percent bias (PBIAS), Standard Error of Estimates (SEE), and two graphical approaches, were

used to assess the model's performance and accuracy in this study. A graphical approach comparison of model simulated values with observed values for a single streamflow gauge in a watershed could be very useful in establishing how well the model works in relation to the study area. The detail description of the statistics can be found in Moriasi *et al.* (2007). NSE is a normalised statistic that compares the magnitude of residual variance ("noise") to the variance of measured data ("information") (Nash and Sutcliffe 1970). The NSE value indicates how closely the observed vs. simulated data graphic fits the 1:1 line. The NSE ranges between -∞ and 1, with a greater value indicating better model performance. The following is the mathematical formula for calculating NSE:

$$NSE = 1 - \frac{\sum_{i=1}^{n}(O_i - P_i)^2}{\sum_{i=1}^{n}(O_i - \bar{O})^2} \quad (3.22)$$

where, O_i is the measured discharge at timestep *i*, $\bar{O}$ is the long-term measured mean discharge, and P_i is the predicted/simulated discharge at timestep *i*. The R^2 numerical notation compares the measured and simulated time series' combined dispersion to their single dispersion (Krause *et al.* 2005). The degree of collinearity between simulated and observed data is assessed by R^2, which ranges from 0 to 1, with higher values suggesting lower error. The mathematical formula for determining R^2 is as follows:

$$R^2 = \left(\frac{\sum_{i=1}^{n}(O_i - \bar{O})(P_i - \bar{P})}{\sqrt{\sum_{i=1}^{n}(O_i - \bar{O})^2}\sqrt{\sum_{i=1}^{n}(P_i - \bar{P})^2}} \right)^2 \quad (3.23)$$

where, $\bar{P}$ is the long-term simulated mean discharge. The average tendency of simulated data to be larger or smaller than their observed counterparts is measured by percent bias (PBIAS). PBIAS has an optimal value of 0, with a negative value indicating overestimation and a positive value indicating underestimate. The following is the mathematical formula for calculating PBIAS:

$$PBIAS = \frac{\sum_{i=1}^{n}(O_i - P_i)}{\sum_{i=1}^{n}(O_i)} \times 100 \quad (3.24)$$

The Standard Error of Estimate (SEE) is a measure of variation in an observation made around a calculated regression line. Simply said, it is used to verify the correctness of regression line predictions. The lower its value, the more accurate the model's prediction.

$$\text{SEE} = \sqrt{\frac{\sum(O_{v,i} - P_{v,i})^2}{n-1}} \quad (3.25)$$

where, $P_{v,i}$ is the predicted or simulated value, $O_{v,i}$ is the observed value, *n* is the number of data used for evaluation.

3.4.3 Return flood and HEC-RAS modelling

On log-probability paper, the frequencies (or probabilities) of the observed flood peaks could be calculated, plotted against the flood peaks, and a smooth curve could be fitted that covered every point. The curve could be extrapolated to get extreme values. Since observed data is typically brief, it may not accurately reflect the population, so we cannot fully rely on the curve derived from observed data. Now that the recorded data are a sample of the parent population drawn at random, a theoretical frequency distribution that fits the data may be created. Extrapolation to get the necessary probabilities can be completed with ease once the distribution has been suitably fitted to the observed data. One of the many techniques used to estimate return flood is the Gumbel method.

3.4.3.1 Gumbel method

The extreme value distribution is the foundation of the Gumbel technique of frequency analysis (Gumbel 1941), which employs frequency factors created for theoretical distribution. Gumbel's annual series of floods are a series of annual maximum series, and he defined a flood as the annual maximum daily flow. According to this method, the probability of occurrence of an event equal to or larger than a value x_0 is:

$$P(X \geq x_0) = 1 - e^{-e^{-y}} \quad (3.26)$$

Where y is a dimensionless variable given by:

$$y = \frac{1.285(x-\bar{x})}{\sigma_x} + 0.577 \quad (3.27)$$

Where $\bar{x}$ = mean and σ_x = standard deviation of the variate *X*. For a particular probability (*P*), Eq. 3.26 becomes:

$$y_P = -ln[-ln\,(1-P)] \quad (3.28)$$

The return period $T = 1/P$, Eq. 3.28 becomes:

$$y_T = -\left[ln.\,ln\frac{T}{T-1}\right] \quad (3.29)$$

Substituting Eq. 3.29 in Eq. 3.27,

$$x_T = \bar{x} + K\sigma_x \quad (3.30)$$

$$Where\ K = \frac{(y_T - 0.577)}{1.2825} = frequency\ factor \quad (3.31)$$

The above equations 3.30 and 3.31 are applicable to an infinite sample size. For practical use, Eqs. 3.30 and 3.31 become:

$$x_T = \bar{x} + K\sigma_{n-1} \quad (3.32)$$

$$K = \frac{(y_T - \overline{y_n})}{S_n} \tag{3.33}$$

Where σ_{n-1}= standard deviation of the sample size $N = \sqrt{\frac{\sum(x-\bar{x})^2}{N-1}}$. Reduce mean $\overline{y_n}$ and reduced standard deviation S_n depends on the sample size and is illustrated in Tables 3.9 and 3.10.

Table 3.9 Reduced mean $\overline{y_n}$ in Gumbel's extreme value distribution (Subramanya 2008)

N = sample size

N	0	1	2	3	4	5	6	7	8	9
10	0.4952	0.4996	0.5035	0.5070	0.5100	0.5128	0.5157	0.5181	0.5202	0.5220
20	0.5236	0.5252	0.5268	0.5283	0.5296	0.5309	0.5320	0.5332	0.5343	0.5353
30	0.5362	0.5371	0.5380	0.5388	0.5396	0.5402	0.5410	0.5418	0.5424	0.5430
40	0.5436	0.5442	0.5448	0.5453	0.5458	0.5463	0.5468	0.5473	0.5477	0.5481
50	0.5485	0.5489	0.5493	0.5497	0.5501	0.5504	0.5508	0.5511	0.5515	0.5518
60	0.5521	0.5524	0.5527	0.5530	0.5533	0.5535	0.5538	0.5540	0.5543	0.5545
70	0.5548	0.5550	0.5552	0.5555	0.5557	0.5559	0.5561	0.5563	0.5565	0.5567
80	0.5569	0.5570	0.5572	0.5574	0.5576	0.5578	0.5580	0.5581	0.5583	0.5585
90	0.5586	0.5587	0.5589	0.5591	0.5592	0.5593	0.5595	0.5596	0.5598	0.5599
100	0.5600									

Table 3.10 Reduced standard deviation S_n in Gumbel's extreme value distribution (Subramanya 2008)

N = sample size

N	0	1	2	3	4	5	6	7	8	9
10	0.9496	0.9676	0.9833	0.9971	1.0095	1.0206	1.0316	1.0411	1.0493	1.0565
20	1.0628	1.0696	1.0754	1.0811	1.0864	1.0915	1.0961	1.1004	1.1047	1.1086
30	1.1124	1.1159	1.1193	1.1226	1.1255	1.1285	1.1313	1.1339	1.1363	1.1388
40	1.1413	1.1436	1.1458	1.1480	1.1499	1.1519	1.1538	1.1557	1.1574	1.1590
50	1.1607	1.1623	1.1638	1.1658	1.1667	1.1681	1.1696	1.1708	1.1721	1.1734
60	1.1747	1.1759	1.1770	1.1782	1.1793	1.1803	1.1814	1.1824	1.1834	1.1844
70	1.1854	1.1863	1.1873	1.1881	1.1890	1.1898	1.1906	1.1915	1.1923	1.1930
80	1.1938	1.1945	1.1953	1.1959	1.1967	1.1973	1.1980	1.1987	1.1994	1.2001
90	1.2007	1.2013	1.2020	1.2026	1.2032	1.2038	1.2044	1.2049	1.2055	1.2060
100	1.2065									

3.4.3.2 HEC-RAS modelling

The U.S. Army Corps of Engineers developed the HEC-RAS (Hydrological Engineering Center River Analysis System), which enables modelling of 1-D and 2-D, steady and unsteady flow, sediment transport, and water quality. It is essentially a piece of software for hydraulic modelling. A hydraulic model is a mathematical description of a water, sewer, or storm system that is used to examine the hydraulic behavior of the system. To comprehend how a hydraulic system would behave in various scenarios at various spatial and temporal scales, hydraulic modelling is widely utilized. Compared to a laboratory experiment, it saves money and time.

The governing equation of 1-D hydraulic models are the Saint-Venant equations:

$$\frac{\partial A}{\partial t} + \frac{\partial \phi Q}{\partial x_c} + \frac{\partial (1-\phi) Q}{\partial x_f} = 0 \tag{3.34}$$

$$\frac{\partial Q}{\partial t}+\frac{\partial}{\partial x_c}\left(\frac{\partial \phi^2 Q^2}{A_c}\right)+\frac{\partial}{\partial x_f}\left(\frac{(1-\phi)^2 Q^2}{A_f}\right)+gA_c\left(\frac{\partial z}{\partial x_c}+S_c\right)+gA_f\left(\frac{\partial z}{\partial x_f}+S_f\right)=0 \quad (3.35)$$

Where A is the cross-sectional area, Q is the discharge, S is the frictional slope, z is the water depth, x is the distance along the flow, f is the fraction to determine channel versus floodplain discharge, and t is the time.

CHAPTER IV
RESULTS AND DISCUSSION

In this chapter, the results obtained from the present study are discussed. Results on preliminary analysis of climate in the study areas, watershed prioritization, hydrological modelling using SWAT and analysis of return floods were discussed in this chapter.

4.1 Preliminary Investigation of Climatic Pattern in Dudhnai and Pare Watershed

Preliminary analysis of climate extremes was carried out to determine the climate extreme indices given in Table 4.1.

Table 4.1 Summary of extreme climate indices in the study

Index	Descriptive name	Definitions	Units
SU25	Summer days	Annual count when TX (daily maximum)>25ºC	days
TR20	Tropical nights	Annual count when TN (daily minimum)>20ºC	days
TN10p	Cool nights	Annual percentage of days when TN<10th percentile	days
TX10p	Cool days	Annual percentage of days when TX<10th percentile	days
TN90p	Warm nights	Annual percentage of days when TN>90th percentile	days
TX90p	Warm days	Annual percentage of days when TX>90th percentile	days
RX1DAY	Max 1-day precipitation amount	Annual maximum consecutive 1-day precipitation	
RX5DAY	Max 5-day precipitation amount	Annual maximum consecutive 5-day precipitation	mm
RX1DAY (monsoon)	-	Maximum 1-day precipitation during monsoon months	mm
RX5DAY (monsoon)	-	Maximum consecutive 5-day precipitation during monsoon months	mm
SDII	Simple daily intensity index	Annual total precipitation divided by the number of wet days (defined as PRCP>=1.0mm) in the year	mm/day
R10	-	Annual count of days when PRCP>=10mm	Days
R20	-	Annual count of days when PRCP>=20mm	Days
R25	-	Annual count of days when PRCP>=25mm	Days
R50	-	Annual count of days when PRCP>=50mm	Days
R100	-	Annual count of days when PRCP>=1000mm	Days
MRI	Moderate rainfall Index	Annual count of days when PRCP is between 10 and 25 mm	Days
HRI	High Rainfall Index	Annual count of days when PRCP is between 25 and 75 mm	Days
R75	Very High Rainfall Index	Annual count of days when PRCP>=75mm	Days
CDD	Consecutive dry days	Maximum number of consecutive days with daily rainfall (RR) <1mm	days
CWD	Consecutive wet days	Maximum number of consecutive days with RR>=1mm	days
R95p	Very wet days	Annual total PRCP when RR>95th percentile	mm
PRCPTOT	Annual total wet-day precipitation	Annual total PRCP in wet days (RR>=1mm)	mm

4.1.1 Climate extremes in Dudhnai watershed during 1981-2013

Climate extreme analysis in Dudhnai watershed was based on administrative sub-division. The watershed has five sub-subdivisions as shown in Table 4.2. The trend analysis on the number of summer days in a year for which daily maximum temperature is greater than 20 ^{o}C (SU25) showed positive trends in all the divisions of Dudhnai (Table 4.2). Kharkutta division showed positive significant trend which increases at the rate of 0.55 days per year. On the other hand, annual counts when daily minimum temperature were greater than 20 ^{o}C (TR20), which is a criterion for tropical nights, have been found to follow a rapid increasing trend at the rate of

more than 0.7 days per year in all the divisions. This result was also in agreement with the significant cooling trends of cool nights (TN10p) and significant warming trends of warm nights (TN90p).

Table 4.2 Mann Kendall's test Z and Sen's slope Q of extreme indices (trends significant at 0.05 level are bold)

Indices	Dudhnai		Songsak		Rongjeng		Kharkutta		Mendipathar	
	Z	**Q**	**Z**	**Q**	**Z**	**Q**	**Z**	**Q**	**Z**	**Q**
SU25	1.92	0.53	1.70	0.48	1.67	0.50	**1.98**	0.55	1.84	0.55
TR20	**2.93**	0.71	**3.19**	0.82	**3.04**	0.75	**2.93**	0.69	**3.01**	0.75
TN10p	**-2.77**	-0.42	**-2.87**	-0.41	**-2.87**	-0.41	**-2.85**	-0.42	**-2.73**	-0.41
TN90p	**3.58**	0.45	**3.77**	0.43	**3.73**	0.43	**3.67**	0.43	**3.64**	0.43
TX10p	-0.33	-0.02	-0.48	-0.04	-0.48	-0.03	-0.43	-0.04	-0.53	-0.03
TX90p	**3.05**	0.34	**2.99**	0.31	**3.11**	0.32	**3.16**	0.34	**3.11**	0.33
SDII	**2.45**	0.12	**2.01**	0.13	**2.08**	0.12	**2.36**	0.12	**2.42**	0.12
R95p	**2.08**	14.58	1.52	11.93	1.74	13.68	**2.08**	14.19	**2.11**	14.50
R20	1.18	0.25	0.57	0.19	0.43	0.12	1.08	0.23	1.01	0.20
PRCPTOT	-0.14	-1.71	-0.29	-4.18	-0.39	-7.07	-0.29	-2.27	-0.11	-1.45
CWD	**-3.41**	-1.39	**-4.31**	-1.85	**-4.34**	-1.86	**-4.17**	-1.89	**-3.69**	-1.63
CDD	1.92	1.02	1.91	0.89	1.91	0.87	**2.51**	1.17	**2.12**	1.00
Rx5day	1.53	1.79	1.35	2.94	1.47	3.21	1.63	2.62	1.78	2.67

Annual percentage of cool days (TX10p) were decreasing, though not significant, whereas annual percentage of warm days were significantly increasing in the study area. Hence, there was a simultaneous warming of both days and nights which were statistically significant at 5% level. As observed from the Sen's slope values (Q) of TR20, TN90p and TX90p in Table 4.1, the warming of the area during nights occurred at a higher rate than warming during days. This study has shown that the number of cold nights and days has decreased and the number of warm nights and days has increased. Such warming trends in both days and nights would increase domestic energy consumption due to rise in energy utilization for cooling, increase water demands in agriculture due to increase in evaporation rate and also increase in the mortality rate. By averaging Sen's slope Q values over the divisions, the rate of change of SU25, TR20, TN10p, TN90p, TX10p and TX90p were 0.52 days/year, 0.74 days/year, -0.41 % days/year, 0.43 % days/year, - 0.03 % days/year and 0.33 % days/year, respectively.

There has been significant increasing trend in simple daily intensity index (SDII) in the area approximately at the rate of 0.12 mm/day per year (Table 4.2). The increasing trend may be attributed to either increase in annual total precipitation represented by PRCPTOT or number of total wet days in a year. However, the trend analysis of PRCPTOT showed the annual total precipitation in the area follows decreasing trend. Therefore, increasing trend in SDII was due to decrease in the wet days. Also, the trend analysis of consecutive wet days (CWD) and

consecutive dry days (CDD) partly supported the positive trend of SDII. Shrinkage of monsoon season i.e., late onset and early withdrawal of southwest monsoon as well as the increase in dry days could possibly the causes of falling trends of PRCPTOT. CWD in the area were significantly following negative trends while on the other hand CDD were following an increasing trend though not significant in all the divisions. The results of trend analysis of very wet days (R95p) showed positive trends also statistically significant in three divisions viz. Dudhnai, Kharkutta and Mendipathar. This indicated that although precipitation amount and number of wet days have decreased, the precipitation were becoming more and more intense. This statement was also supported by the positive trends of annual counts of days when precipitation is greater than 20 mm (R20) and annual maximum consecutive 5-days precipitation amount (Rx5day) as shown in Table 4.2. Despite insignificant trends in R20 and Rx5day, it could unarguably state that precipitation of the nature of short duration high intensity is occurring very frequently in the area. By averaging Sen's slope Q values over the divisions, the rate of change of SDII, R95p, R20, PRCPTOT, CWD, CDD and Rx5day were respectively 0.12 mm/day/year, 13.78 mm/year, 0.20 days/year, -3.34 mm/year, -1.72 days/year, 0.99 days/year and 2.65 mm/year.

The three precipitation extreme indices- CWD, CDD and Rx5day are plotted as shown in Fig. 4.1. The consecutive wet days were found to be higher (around 100 days) in the initial years but in the later end of the study period, CWD becomes lower almost below 40 days. In case of consecutive dry days, the trends were found exactly the opposite of CWD. This rapid rise and fall of CCD and CWD respectively are warning signal of future water scarcity and it could bring an alarming situation of socio-economic and hydrological condition. The maximum 5 days precipitation in the study area ranged from 150 to 500 mm for all station except Dudhnai that ranges from 115 to 425 mm. Despite being insignificant trends in maximum 5 days rainfall in all stations, the decrease in CWD and increase in CDD indicated water stress conditions i.e., drought. This is due to the fact that, the reduction in annual precipitation and number of CWD occurred along with increase in occurrence of higher intensity and lower duration precipitation.

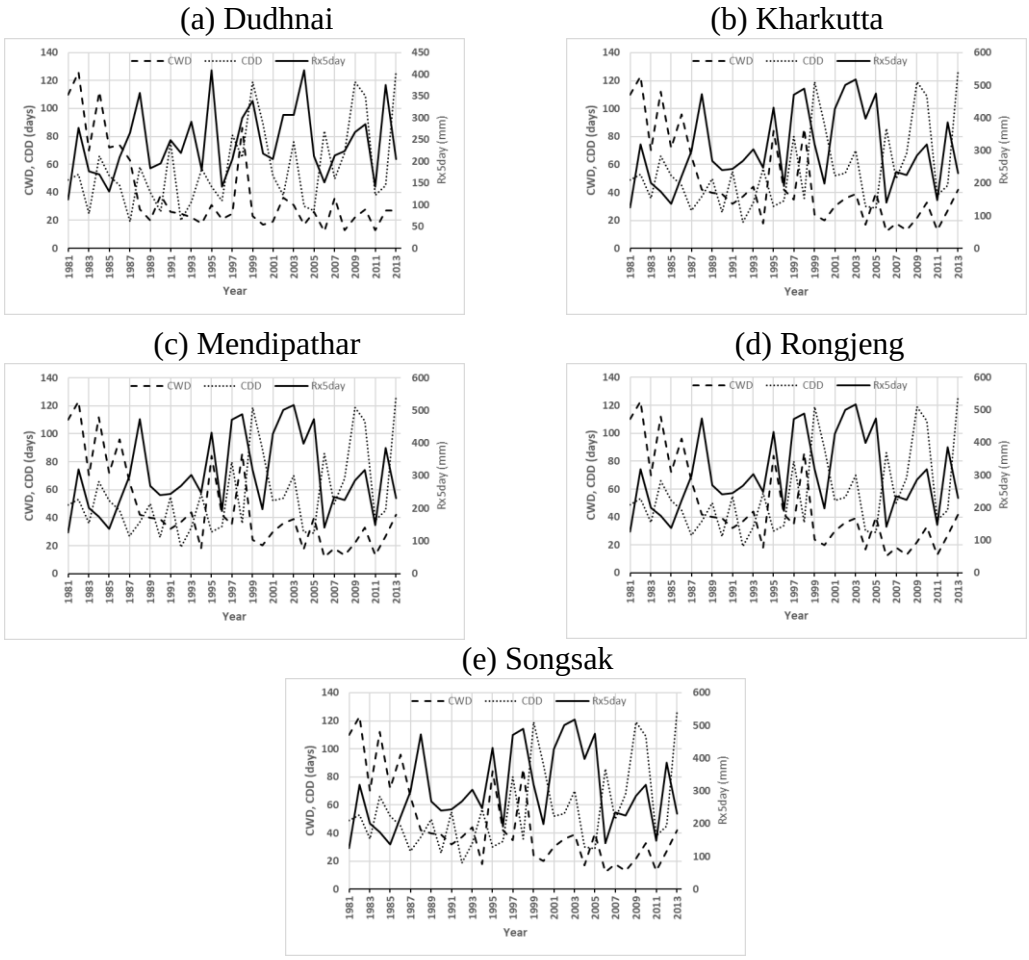

Fig. 4.1 Consecutive wet days (CWD), consecutive dry days (CDD) and maximum 5 days precipitation amount (Rx5day) for (a) Dudhnai, (b) Kharkutta, (c) Mendipathar, (d) Rongjeng and (e) Songsak divisions

4.1.2 Precipitation extremes in Pare watershed during 1981-2019

The Mann–Kendall test Z and Sen's slope Q values for different extreme precipitation indices in the Pare watershed are illustrated in Table 4.3. Majority of the precipitation extreme indices indicated falling trends, and majority were found statistically insignificant at 0.05 level. Statistically significant trends were observed in indices such as SDII, CDD, CWD and MRI. The annual total precipitation indicated by PRCPTOT has shown falling trends in every subbasin as whole as the whole watershed (Pare). Although the results were not statistically significant at 0.05 level, the annual precipitation was found decreasing at a rate of 3.3 mm per year in the Pare watershed. The trend of SDII at each sub-watershed was found rising indicating rainfall intensities in the area. Also, the trend of SDII in Pare watershed was found significantly increased during the period of 1981–2019. The trend of consecutive dry days (CDD), though

found increasing in all the sub-watersheds, was statistically significant in SW7 at the rate of 0.3 days per year. On the contrary, consecutive wet days (CWD) exhibited significant decreasing trends in all sub-watersheds except in SW5, SW9 and SW12.

Table 4.3 Trend direction and magnitudes for various precipitation extremes during 1981- 2019 in Pare watershed

Indices	SW1	SW2	SW3	SW4	SW5	SW6	SW7	SW8	SW9	SW10	SW11	SW12	SW13	Pare
RX1DAY														
Z	−0.6	−0.5	−0.5	0.0	−0.9	−0.6	−0.3	−0.7	−0.7	0.0	−0.7	−0.6	−0.5	0.8
Q	−0.2	−0.2	−0.2	0.0	−0.5	−0.2	−0.2	−0.2	−0.2	0.0	−0.3	−0.2	−0.2	0.3
RX5DAY														
Z	−1.2	−0.8	−1.1	−0.9	−1.3	−1.2	−1.0	−0.9	−1.0	−0.9	−1.1	−1.2	−0.9	0.1
Q	−1.2	−1.0	−1.0	−0.7	−1.4	−1.2	−0.8	−1.0	−0.9	−0.6	−1.1	−1.2	−0.8	0.2
SDII														
Z	1.2	1.4	1.0	1.5	1.0	1.1	1.4	1.1	1.4	1.2	1.1	1.0	1.2	**2.4**
Q	0.0	0.1	0.0	0.0	0.0	0.0	0.0	0.1	0.1	0.0	0.0	0.0	0.1	0.1
R10														
Z	−1.5	−0.8	−1.5	−1.8	−1.2	−1.5	−1.7	−0.3	−0.8	−1.7	−1.3	−1.5	−0.8	−1.6
Q	−0.2	−0.2	−0.3	−0.3	−0.2	−0.2	−0.2	−0.1	−0.2	−0.3	−0.2	−0.3	−0.2	−0.3
R25														
Z	0.4	0.5	0.3	0.1	0.5	0.5	−0.7	0.3	0.4	0.0	0.3	0.2	0.3	0.7
Q	0.1	0.1	0.0	0.0	0.1	0.1	−0.1	0.1	0.1	0.0	0.0	0.0	0.0	0.1
CDD														
Z	1.2	1.3	1.4	1.8	0.6	1.2	**2.1**	0.8	1.8	1.4	1.1	1.1	1.2	1.5
Q	0.2	0.1	0.2	0.3	0.1	0.2	0.3	0.1	0.2	0.2	0.2	0.2	0.1	0.2
CWD														
Z	***−3.5***	***−2.6***	***−3.1***	***−3.8***	−1.5	***−2.8***	***−2.4***	***−2.1***	−1.8	***−3.4***	***−2.1***	−1.9	***−2.1***	***−3.8***
Q	−0.5	−0.4	−0.5	−0.7	−0.2	−0.4	−0.3	−0.2	−0.3	−0.6	−0.3	−0.3	−0.3	−0.7
PRCPTOT														
Z	−0.9	−0.3	−1.0	−1.2	−0.8	−0.9	−1.1	−0.1	−0.6	−1.3	−0.7	−0.8	−0.3	−0.3
Q	−7.9	−1.9	−9.5	−8.4	−5.9	−7.5	−7.5	−1.4	−3.0	−7.6	−5.7	−6.0	−2.5	−3.3
RX1DAY (monsoon)														
Z	0.0	0.0	−0.1	0.3	0.1	0.2	−0.3	0.2	0.0	0.3	0.0	0.1	0.3	1.0
Q	0.0	0.0	0.0	0.1	0.1	0.1	−0.2	0.1	0.0	0.1	0.0	0.0	0.1	0.4
RX5DAY (monsoon)														
Z	−0.9	−0.5	−0.9	−0.7	−0.9	−0.9	−1.1	−0.5	−0.4	−0.7	−0.8	−1.0	−0.4	0.2
Q	−0.7	−0.5	−0.7	−0.5	−1.0	−0.7	−0.9	−0.4	−0.4	−0.5	−0.7	−0.8	−0.4	0.2
MRI														
Z	***−3.1***	***−2.8***	***−3.1***	***−3.4***	***−2.4***	***−3.2***	−1.8	−0.8	***−2.3***	***−2.9***	***−2.6***	***−2.6***	***−2.2***	***−3.7***
Q	−0.3	−0.2	−0.3	−0.3	−0.2	−0.3	−0.2	−0.1	−0.2	−0.2	−0.3	−0.3	−0.2	−0.4
HRI														
Z	0.6	0.5	0.5	0.2	0.7	0.6	−0.8	0.7	0.5	0.1	0.4	0.5	0.5	0.4
Q	0.1	0.1	0.1	0.0	0.1	0.1	−0.1	0.1	0.1	0.0	0.1	0.1	0.1	0.1
R75														
Z	−0.5	−0.1	0.1	−0.1	−1.0	−0.7	0.0	−0.6	0.0	0.4	−0.6	−0.4	−0.3	1.6
Q	0.0	0.0	0.0	0.0	0.0	0.0	0.0	0.0	0.0	0.0	0.0	0.0	0.0	0.0
R50														
Z	−1.4	0.4	−0.9	0.0	−1.3	−0.9	−0.7	0.2	0.4	−0.4	−0.4	−0.8	0.4	0.0
Q	−0.1	0.0	0.0	0.0	−0.1	0.0	0.0	0.0	0.0	0.0	0.0	0.0	0.0	0.0
R100														
Z	−0.4	−0.6	0.0	0.4	−0.7	−0.6	−0.8	−0.5	−0.7	0.0	−0.8	−0.6	−0.6	−0.4
Q	0.0	0.0	0.0	0.0	0.0	0.0	0.0	0.0	0.0	0.0	0.0	0.0	0.0	0.0

Singnificant negative trends at 0.05 level are bold-italic while significant positive trends at 0.05 level are bold

Precipitation extremes such as RX1DAY, RX5DAY, R10 and RX5DAY (monsoon) were found decreasing though statistically insignificant at 0.05 level. The moderate rainfall index (MRI) was found to be decreasing significantly at all the sub-watersheds except SW7 and SW8. However, high rainfall index (HRI), though statistically insignificant at 0.05 level, was found to be increasing at all sub-watersheds except SW7. On the other hand, trends in very high rainfall index (R75) indicated decreasing trends for majority of the sub-watersheds. The overall trends of Pare watershed indicated statistically significant increasing trends for the index SDII and negative trends for the indices CWD and MRI. It was observed that there have been rapid decreasing trends in the total annual precipitation (PRCPTOT) in all the sub-watersheds. This is an indication of diminishing water resource potential in the region. This particular finding was in agreement with the village survey conducted in 2016 regarding the hydrometeorological conditions and agricultural activities in the study area. During the survey, the participants were asked about the water flow regime of the Pare River. Most of the participants claimed diminishment of water level depths at various sections of the Pare River. The reason behind may be due to decrease in rainfall in the study area since there are no structures such as reservoirs, dams, etc. which could regulate the flow. Further, the statistically significant decreasing trends in the consecutive wet days (CWD) and increasing trends in the consecutive dry days (CDD) also suggested and support the diminishing water resource potential in the study area. Our findings also agree with the results of the studies conducted by Rupakumar et al. (1992), Bhagawati et al. (2016), Patle et al. (2016) and Bhagawati et al. (2017) over the regions in which this study area is situated. Their findings illustrated decrease in annual total precipitation as well as monsoonal precipitation approximately during the same historical period in this study.

The results suggested that the precipitation regime in the study area had been accompanied by overall reduction in precipitation amount, milder rainfall events, reduction in monsoon (June–September) rainfall and drier climatic conditions. The results suggest that precipitation events are becoming milder in the region and the decreasing magnitude values of trends in precipitation total in almost all the sub-watersheds suggest harmful consequences associated with the shortage of water in the years to come. Despite the results above, almost future projections of precipitation showed increase in rainfall amount with higher intensity rainfall.

4.2 Morphometric Analysis and Watershed Prioritization in Dudhnai and Pare Watersheds

4.2.1 Morphometric analysis and watershed prioritization in Dudhnai watershed

The results of the execution of morphometric tool in Dudhnai watershed and its seven sub-watersheds are illustrated in Table 4.4. It showed that Dudhnai River is a 6^{th} order river formed by 2122, 505, 107, 26 and 7 numbers of 1st, 2nd, 3rd, 4th and 5th order streams, respectively. The total length of the streams in the watershed is 1327.6 km with average bifurcation ratio of 4.75. Kale and Gupta (2001) mentioned that bifurcation ratio ranging between 3 and 5 indicate natural drainage system within a homogenous rock. Higher bifurcation ratio indicates well-dissected drainage basins (Horton 1945) leading to less chances of flood and erosion risk (Eze and Efong 2010). The form factor of the watershed was found as 0.28 indicating elongated watershed. Higher values signify circular watershed with a value of 0.754 for perfectly circular watershed (Pareta and Pareta 2011). Similarly, elongation ratio of 0.59 also proved the elongated nature of the watershed. According to Pareta ana Pareta (2011), based on elongation ratio, a watershed could be classified as circular (0.9–0.1), oval (0.8–0.9), less elongated (0.7–0.8), elongated (0.5–0.7), and more elongated (< 0.5). The stages of a watershed can be indicated by circularity ratio with low, medium and high values representing youth, mature and old stages of the watershed. The circularity ratio for Dudhnai watershed is 0.21 indicating elongated and youth stage. The compactness coefficient of the Dudhnai watershed is 2.19 which is a parameter, dependent only on the slope and independent of the size of watershed. Drainage texture can be classified into five different textures i.e., very coarse (8) as given in Pareta and Pareta (2011). For the Dudhnai watershed, this value is 16.4 which can be categorized as very fine drainage texture. Stream frequency are categorized into five different classes viz., low (20). The stream frequency in Dudhnai watershed is 5.76 no. of streams/km2 indicating moderate nature. In general, high drainage density reflects rapid hydrological response to the rainfall events while low drainage density means slow hydrological response. The drainage density of the Dudhnai watershed is 2.76 km/km^2. According to Schumm (1956), landforms are classified based on constant of channel maintenance as more erodible (0.5).

Table 4.4 Analysis results of the morphometric parameters of Dudhnai watershed and its seven sub-watersheds

Morphometric parameters		Dudhnai	Rongma	Rongitt	Manda	Chil	Sarangma	Chitukona	Chilapara
Number of streams	1st order	2122	302	162	450	376	158	193	96
	2nd order	505	66	39	109	93	32	41	29
	3rd order	107	11	7	22	24	9	9	5
	4th order	26	3	2	6	7	2	2	2
	5th order	7	1	1	1	1	1	1	1
	6th order	1	-	-	-	-	-	-	-
	Total	2768	383	211	588	501	202	246	133
Length of streams	1st order	670.7	90.9	54.3	142.1	121.0	48.9	58.7	31.2
	2nd order	309.6	39.6	29.1	64.2	55.0	21.9	31.4	11.4
	3rd order	161.5	21.5	11.6	43.6	23.4	8.0	20.1	7.5
	4th order	89.0	12.0	5.9	13.2	21.4	16.3	13.8	4.1
	5th order	61.5	8.8	6.5	21.9	13.7	3.8	1.4	4.7
	6th order	35.3	-	-	-	-	-	-	-
	Total	1327.6	172.7	107.5	285	234.6	98.9	125.4	58.9
Bifurcation ratio	1:2	4.20	4.58	4.15	4.13	4.04	4.94	4.71	3.31
	2:3	4.72	6.00	5.57	4.95	3.88	3.56	4.56	5.80
	3:4	4.12	3.67	3.50	3.67	3.43	4.50	4.50	2.50
	4:5	3.71	3.00	2.00	6.00	7.00	2.00	2.00	2.00
	5:6	7.00	-	-	-	-	-	-	-
	Average	4.75	4.31	3.81	4.69	4.57	3.75	3.94	3.40
Basin area (km^2)		480.4	60.56	38.9	101.89	84.77	38.35	46.57	20.14
Basin surface area (km^2)		500.18	104.98	58.39	161.02	144.18	63.63	63.77	32.41
Basin perimeter (km)		168.79	42.29	38.36	79.5	52.91	43.17	48.02	29.89
Basin Length (km)		41.71	8.77	11.01	22.25	11.24	11.61	12.75	9.82
Main channel length (km)		54.66	18.9	16.54	29.8	16.00	16.98	14.25	11.09
Fitness ratio		0.32	0.45	0.43	0.37	0.30	0.39	0.30	0.37
Form factor		0.28	0.79	0.32	0.21	0.67	0.28	0.29	0.21
Shape factor ratio		3.62	1.27	3.11	4.86	1.49	3.52	3.50	4.79
Relative perimeter		2.85	1.43	1.01	1.28	1.60	0.89	0.97	0.67
Length area relation		56.9	16.42	12.59	22.44	20.09	12.48	14.03	8.48
Rotundity coefficient		2.85	0.99	2.45	3.82	1.17	2.76	2.74	3.76
Mean basin width		11.52	6.91	3.53	4.58	7.54	3.30	3.65	2.05
Drainage texture		16.4	9.06	5.5	7.39	9.47	4.68	5.12	4.45
Compactness coefficient		2.19	1.54	1.75	2.24	1.63	1.98	2.00	1.89
Circulatory ratio		0.21	0.43	0.33	0.20	0.38	0.26	0.25	0.28
Elongation ratio		0.59	1.001	0.64	0.51	0.92	0.60	0.60	0.51
Drainage density (km/km^2)		2.76	2.85	2.76	2.8	2.77	2.58	2.69	2.92
Stream frequency (number/km^2)		5.76	6.32	5.42	5.77	5.91	5.27	5.28	6.60
Constant of channel maintenance (km^2/km)		0.36	0.35	0.36	0.36	0.36	0.39	0.37	0.34
Infiltration number		15.92	18.04	14.99	16.14	16.36	13.59	14.23	19.29
Drainage intensity		2.08	2.22	1.96	2.06	2.14	2.04	1.96	2.26
Average length of overland flow (km)		0.18	0.18	0.18	0.18	0.18	0.19	0.19	0.17
Height of basin outlet (m)		47	286	286	86	75	61	51	48
Maximum height of basin (m)		688	688	659	604	720	643	592	605
Total basin relief (m)		641	502	373	518	645	582	541	557
Relief ratio		0.0154	0.0573	0.0339	0.0233	0.0574	0.0501	0.0424	0.0567
Relative relief ratio		0.38	1.19	0.97	0.65	1.22	1.35	1.13	1.86
Gradient ratio		0.0154	0.0573	0.0339	0.0233	0.0574	0.0501	0.0424	0.0567
Ruggedness number		1.77	1.43	1.03	1.45	1.79	1.50	1.46	1.63
Melton Ruggedness number		29.25	64.5	59.8	51.32	70.06	93.99	79.27	124.11
Modified Melton Ruggedness number		28.66	48.99	48.81	40.82	53.72	72.96	67.75	97.84
Terrain undulation index		1.04	1.73	1.50	1.58	1.7	1.66	1.37	1.61

Channel maintenance constant of Dudhnai watershed is 0.36 km^2/km indicating moderately low erodibility nature of the watershed. Drainage intensity of a watershed is indicative of the effectivity of both drainage density and stream frequency together on the surface denudation. The drainage intensity in the Dudhnai watershed is moderate having a value of 2.08. High infiltration number of 15.92 found for Dudhnai watershed is an indicative of low infiltration and high runoff. According to Horton (1945), lower values of the length of overland flow (<0.4) are indicative of strong channel erosion while higher values indicate stronger sheet erosion. Dudhnai has 0.18 km average length of overland flow signifying pronounced channel erosion in the whole watershed. Relief ratio measures the overall steepness of a watershed and can be used to represent intensity of erosion process (Schumm 1956). In the Dudhnai watershed, the value of relief ratio is 0.0154. The watershed has a high ruggedness number of 1.77 indicating high risk of soil erosion.

All the seven sub-watersheds of Dudhnai are 5th order streams. In terms of area, Manda sub-watershed is the largest while Chilapara sub-watershed is the smallest. Morphometric parameters such as bifurcation ratio, length of overland flow, drainage density, drainage texture and stream frequency have direct effects on soil erosion while other parameters such as form factor, elongation ratio, circularity ratio and compactness coefficient have inverse effects on soil erosion. This can be understood as, in those parameters which have direct relationship with soil erosion, higher rank (lower values) should be assigned for higher values of the morphometric parameters. The derivative parameters of relief ratio and ruggedness number also have a direct relationship with soil erosion. As a result of such interpretation, the seven tributaries sub-watersheds of Dudhnai watershed are prioritized as shown in Table 4.5.

Table 4.5 Sub-watershed ranks based on the morphometric parameters w.r.t. soil erosion in Dudhnai watershed

Sub-watershed	R_{b_m}	L_g	D_d	D_t	F	F_f	R_e	R_c	C_c	Rhl	R_n	**Compound rank**	**Priority**
Weightage	0.30		0.40							0.30			
Rongma	3	6	2	2	2	7	7	7	1	2	6	4.15	**6**
Rongitt	5	3	5	4	5	5	5	5	3	6	7	4.98	**7**
Manda	1	5	3	3	4	1	1	1	7	7	5	3.84	**2**
Chil	2	4	4	1	3	6	6	6	2	1	1	2.80	**1**
Sarangma	6	1	7	6	7	3	3	3	5	4	3	4.04	**3**
Chitukona	4	2	6	5	6	4	4	2	6	5	4	4.14	**5**
Chilapara	7	7	1	7	1	2	2	4	4	3	2	4.05	**4**

The sub-watershed Manda has been assigned the rank 1, meaning this sub-watershed has the highest probability of soil erosion with respect to bifurcation ratio. Similar interpretation can be made from Table 4.5. Based on the compound rank obtained, the priority rank of the sub-

watersheds has been assigned in the order as Chil, Manda, Sarangma, Chilapara, Chitukona, Rongma and Rongitt. This result of the study indicated that the sub-watershed Chil, the second largest sub-watershed, is the most vulnerable watershed to soil erosion and therefore, it should be taken as the first priority for carrying out conservation and mitigation intervention while Rongitt could be given the least priority.

Watersheds are used for different purposes such as cultivation, infrastructural development, recreational activities, forestry etc. Therefore, it is important to know the purpose of the watershed in its prioritization. Also, soil characteristics such as texture, soil depth etc. are important parameters which knowledge could aid in watershed prioritization. In the present study, only morphometric parameters resulted from combine dataset of DEM and toposheets were considered for watershed prioritization. However, it can be further improved through incorporation of information regarding land use land cover and soil characteristics.

4.2.2 Morphometric analysis and watershed prioritization in Pare watershed

The results of the morphometric analysis of Pare watershed and its sub-watersheds are presented in Table 4.6 and Table 4.7. In the Table 4.6, the length and number of streams of various order and their totals are shown while Table 4.7 presented the various morphometric parameters. The drainage network delineation of Pare watershed with a stream threshold value of 50 cells results in 7^{th} order stream network as shown in Fig. 4.2. Also, we divided the whole watershed into 26 sub-watersheds (Fig. 4.2) to cover the major tributaries as well as looking at the importance of sub-watersheds to the inhabitants.

The geological and tectonic characteristics of a watershed are reflected in bifurcation ratio of the watershed. A bifurcation ratio between 3 and 5 indicates a watershed of natural drainage system within a homogenous rock. Watershed having high bifurcation ratio have less chance of being flooded and eroded as higher bifurcation ratio indicates well-dissected drainage basins. The mean bifurcation ratio of Pare watershed was found as 4.29 (Table 4.7) indicating well dissected drainage basin. A perfectly circular watershed will have a form factor value of 0.785 and any deviation from it indicates elongated watershed. The form factor of Pare watershed was found as 0.24 (Table 4.7) indicating highly elongated watershed. The drainage texture of Pare watershed was found as 38.31 (number/km) indicating very fine texture. The high value of drainage texture indicates that the basin is crowded with numerous stream segments with higher degree of slopes. As presented in Table 4.7, the compactness coefficient of Pare

watershed is 1.64 indicating compact watershed. For a perfectly circular watershed, the compactness coefficient is 1, and is the most hazardous condition, since it will yield the shortest time of peak flow in the watershed. Circularity ratio is one of the morphometric parameters which reflects the nature of elongation and stages of watershed development. Circulatory ratio with low, medium and high values are indicative of youth, mature and old stages of the watershed development respectively. In the present study, the circulatory ratio of Pare watershed was found as 0.38 indicating elongated watershed and in youth stage. The elongation ratio of Pare watershed was found as 0.56 indicating elongated watershed. An elongation value of close to unity indicates circular watershed. Drainage density is one of the most important morphometric parameters in a watershed since it provides a rough idea of how the fate of precipitation will turn once it reaches the ground. Higher the drainage density lesser will be the time of peak runoff, also indicating quicker transportation of sediment load given the condition that soils are being eroded. The drainage density in Pare watershed was found as 3.18 km/km^2 and the values ranges from 0.31 to 3.64 km/km^2 in the sub-watersheds. Stream frequency of a watershed is directly proportionate to the number of streams indicating close correlation with drainage density. The stream frequency in Pare was found as 7.95 per square kilometer of area and it ranges from 1.2 to 14.05 per square kilometer area across the sub-watersheds. According to Horton (1945), a watershed has a pronounced channel erosion if the average length of overland flow is less than 0.4, otherwise, sheet erosion is prominent in the watershed. As per the result as presented in Table 4.7, Pare watershed has a characteristics of strong channel erosion as indicated by a value of Lg = 0.16 km. The relief ratio in Pare watershed was found as 0.05. The ruggedness number is a combined index of drainage density and total basin relief with higher value indicating higher risk of soil erosion. As per the results of morphometric analysis in Pare watershed, a very high value of ruggedness number was obtained for the watershed indicating very high risk of soil erosion occurring on the steep watershed slopes.

Table 4.6 Stream order, number of streams and their lengths in Pare and its sub-watersheds

Name	Number of Streams								Length of Streams							
	N1	*N2*	*N3*	*N4*	*N5*	*N6*	*N7*	*Nu*	*L1*	*L2*	*L3*	*L4*	*L5*	*L6*	*L7*	*Lu*
SW1	354	82	18	2	1	-	-	457	103.42	40.98	25.00	9.60	7.32	-	-	186.32
SW2	311	74	16	4	1	-	-	406	86.37	42.82	21.35	5.48	11.41	-	-	167.42
SW3	173	44	7	2	1	-	-	227	52.34	25.31	6.04	8.89	1.55	-	-	94.14
SW4	26	14	-	-	2	13	-	55	8.74	2.52	-	-	0.89	2.69	-	14.84
SW5	197	45	11	2	1	-	-	256	51.44	24.23	13.30	6.09	5.28	-	-	100.33
SW6	148	34	7	2	1	-	-	192	45.79	15.71	9.28	2.44	3.68	-	-	76.90
SW7	192	86	29	25	-	-	44	376	51.38	22.64	7.38	6.25	-	-	8.07	95.72
SW8	173	47	10	3	1	-	-	234	56.05	20.02	9.06	6.39	3.89	-	-	95.40
SW9	108	29	7	1	-	-	-	145	31.56	16.70	7.16	6.02	-	-	-	61.44
SW10	107	42	19	21	-	25	-	214	28.05	10.01	4.51	4.35	-	4.84	-	51.75
SW11	213	51	8	2	1	-	-	275	54.96	23.68	18.10	7.21	1.34	-	-	108.28
SW12	101	23	5	2	1	-	-	132	30.50	16.48	10.09	3.48	1.29	-	-	61.85
SW13	81	33	17	4	-	28	-	163	22.30	10.47	5.14	1.29	-	5.00	-	44.20
SW14	132	27	4	1	-	-	-	164	35.34	12.63	5.07	8.19	-	-	-	61.23
SW15	51	21	19	-	-	2	9	102	14.46	3.91	5.28	-	-	0.56	1.83	26.04
SW16	95	36	24	2	2	26	-	185	23.61	6.41	7.43	0.41	0.93	6.06	-	44.85
SW17	110	28	6	1	-	-	-	145	34.33	11.14	6.09	6.47	-	-	-	58.03
SW18	77	33	19	5	1	18	-	153	21.80	9.36	5.33	1.59	0.04	4.55	-	42.66
SW19	84	45	9	7	1	22	-	168	21.45	13.85	1.98	2.79	0.66	5.16	-	45.87
SW20	60	17	18	5	1	19	-	120	17.27	3.62	3.57	1.33	0.35	4.11	-	30.25
SW21	373	87	20	4	1	-	-	485	103.05	46.17	28.15	9.17	9.26	-	-	195.80
SW22	187	85	43	14	1	37	-	367	48.87	33.47	15.90	3.61	0.59	6.66	-	109.10
SW23	299	69	18	4	1	-	-	391	87.36	41.10	18.09	9.62	8.86	-	-	165.04
SW24	95	40	27	10	1	18	-	191	30.12	10.67	6.33	1.55	0.43	4.28	-	53.38
SW25	747	314	195	92	1	111	-	1460	186.26	77.31	46.60	20.10	0.29	20.14	-	350.70
SW26	217	49	9	3	1	-	-	279	61.49	27.43	12.35	10.83	5.03	-	-	117.12
Pare	4718	1113	233	49	11	2	1	6127	1308.96	568.77	298.55	142.26	58.92	61.59	9.17	2448.22

Table 4.7 Morphometric parameters of Pare and its sub-watersheds

Name	Rb_m	F_f	D_t	C_c	R_c	R_e	D_d	F	L_g	Rhl	R_n
SW1	4.97	0.50	9.28	1.86	0.29	0.79	3.29	8.07	0.15	0.15	5.24
SW2	4.21	0.33	7.88	2.05	0.24	0.64	3.28	7.95	0.15	0.11	4.42
SW3	3.93	0.48	7.24	1.67	0.36	0.78	3.31	7.97	0.15	0.16	4.18
SW4	3.00	0.47	4.42	1.74	0.33	0.77	3.64	13.47	0.14	0.24	2.56
SW5	3.99	0.25	6.18	2.04	0.24	0.56	3.00	7.67	0.17	0.13	4.43
SW6	3.68	0.57	6.93	1.60	0.40	0.85	3.17	7.93	0.16	0.21	4.38
SW7	1.73	5.67	9.32	0.64	2.41	2.69	0.31	1.20	1.63	0.23	0.53
SW8	3.68	0.43	7.10	1.75	0.33	0.74	3.34	8.20	0.15	0.16	4.31
SW9	4.96	0.32	5.56	1.72	0.34	0.64	3.30	7.79	0.15	0.18	4.45
SW10	1.63	0.45	8.28	1.85	0.29	0.76	3.32	13.71	0.15	0.17	3.25
SW11	4.14	0.49	8.26	1.66	0.37	0.79	3.25	8.49	0.15	0.17	4.44
SW12	3.37	0.49	5.35	1.65	0.37	0.79	3.44	7.33	0.15	0.19	4.01
SW13	2.20	0.46	7.62	1.73	0.33	0.77	3.63	13.38	0.14	0.19	3.50
SW14	5.21	0.29	5.61	1.93	0.27	0.61	3.31	8.87	0.15	0.23	6.01
SW15	3.31	0.38	4.85	2.13	0.22	0.70	3.35	13.11	0.15	0.28	4.30
SW16	3.44	0.27	7.16	1.91	0.27	0.58	3.07	12.67	0.16	0.18	4.13
SW17	4.87	0.26	4.88	2.00	0.25	0.58	3.25	8.11	0.15	0.15	4.04
SW18	2.59	0.85	6.61	1.83	0.30	1.04	3.35	12.02	0.15	0.28	3.68
SW19	3.04	0.79	8.30	1.52	0.43	1.00	3.24	11.88	0.15	0.25	3.40
SW20	2.63	0.39	5.75	2.01	0.25	0.70	3.54	14.05	0.14	0.24	3.95
SW21	4.41	0.38	9.14	1.88	0.29	0.70	3.05	7.55	0.16	0.12	4.63
SW22	4.26	0.58	10.55	1.66	0.36	0.86	3.13	10.54	0.16	0.17	4.18
SW23	4.17	0.32	8.81	1.77	0.32	0.64	3.27	7.75	0.15	0.13	5.49
SW24	3.32	0.56	7.04	1.88	0.28	0.85	3.23	11.55	0.15	0.15	2.62
SW25	19.62	0.31	18.25	2.11	0.22	0.63	3.07	12.76	0.16	0.10	5.68
SW26	3.97	0.41	6.60	1.98	0.26	0.72	3.19	7.61	0.16	0.13	4.01
Pare	4.29	0.24	38.31	1.64	0.38	0.56	3.18	7.95	0.16	0.05	8.46

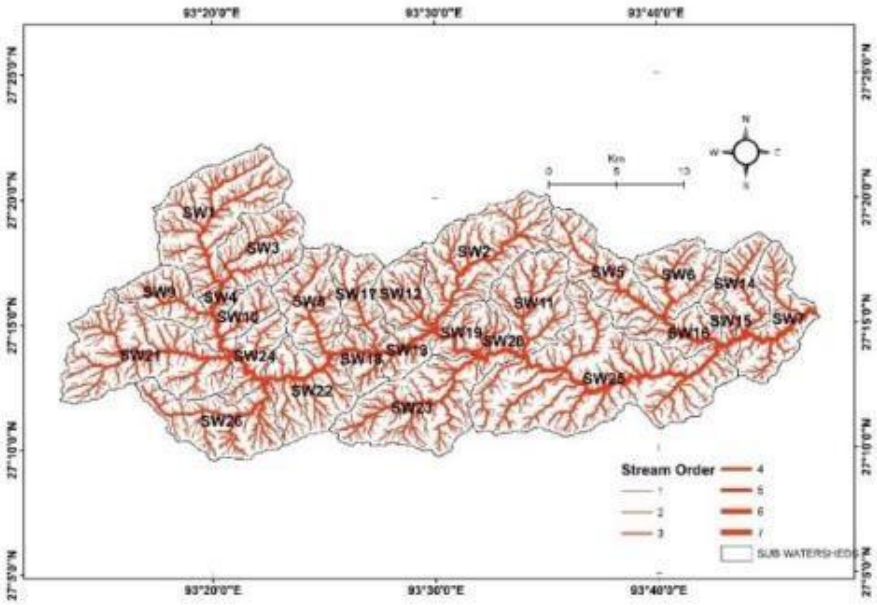

Fig. 4.2 Sub-watersheds and stream order of Pare watershed

Eleven morphometric were considered while prioritizing sub-watersheds. The definitions of all the parameters are correlated with various hydrological aspects such as topography, potentiality of runoff volume generation and time of peak attainment in order to develop relationships regarding whether higher or lower values of these morphometric parameters will cause higher or lower soil erosion. The results of the prioritization of sub-watersheds in Pare are illustrated in Table 4.8 and the final priority map is shown in Fig. 4.3. Linear morphometric parameters such as bifurcation ratio, drainage texture, drainage density, stream frequency and length of overland flow have direct relationship with soil erodibility while shape morphometric parameters such as form factor, compactness coefficient, circulatory ratio and elongation ratio are inversely proportional to soil erodibility. The two relief morphometric parameters i.e., relief ratio and ruggedness number, considered in the study are directly proportional to soil erodibility. The maximum value in linear and relief parameters among the sub-watersheds has been assigned as rank 1 and the least value as rank 26. On the opposite, the maximum value in shape parameters among the sub- watersheds has been assigned as rank 26 and the least as rank 1. Compound scores are determined by averaging all over the linear, shape and relief parameters for each sub-watershed, as illustrated in Table 4.8. The maximum and minimum compound prioritized score of the sub-watersheds are 7 (SW25) and 19.73 (SW7) respectively indicating SW25 has the priority rank of 1 while SW7 has the lowest priority rank of 26. This can be interpreted in a way that SW25 has been found to be the most vulnerable to soil erosion requiring highest priority for carrying out soil, land and water conservation measures while such mitigation and intervention measures could be taken up at last for SW7. As mentioned in Chandniha and Kansal (2014), morphometric study is one of the most appropriate techniques to address issues related to water distribution and erosion problems over the watershed, we suggest various decision makers and stakeholders to get interest in this paper in order to manage various sub-watersheds in the Pare catchment.

Table 4.8 Priority ranks of sub-watersheds in Pare watershed in relation to soil erosion problems

Name	Rb_m	F_f	D_t	C_c	R_c	R_e	D_d	F	L_g	Rhl	R_n	Compound Score	Final Priority
SW1	3	20	4	12	12	18	12	16	19	19	4	12.64	11
SW2	8	8	10	3	3	8	13	18	14	25	9	10.82	5
SW3	13	17	12	20	21	17	10	17	16	16	14	15.73	20
SW4	21	16	26	17	17	16	1	3	26	4	25	15.64	19
SW5	11	1	19	4	4	1	25	22	2	23	8	10.91	6
SW6	15	22	16	24	24	22	20	19	7	8	10	17.00	24
SW7	25	26	3	26	26	26	26	26	1	6	26	19.73	26
SW8	14	13	14	16	16	13	7	14	20	17	11	14.09	14
SW9	4	6	22	19	19	6	11	20	15	12	6	12.73	12
SW10	26	14	8	13	13	14	8	2	18	15	23	14.00	13
SW11	10	18	9	22	22	19	15	13	12	14	7	14.64	17
SW12	17	19	23	23	23	20	4	25	23	9	17	18.45	25
SW13	24	15	11	18	18	15	2	4	25	10	21	14.82	18
SW14	2	4	21	8	8	4	9	12	17	7	1	8.45	2
SW15	19	10	25	1	1	10	6	5	21	1	12	10.09	3
SW16	16	3	13	9	9	3	22	7	5	11	15	10.27	4
SW17	5	2	24	6	6	2	16	15	11	18	16	11.00	7
SW18	23	25	17	14	14	25	5	8	22	2	20	15.91	21
SW19	20	24	7	25	25	24	17	9	10	3	22	16.91	23
SW20	22	11	20	5	5	11	3	1	24	5	19	11.45	8
SW21	6	9	5	11	11	9	24	24	3	24	5	11.91	9
SW22	7	23	2	21	20	23	21	11	6	13	13	14.55	16
SW23	9	7	6	15	15	7	14	21	13	21	3	11.91	9
SW24	18	21	15	10	10	21	18	10	9	20	24	16.00	22
SW25	1	5	1	2	2	5	23	6	4	26	2	7.00	1
SW26	12	12	18	7	7	12	19	23	8	22	18	14.36	15

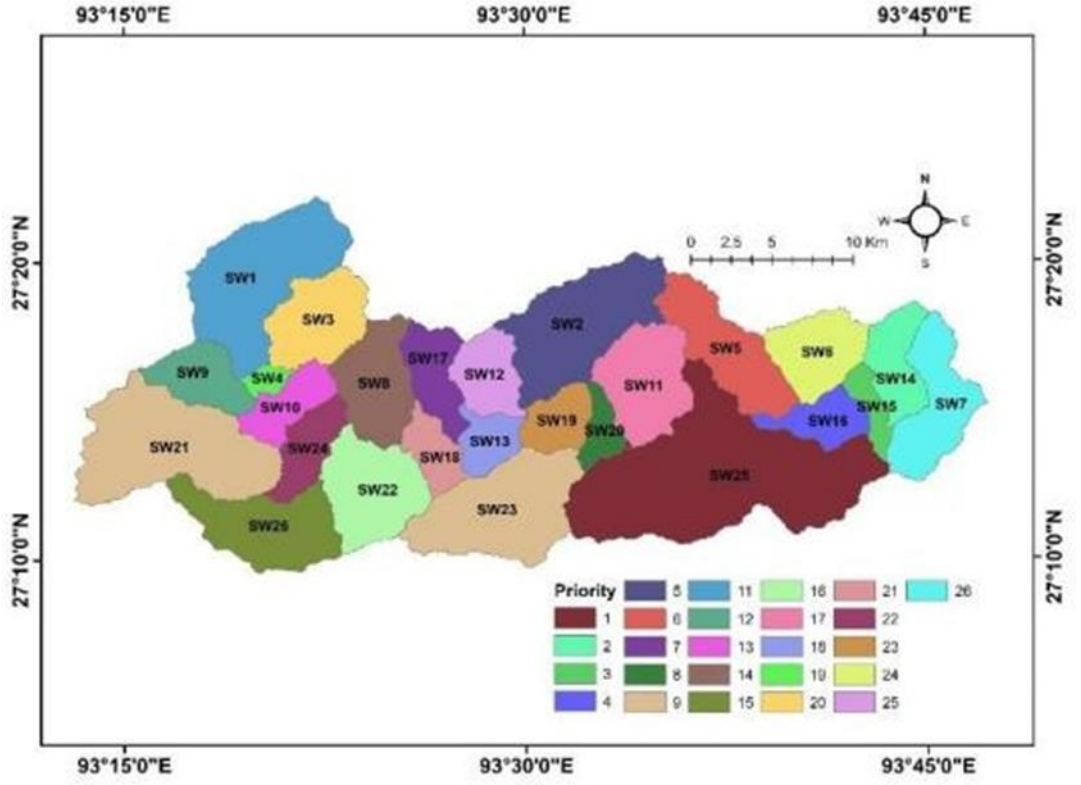

Fig. 4.3 Priority map of sub-watersheds in Pare watershed

4.3 Hydrological Modelling of SWAT Model in Pare Watershed

4.3.1 Precipitation regime during calibration and validation periods in Pare

To understand the seasonal pattern of rainfall in the Pare watershed, monthly average rainfall is plotted, as shown in Fig. 4.4. The plot revealed that the majority of the rainfall in a year in

the watershed occurred during monsoon season. However, abundant amount of rainfall also occurred during pre-monsoon season, especially during the month of May. Rainfall in the pre-monsoon (from March to May) was higher than the rainfall in post-monsoon (October to November). The rainfall share of each season in the watershed in a year were 4.1 percent (winter), 26.4 percent (pre-monsoon), 63 percent (monsoon), and 6.5 percent (post-monsoon). This shows that almost 90 percent of the annual rainfall in the Pare watershed received during the months of March to September, which infers that the hydrology of the watershed is majorly controlled during these months.

4.3.2 Temperature regime during calibration and validation periods in Pare

Temperature data analysis in the Pare watershed over these periods revealed that the mean daily TMAX and TMIN in the area was about 28.66 °C and 18.79 °C, respectively. The lowest recorded temperature in the study area during these periods was 6.62 °C and the highest recorded temperature during the same period was 36.89 °C. The standard deviation of TMAX and TMIN around their mean values were found as 3.7 and 5.51 °C, indicating greater variation for minimum temperature. Seasonal variation of TMIN and TMAX are shown in Fig. 4.5. The temperature in the study area peaks in the month of August while January is the coldest month with average night temperature of about 9.98 °C. The diurnal temperature difference in the study area was found highest in the month of January.

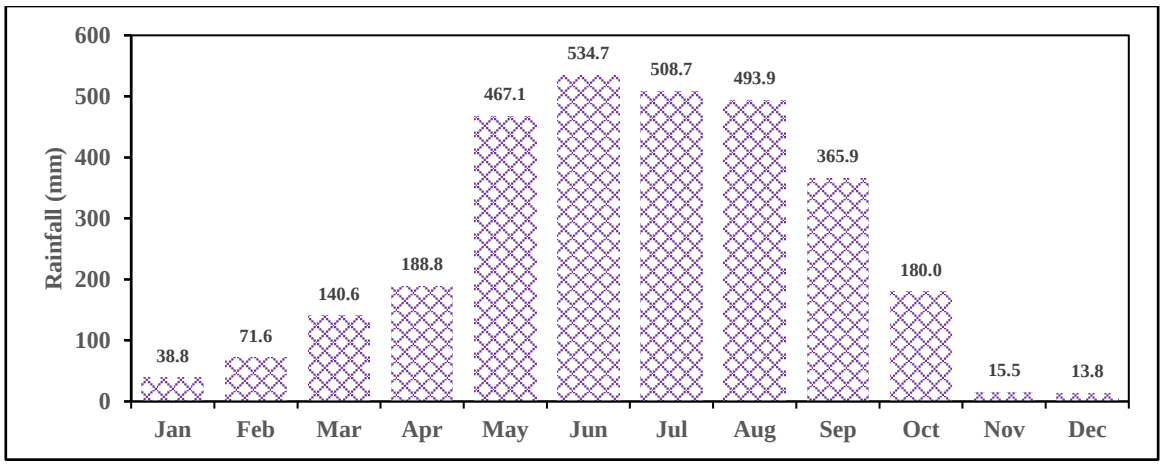

Fig. 4.4 Monthly average rainfall in Pare watershed during combined periods of 1991-1997 and 2003-2005

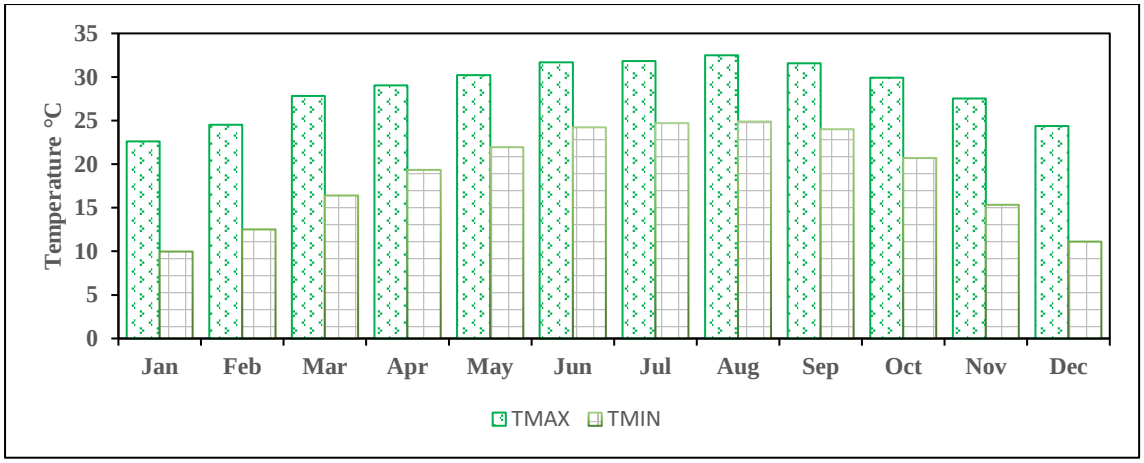

Fig. 4.5 Seasonal variation of TMAX and TMIN in Pare watershed during combined periods of 1991-1997 and 2003-2005

4.3.3 Climate regime in Pare watershed according to NEX-GDDP

The range of projections of yearly rainfall given by the four climate models along with their ensembles during baseline, near future, mid future and far future periods under RCPs 4.5 and 8.5 are shown in Fig. 4.6. The mean annual rainfall of each of the models and their ensembles during baseline and three different future periods under RCPs 4.5 and 8.5 are illustrated in Table 4.9. Also, the percentage changes of the climate models in future periods w.r.t. baseline (1976-2005) are also illustrated in Table 4.9. There was a clear indication that, the general trend of annual rainfall in the study area was projected to increase in the future. Also, the projections were projected higher under RCP 8.5 scenarios as compared to RCP4.5 scenarios. The mean annual rainfall given by CCSM4, CNRM-CM5, MPI-ESM-LR, NorESM1-M and their ensemble during the baseline era were found as 1835.1 mm, 1916.5 mm, 1905.8 mm, 1866.5 mm, and 1881 mm, respectively. Of all the future scenarios, near future period (2030s) of the climate model NorESM1-M under RCP 8.5 was seen to have lesser mean annual rainfall than its baseline period. In this particular scenario, it was projected to decrease in mean annual rainfall to the amount of 7.5 percent lesser than the baseline. The ensemble climate model under RCP 4.5 were projected to be 8.3, 17.0, and 14.6, percent higher than the baseline mean during 2030s (near future), 2050s (mid future) and 2080s (far future), respectively. While under RCP 8.5, it projected to be 7.1, 19.9, and 38.6, percent higher than the historical mean during 2030s, 2050s and 2080s, respectively. All scenarios under RCP 8.5 and also the scenarios of the climate model CNRM-CM5 under RCP 4.5 projected increasing mean annual rainfall as time frames moves from near to far future. However, the other four remaining climate models under

RCP 4.5 including the ensemble projected highest increased during mid future as compare to near and far future eras. Analyzing the seasonal variation of rainfall of all climate scenarios (not shown in this paper) indicated that monsoonal and pre-monsoonal share of the ensemble model in the baseline period were respectively, 68.4 percent and 25 percent. The share of these two seasons was found highest for the model NorESM1-M (94.2%) and lowest for the model MPI-ESM-LR (92.1%), indicating that in the Pare watershed, its hydrology is controlled majorly during these two seasons. Further analyzing the percentage changes in rainfall in each month of the year w.r.t. the baseline period suggested that significant amount of rainfall increase was observed during monsoon as well as pre-monsoon season. On the other hand, decrease in rainfall was generally observed during months of November-March. These observations suggested that, the precipitation pattern in the watershed would witness shrinking of rainy days with higher intensity rainfall during monsoon and pre-monsoon seasons.

The range of projections of yearly average maximum temperature (TMAX) given by the four climate models along with their ensembles during baseline, near future, mid future and far future periods under RCPs 4.5 and 8.5 are shown in Fig. 4.7. The mean annual TMAX of each of the models and their ensembles during baseline period and three different future periods under RCPs 4.5 and 8.5 are illustrated in Table 4.10. Also, the absolute changes in temperature of the climate models in future periods w.r.t. baseline period are also shown in the table. Similarly for yearly average minimum temperature (TMIN), the corresponding figure is shown in Fig. 4.8. Further, the corresponding mean annual minimum temperature along with the absolute change in temperature in the future periods w.r.t. baseline is illustrated in Table 4.11. The trends in the plots indicate that both TMAX and TMIN are expected to increase in the future years and the magnitude of increment under RCP 8.5 projection scenarios would be higher than RCP 4.5 projection scenarios. The ensemble climate model has indicated that the mean minimum temperature would be increased by about 1.2 ºC, 1.7 ºC, and 2.1 ºC in 2030s, 2050s and 2080s, respectively from the baseline era (1976-2005) under RCP 4.5 scenario, while under RCP 8.5, these values were 1.2 ºC, 2.4 ºC, and 3.8 ºC, respectively. In case of maximum temperature, these increased values were 1.0 ºC, 1.7 ºC, and 2.1 ºC under RCP 4.5 scenarios and 1.1 ºC, 2.3 ºC, and 3.7 ºC, respectively. Analyzing these absolute changes and also at the seasonal level (monthly variation in a year), relatively greater changes were obtained for TMIN indicating that night temperature would increase at greater pace than daytime temperature.

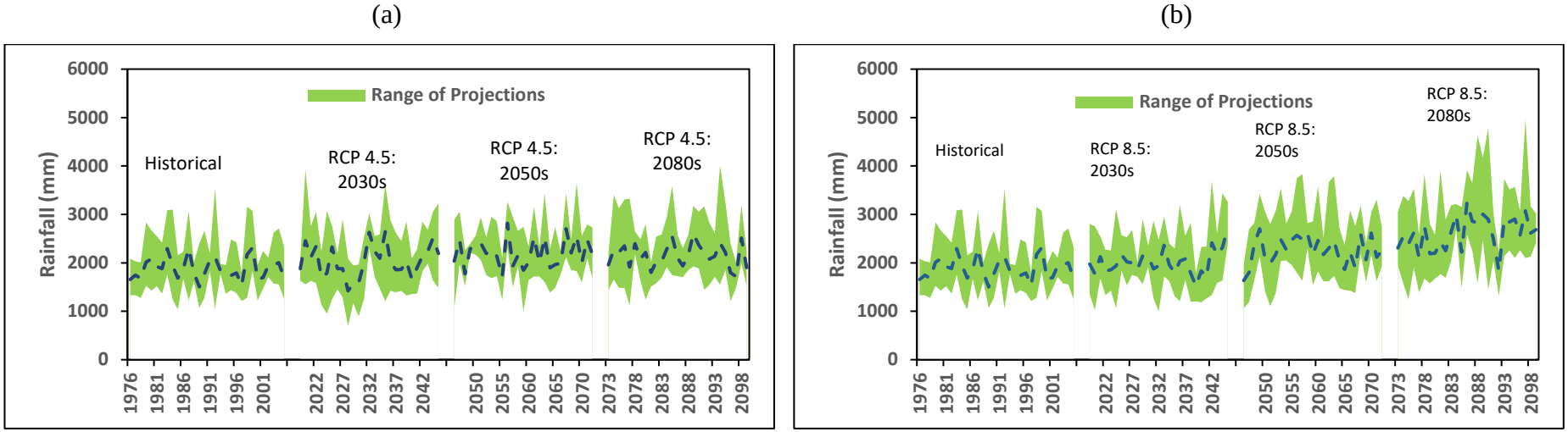

Fig. 4.6 Rainfall projections of the climate models and their ensemble in Pare watershed during baseline and future period under (a) RCP 4.5 and (b) RCP 8.5 projection scenarios

Table 4.9 Mean annual rainfall of climate models in Pare watershed and their percentage change w.r.t. baseline period

		CCSM4 (mm)	% Change	CNRM-CM5 (mm)	% Change	MPI-ESM-LR (mm)	% Change	NorESM1-M (mm)	% Change	Ensemble (mm)	% Change
Historical (1976-2005)		1835.1		1916.5		1905.8		1866.5		1881.0	
RCP 4.5	**2030s**	1936.1	5.5	2131.0	11.2	2105.9	10.5	1972.1	5.7	2036.3	8.3
	2050s	2190.0	19.3	2159.7	12.7	2308.7	21.1	2141.0	14.7	2199.9	17.0
	2080s	2106.7	14.8	2470.5	28.9	2137.5	12.2	1908.8	2.3	2155.9	14.6
RCP 8.5	**2030s**	1907.4	3.9	2265.1	18.2	2155.3	13.1	1727.3	-7.5	2013.8	7.1
	2050s	2179.7	18.8	2533.2	32.2	2243.5	17.7	2068.0	10.8	2256.1	19.9
	2080s	2493.1	35.9	2701.6	41.0	2571.4	34.9	2660.7	42.5	2606.7	38.6

(a) (b)

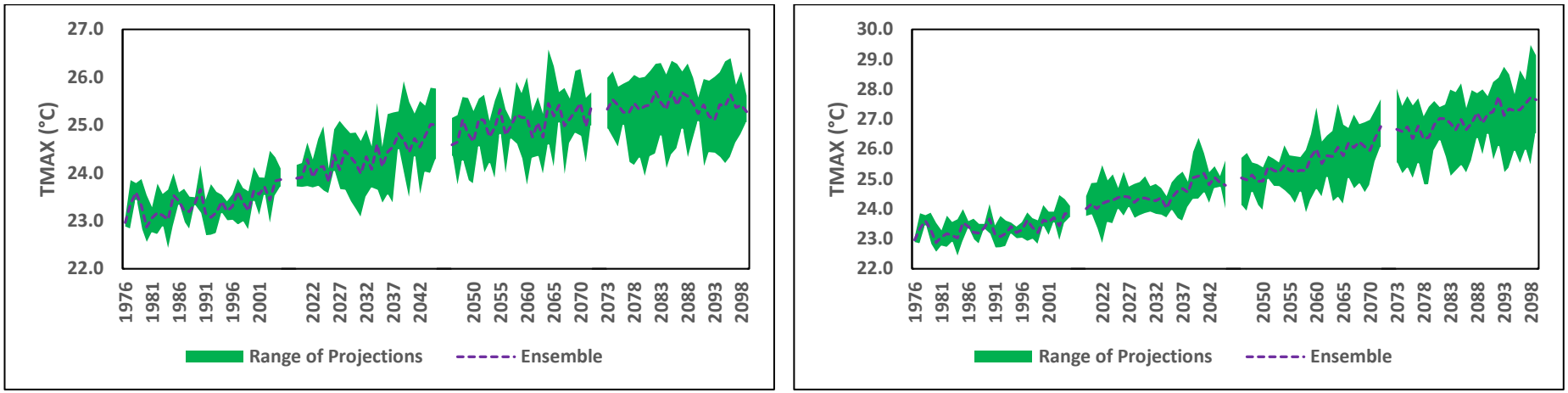

Fig. 4.7 TMAX projections of the climate models and their ensemble in Pare watershed during baseline and future period under (a) RCP 4.5 and (b) RCP 8.5 projection scenarios

Table 4.10 Mean annual TMAX of climate models in Pare watershed and their absolute change w.r.t. baseline period

		CCSM4 (°C)	Absolute Change (°C)	CNRM-CM5 (°C)	Absolute Change (°C)	MPI-ESM-LR (°C)	Absolute Change (°C)	NorESM1-M (°C)	Absolute Change (°C)	Ensemble (°C)	Absolute Change (°C)
Historical (1976-2005)		**23.38**		**23.22**		**23.47**		**23.31**		**23.35**	
RCP 4.5	**2030s**	24.40	1.02	23.70	0.48	24.76	1.29	24.57	1.26	24.36	1.01
	2050s	25.26	1.88	24.30	1.07	25.31	1.83	25.32	2.01	25.05	1.70
	2080s	25.73	2.35	24.50	1.27	25.74	2.27	25.70	2.38	25.42	2.07
RCP 8.5	**2030s**	24.54	1.16	23.91	0.69	24.93	1.45	24.56	1.24	24.48	1.14
	2050s	25.82	2.44	24.55	1.33	26.22	2.75	25.89	2.57	25.62	2.27
	2080s	27.24	3.86	25.57	2.35	27.89	4.42	27.28	3.97	27.00	3.65

(a) (b)

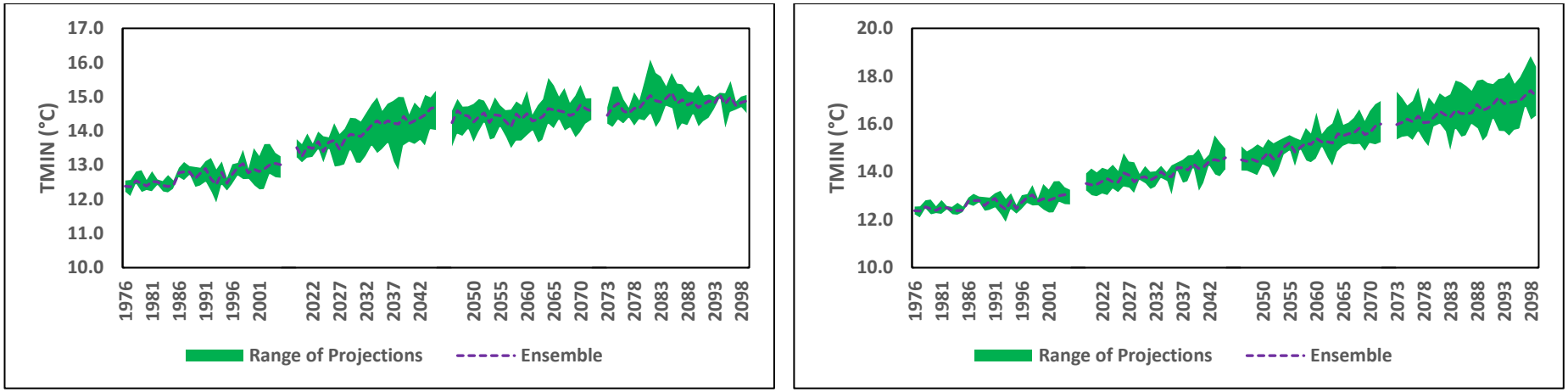

Fig. 4.8 TMIN projections of the climate models and their ensemble in Pare watershed during baseline and future period under (a) RCP 4.5 and (b) RCP 8.5 projection scenarios

Table 4.11 Mean annual TMIN of climate models in Pare watershed and their absolute change w.r.t. baseline period

		CCSM4 (°C)	Absolute Change (°C)	CNRM-CM5 (°C)	Absolute Change (°C)	MPI-ESM-LR (°C)	Absolute Change (°C)	NorESM1-M (°C)	Absolute Change (°C)	Ensemble (°C)	Absolute Change (°C)
Historical (1976-2005)		**12.72**		**12.58**		**12.76**		**12.65**		**12.67**	
RCP 4.5	**2030s**	14.27	1.55	13.37	0.79	14.14	1.38	14.15	1.50	13.88	1.21
	2050s	14.51	1.79	13.92	1.33	14.85	2.08	14.54	1.89	14.40	1.72
	2080s	14.87	2.15	14.38	1.80	15.15	2.39	14.83	2.18	14.79	2.12
RCP 8.5	**2030s**	13.99	1.27	13.48	0.89	14.36	1.60	13.88	1.23	13.87	1.20
	2050s	15.18	2.45	14.57	1.99	15.75	2.99	15.15	2.50	15.11	2.43
	2080s	16.54	3.82	15.65	3.07	17.58	4.82	16.54	3.89	16.48	3.81

4.3.4 Sensitivity analysis in SWAT in Pare watershed

To examine the influence of each parameter on the performance of streamflow simulation, sensitivity analysis, a technique for determining the degree of responsiveness of parameters, was used. The uncalibrated SWAT streamflow was compared to observed streamflow before selecting the parameters to be included in model calibration. The timing of peaks, their magnitudes, and the shapes of hydrographs were studied, and 12 model parameters that will affect these aspects of hydrographs were chosen. The uncalibrated SWAT streamflow have major disagreement from the observed streamflow in terms of base flow and magnitude of runoff peaks, while the timings were mostly accurate. Sensitivity analysis were performed on these 12 SWAT model parameters during the calibration process in SWAT-CUP. After assigning initial ranges of the 12 model parameters, an iteration of 1000 simulations are performed. The rankings of the 12 model parameters are displayed in Table 4.12. Sensitivity of parameters to streamflow can be determined based on t-stat and p-value, with bigger absolute t-stat values suggesting higher sensitivity (Abbaspour, 2015) and p-values showing their significant level. The results revealed that channel hydraulic conductivity is the most sensitive parameter in simulating streamflow in Pare River. Based on p-value and t-stat, channel hydraulic conductivity (CH_K2), curve number (CN2) and recession constant of bank (ALPHA_BNK) are the three most sensitive parameters. CN2 and CH_K2 are two model parameters which strongly influence the peaks of hydrograph. CN2 is a dimensionless quantity that is linked to the permeability of soil, land usage, and previous moisture conditions. Reduced surface runoff and increased infiltration were the results of a low CN value. Other sensitive variables like ALPHA_BNK, GWQMN, GW_REVAP, and REVAPMN have a big impact on the hydrograph's low flows (baseflow components).

4.3.5 Calibration of streamflow in SWAT model

SWAT model was calibrated using observed streamflow at the outlet of the Pare watershed for a period of seven years (1991-1997). The parameter range (minimum and maximum) and the method of parameter modification are illustrated in Table 4.13. Two modification methods viz. replace and relative, were employed in the calibration. The replace method simply replaces the original value with a specified value from within the parameter range and in the process loses spatial heterogeneity. In relative method, instead of providing parameter values, range of multiplier

constant is provided to conserve spatial heterogeneity. Relative method multiplies the original value with 1 plus the multiplier constant.

Table 4.12 Sensitivity ranks of the SWAT model parameters in Pare watershed

Parameter	Definition	p-value	t-stat	Rank
CH_K2.rte	Channel hydraulic conductivity	0.000	41.601	**1**
CN2.mgt	CN number for moisture condition II	0.000	-39.509	**2**
ALPHA_BNK.rte	Bank storage's recession constant	0.000	-13.813	**3**
GWQMN.gw	Threshold water's depth in shallow aquifer required for occurrence of return flow	0.087	-1.712	**4**
GW_REVAP.gw	Groundwater "revap" coefficient	0.130	-1.514	**5**
REVAPMN.gw	Threshold water's depth in shallow aquifer for occurrence of percolation to deep aquifer	0.289	-1.061	**6**
SOL_K(..).sol	Soil's saturated hydraulic conductivity	0.466	-0.730	**7**
ALPHA_BF.gw	Baseflow recession constant	0.498	-0.677	**8**
ESCO.hru	Compensation factor for soil evaporation	0.669	-0.428	**9**
GW_DELAY.gw	Groundwater delay	0.876	-0.156	**10**
CH_N2.rte	Manning's roughness *n* of main channel	0.877	-0.154	**11**
SOL_AWC(..).sol	Available water capacity of soil layer	0.962	-0.048	**12**

Table 4.13 Parameter range, parameter change method and fitted model parameter values in SWAT-CUP

Sl. No.	Parameter	Minimum	Maximum	Fitted Value	Method
1.	CN2.mgt	-0.20	0.20	**-0.1002**	Relative
2.	GW_DELAY.gw	5	450	**17.68**	Replace
3.	ALPHA_BF.gw	0	1	**0.40**	Replace
4.	GWQMN.gw	0	2000	**315.00**	Replace
5.	ESCO.hru	0.70	0.99	**0.87**	Replace
6.	SOL_AWC(..).sol	-0.20	0.20	**0.0126**	Relative
7.	SOL_K(..).sol	-0.30	0.30	**0.0009**	Relative
8.	CH_N2.rte	0.05	0.30	**0.09**	Replace
9.	CH_K2.rte	0	150	**142.13**	Replace
10.	REVAPMN.gw	0	500	**433.25**	Replace
11.	GW_REVAP.gw	0.02	0.20	**0.04**	Replace
12.	ALPHA_BNK.rte	0	1	**0.12**	Replace

Twelve model parameters were modified in the calibration process. Best fit set of parameters was selected out of the 1000 sets of parameters based on the best Nash-Sutcliffe values. The best-fitted values (calibrated model parameters) of the 12 SWAT model parameters are shown in Table 4.13. The best fit values of ALPHA_BF, GW_DELAY, GWQMN, ESCO, CH_N2, CH_K2,

GW_REVAP, REVAPMN, and ALPHA_BNK are found as 0.4, 17.68 days, 315 mm, 0.87, 0.09, 142.13 mm/hr, 0.04, 433.25 mm, and 0.12, respectively. The best fit multipliers for CN2, SOL_AWC(..), and SOL_K(..) are (1 - 0.1002 = 0.8998), (1 + 0.0126 = 1.0126), and (1 + 0.0009 = 1.0009), respectively. The uncertainty of the SWAT model can be implicated from p-, and r-factors. These two factors are in such a way that one can be optimized at the cost of the other. Any SWAT calibration processes aims to balance between these two factors. In this study, based on expert knowledge, calibration was attempted to get p-factor more than 0.75 and r-factor less than 1.2. The fitted values in Table 4.13 are the outcome of 1000 simulations in an iteration of SWAT calibration. Second iteration was also attempted in vain to optimize the NSE. Slight increment of NSE in the second iteration cannot be compromised by larger reduction in p-factor, leading to increase in model uncertainty.

Fig. 4.9 depicts daily time series plots of observed and simulated runoffs in the SWAT model for the calibration period (1991-1997). Fig. 4.10 depicts the monthly fluctuation of observed and simulated runoffs throughout the same time period. The model reflects the runoff changes reasonably well, according to a qualitative comparison of observed and simulated daily and monthly runoff. The calibration years accurately recreate the magnitude, evolution, and fluctuation of streamflow. The low flow components of the hydrographs were found to be mismatched in all years from 1991 to 1997, where the SWAT model was unable to capture it in the Pare watershed.

The model's simulated runoff matches the rainfall pattern better than the observed runoff. Although the peaks of the simulated and actual runoffs differ somewhat, their volumes are nearly identical. The most obvious mismatch occurred in 1992, when the SWAT model anticipated a peak discharge of roughly 111 cumecs but the actual peak discharge was 170 cumecs. After a thorough examination of rainfall patterns, observed discharge, and simulated discharge over multiple years, there appears to be some uncertainty in the observed data. On the 26th March 1994, Pare watershed received a rainfall amount of 168.29 mm which resulted a discharge of 85 cumecs. On the other hand, SWAT predicted a discharge of 714 cumecs. Through examination, it was observed that in the preceding 10 days prior to this day, Pare watershed received a cumulative rainfall amount of 185.55 mm. Due to this, the watershed was already saturated and critical and cause a sudden flood of discharge on 26th March 1994 aided by 168.29 mm of rainfall that day.

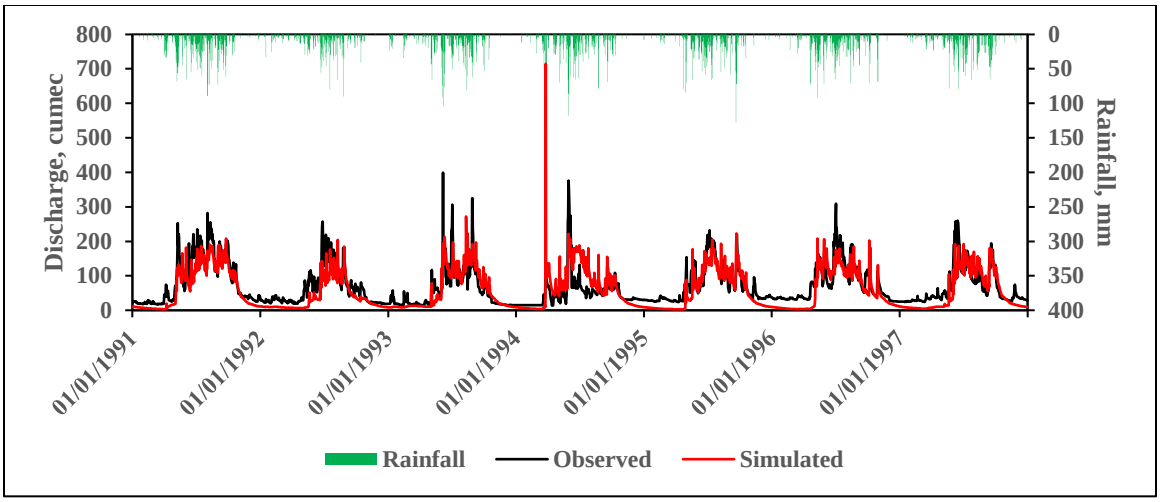

Fig. 4.9 Daily variation of observed and simulated discharge in SWAT model for Pare River during calibration period

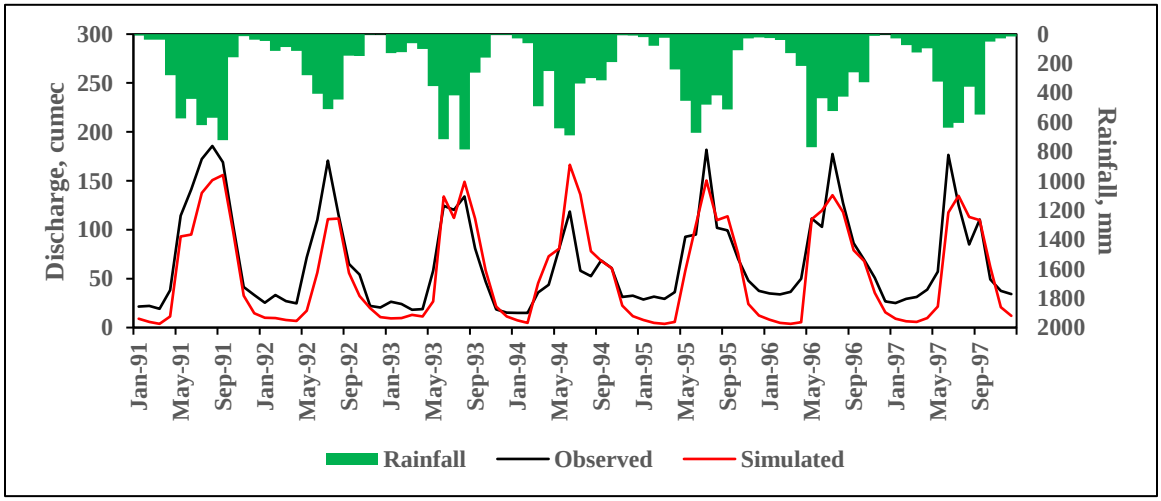

Fig. 4.10 Monthly variation of observed and simulated discharge in SWAT model for Pare River during calibration period

The average daily actual runoff in the Pare watershed was 67.67 cumecs throughout this timeframe, while the average daily simulated runoff was at 55.94 cumecs. It means that the discharge in the Pare watershed was slightly underestimated by the SWAT model. During low flow (dry period) periods, the degree of underestimation was shown to be larger than during wet period periods. Scatter plot between the observed and simulated runoff is shown in Fig. 4.11 along with the 1:1 line. The plot shows R^2 value of 0.6148 which is reasonably good for mountainous watersheds. It implies that the constructed SWAT model for the Pare watershed was able to explain almost 61 %

of the actual runoff variation. Comparing the data points with the 1:1 line revealed good model performance, however, some dispersions of points were also observed.

Table 4.14 shows the model performance indicators for the constructed SWAT model in the Pare watershed during calibration period. As mentioned earlier, a hydrological model be considered suitable if the NSE is greater than 0.50, the PBIAS is less than 25%, and R^2 values greater than 0.50. Based on these, the SWAT model developed in the Pare watershed functioned satisfactorily on daily and monthly timesteps. The SWAT model was found to be 52 percent and 72 percent efficient at daily and monthly timesteps, respectively. The SWAT model's PBIAS was calculated to be 17.3 and 17.44 for daily and monthly timesteps, respectively, showing that the runoff was underestimated by the SWAT model. At daily and monthly timesteps, the standard error of estimates (SEE) was calculated to be 38.5 cumecs and 25.54 cumecs, respectively. For daily and monthly timesteps, the coefficient of determination (R^2) values was estimated to be 0.61 and 0.80, respectively, demonstrating good model prediction.

4.3.6 Validation of streamflow in SWAT model

The setup SWAT model was validated for three years, from 2003 to 2005, using the calibrated model parameters in Table 4.13. The measured versus simulated discharge for daily and monthly timescales are shown in Figs. 4.12 and 4.13, respectively. According to comparisons of observed and simulated daily discharge, it is revealed that the SWAT model reflects the observed discharge well better than the calibration years in the validation period. Unlike the calibration phase, the SWAT model predicted the low flow components of the hydrographs better in the validation period, both at daily and monthly timesteps. In the validation phase, the model's predicted runoff follows the rainfall pattern better than the observed runoff.

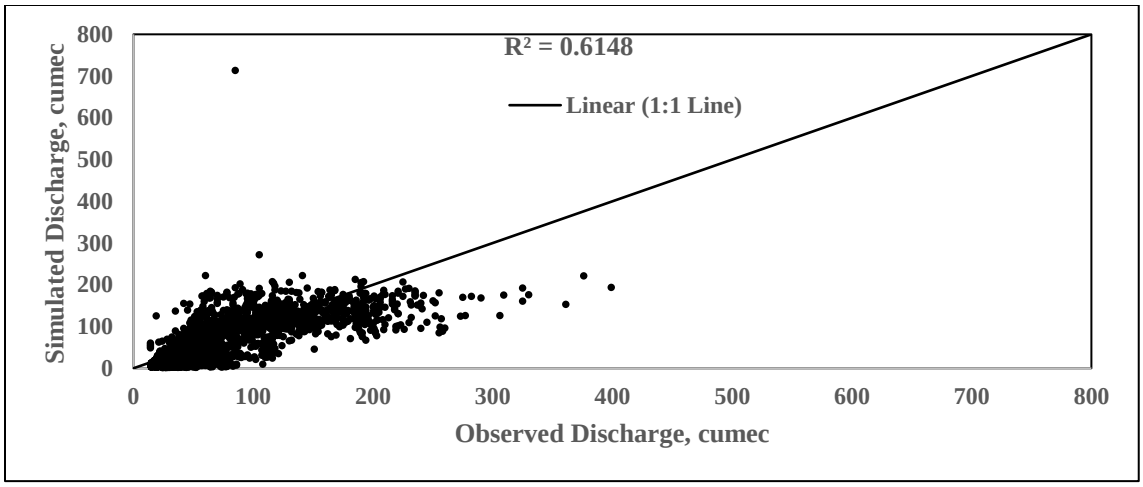

Fig. 4.11 Scatter plot between daily observed and simulated discharge during calibration period in SWAT model

Table 4.14 SWAT model performance indices for daily and monthly timesteps during calibration

Performance Indicators	Timestep	
	Daily	Monthly
NSE	0.52	0.72
R^2	0.61	0.80
PBIAS	17.3	17.44
SEE	38.5	25.54

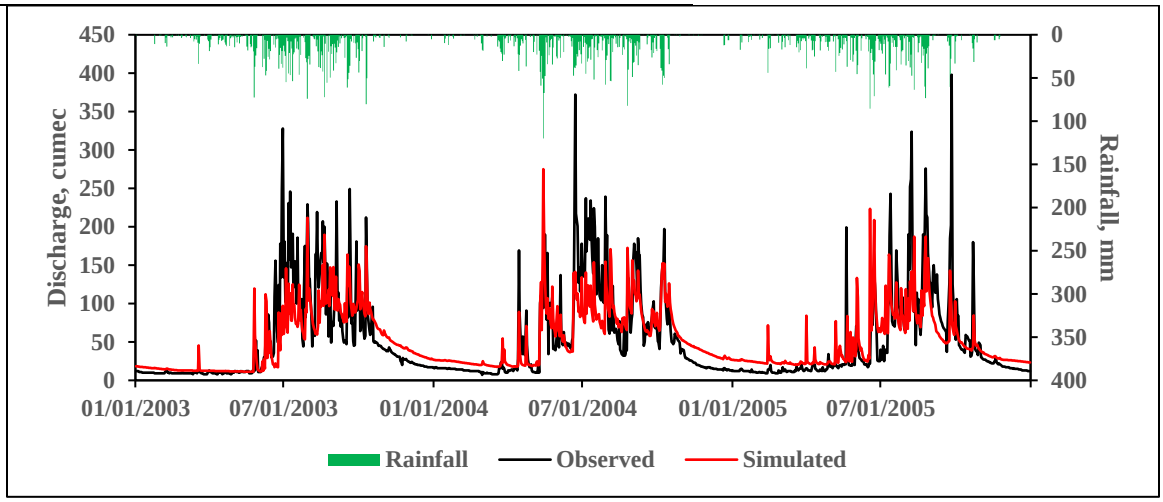

Fig. 4.12 Daily variation of observed vs simulated discharge in SWAT model for Pare River during validation period

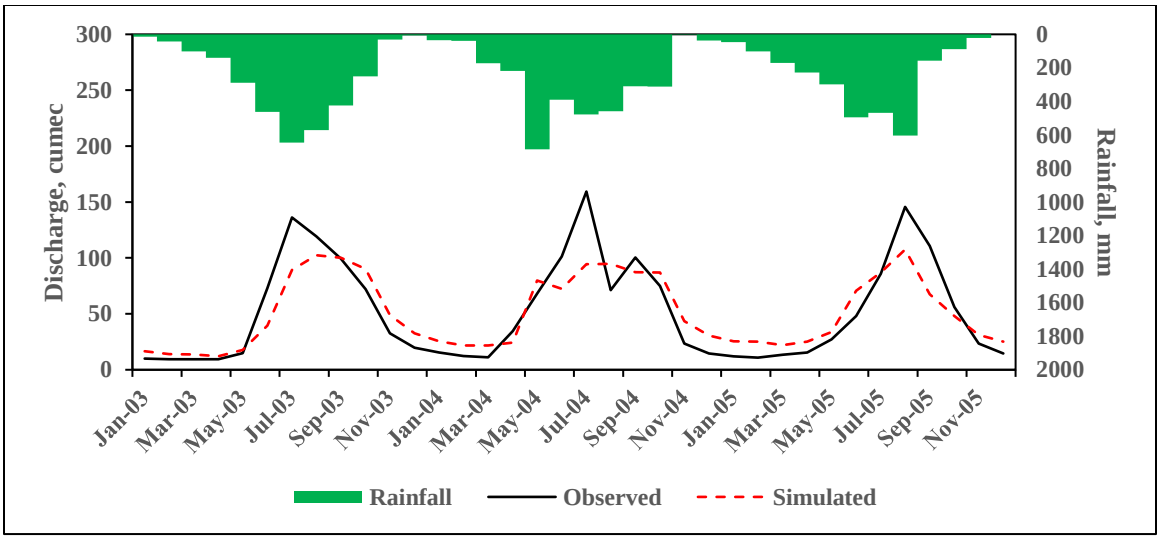

Fig. 4.13 Monthly variation of observed vs simulated discharge in SWAT model for Pare River during validation period

During the validation period, the mean daily actual runoff in the Pare watershed was estimated to be 51.8 cumecs, while the mean daily simulated runoff was around 51 cumecs. It means that throughout the validation period, the SWAT model somewhat underestimated (negligible) the discharge in the Pare watershed. Fig. 4.14 shows a scatter plot of observed and modelled runoff, as well as the 1:1 line. The figure indicates an R^2 of 0.6073, which is reasonably good indication. It means that the Pare watershed SWAT model was able to explain nearly 61 percent of the variance.

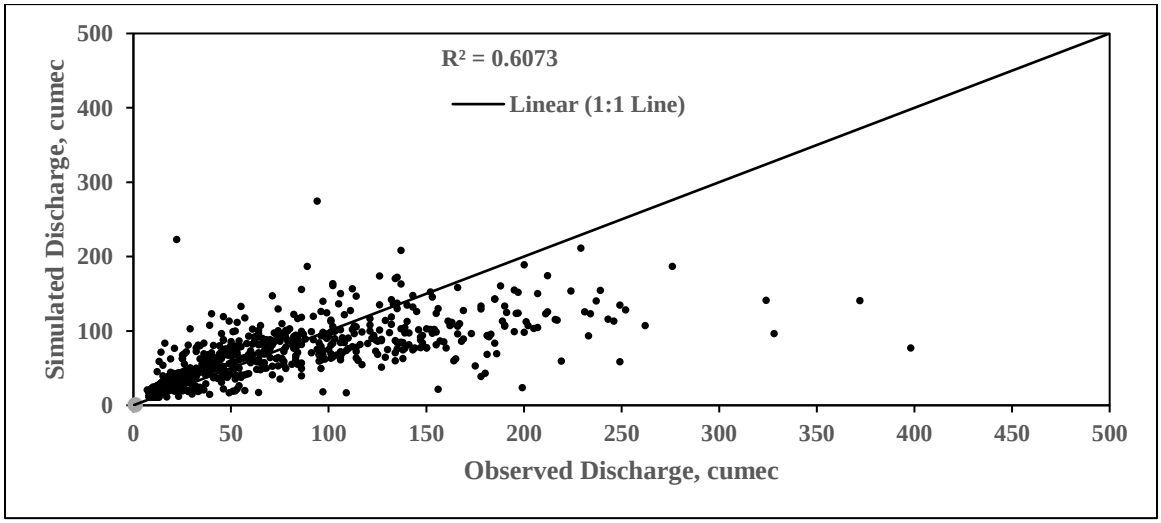

Fig. 4.14 Scatter plot between daily observed and SWAT simulated discharge during validation period

Table 4.15 shows the model performance indicators, which show that the SWAT model performs satisfactorily. On daily and monthly timesteps, the SWAT model constructed in the Pare watershed functioned admirably. The SWAT model's efficiencies were determined to be 60% and 78%, respectively, at daily and monthly timesteps. For daily and monthly timesteps, the SWAT model's PBIAS was predicted to be 1.6 and 1.5, respectively, indicating that the model underestimated discharge. For daily and monthly timesteps, the standard error of estimates (SEE) was calculated to be 36.17 cumecs and 21.26 cumecs, respectively. During the validation period, the SWAT model's coefficient of determination (R^2) values was estimated to be 0.61 and 0.82 for daily and monthly timesteps, respectively. All of the performance measures indicated that the model was capable to represent the watershed's hydrologic response and simulate the water yield while taking into account streamflow variability. It's worth noting that over the validation period from 2003 to 2005, all model performance measures indicated improved model performance. The constructed SWAT model has demonstrated to be extremely satisfactory in terms of runoff volume simulated by the model.

Table 4.15 SWAT model performance indices for daily and monthly timesteps during validation

Performance Indicators	Timestep	
	Daily	Monthly
NSE	0.60	0.78
R^2	0.61	0.82
PBIAS	1.6	1.5
SEE	36.17	21.26

4.3.7 Uncertainties in SWAT model's prediction of streamflow

Uncertainty analysis was carried out for the calibration and validation periods in SWAT-CUP. The measures of uncertainties in the prediction were determined from p-factor and r-factor of the 95PPU. The p-factor and r-factor are closely related to each other, which indicated that a larger p-factor can be achieved only at the expense of a higher r-factor. The values of these factors achieved during calibration and validation of daily discharge data are illustrated in Table 4.16. To ease in comparison and understandings, observed discharge, best fit simulated discharge, rainfall and 95PPU uncertainty band of the calibration and validation periods were plotted and shown in Figs.

4.15 and 4.16, respectively.

Table 4.16 Measures of SWAT model uncertainties during calibration and validation in Pare

Performance Indicators	Periods	
	Calibration	Validation
p-factor	0.76	0.88
r-factor	1.19	1.07

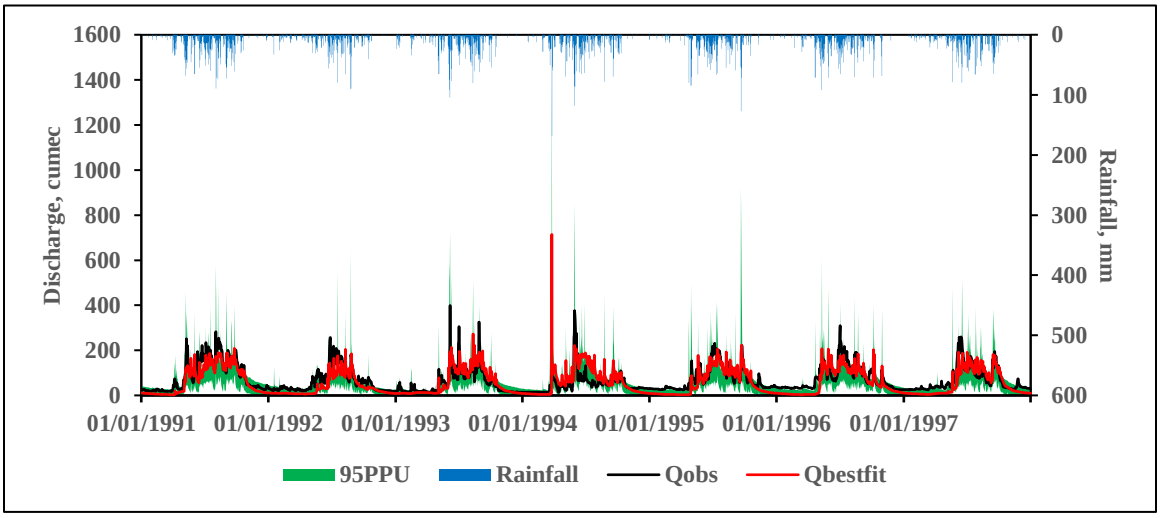

Fig. 4.15 95PPU, rainfall, measured and best fit predicted discharge during calibration in SWAT for Pare watershed

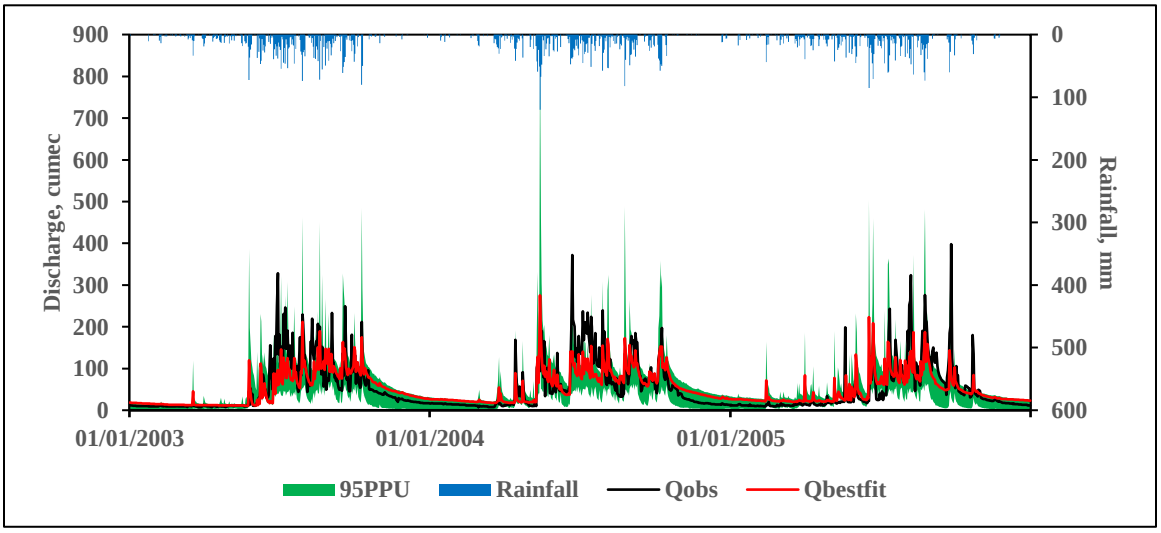

Fig. 4.16 95ppu, rainfall, measured and best fit predicted discharge during validation in SWAT for Pare watershed

The SWAT model could not accurately reflect the watershed in low flow circumstances during the calibration period of 1991-1997, as shown in Figs. 4.9 and 4.10. While in the validation period of 2003-2005, the model could satisfactorily represent low flow conditions, however, the peaks couldn't be matched accurately. The p- factors of the SWAT model during calibration and validation periods were found as 0.76 and 0.88, respectively. It indicates that 76 percent of the measured data was bracketed within the 95ppu band during model calibration and 88 percent during model validation. The average measure of thickness of the 95ppu bands (r-factors) during model training and validation were found as 1.19 and 1.07, respectively. Based on these values, the SWAT model developed for the Pare watershed could be considered satisfactory. The model uncertainties may be due to various reasons. Singh *et al.* (2007) described five different sources of uncertainties in hydrological modelling, which are listed below:

(a) natural uncertainties: randomly associated in spatial and temporal fluctuations of natural processes;
(b) model structure uncertainties, which are the model's inability to accurately represent the system;
(c) parameters' uncertainty: it is the inability to determine and use right values of the parameters;
(d) uncertainty in the measured/observed data: this is the most common uncertainties associated with inadequate gauging networks and inaccurate measurement and data entry; and
(e) uncertainties in computation.

The magnitude of uncertainties is higher, particularly in mountainous watershed (Das *et al.* 2019) due to various reasons such as sparse gauging networks, complexity and variation in topography and lack of logistics. Bhattacharya *et al.* (2019) compared the suitability of ERA-Interim reanalysis data with IMD gridded weather data resulted in lesser NSE (ranges between 0.22 and 0.5) for SWAT model with IMD gridded weather data in simulating snowmelt runoff at Pong and Pandoh dam in Beas River basin. Low NSE of SWAT model in mountainous watershed can also be evident in Singh and Goyal (2017) in which the NSE values obtained during calibration were 0.46 and 0.48 at Lachung and Chungthang gauging sites, respectively. Low NSE value, also obtained in this

study (NSE = 0.52), although satisfactory, may be attributed to uncertainties in the measured data described by Singh *et al.* (2007). In mountainous watershed such as the Pare watershed, orographic effects of precipitation are very prominent and hence require good adequacy of rainfall gauging networks. Three IMD precipitation grids used in the study are relatively sparse. It can also be noted that, the streamflow gauging station in the watershed is a single measurement point staff gauge and therefore required accurate measurement of river cross-section. With the amount of uncertainties possibilities in the watershed, the results obtained are quite satisfactory.

4.3.8 Projection of future streamflow using SWAT

Figures 4.17 (a) and (b) show the yearly total runoff in the Pare watershed simulated using an ensemble climate model in SWAT from 1976 to 2005 and from 2019 to 2099 under RCPs 4.5 and 8.5. The four climate models' projection ranges are also depicted in the graphics. In comparison to the baseline/historical period, the predicted yearly runoff in the Pare watershed is expected to increase under both RCP 4.5 and RCP 8.5. The amount of projected streamflow increase was found to be greater under RCP 8.5 than under RCP 4.5, as shown by the trend lines in Figs. 4.17 (a) and (b). The trends were indicative of greater variation in future periods as compare to the historical period.

Figures 4.18 (a) and (b) demonstrate the relative percentage change in mean annual total runoff simulated by SWAT with respect to historical era under RCPs 4.5 and 8.5. Climate models-CCSM4, CNRM-CM5, MPI-ESM-LR, NorESM1-M, and their ensemble had baseline average annual runoff of 1288.9, 1381.1, 1365.4, 1345.3, and 1343.7 mm, respectively. The highest growth was shown by the NorESM1-M model during the 2080s (far future era) under the RCP 8.5 projection scenarios, with a 54.5 percent increase over its historical period. The only reduction in streamflow scenario was seen for the NorESM1-M model with a reduction of about 10.6 percent over its historical period. The percentage change in ensemble discharge revealed a rising trend in streamflow for both RCPs and also increased further as time slice shifts from near to far future periods under RCP 8.5 projection scenarios, indicating a generic rising situation. However, in case of RCP 4.5 projection, runoff increased in the 2030s and 2050s and then slightly reduced in the 2080s.

(a) (b)

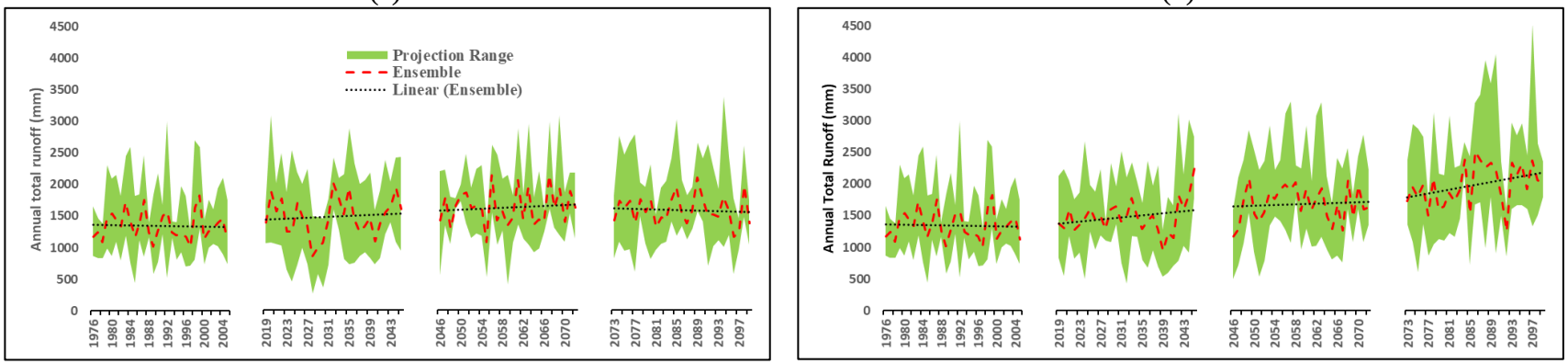

Fig. 4.17 Average yearly discharge projections by ensemble climate in the Pare watershed during (a) RCP 4.5 and (b) RCP 8.5

(a) (b)

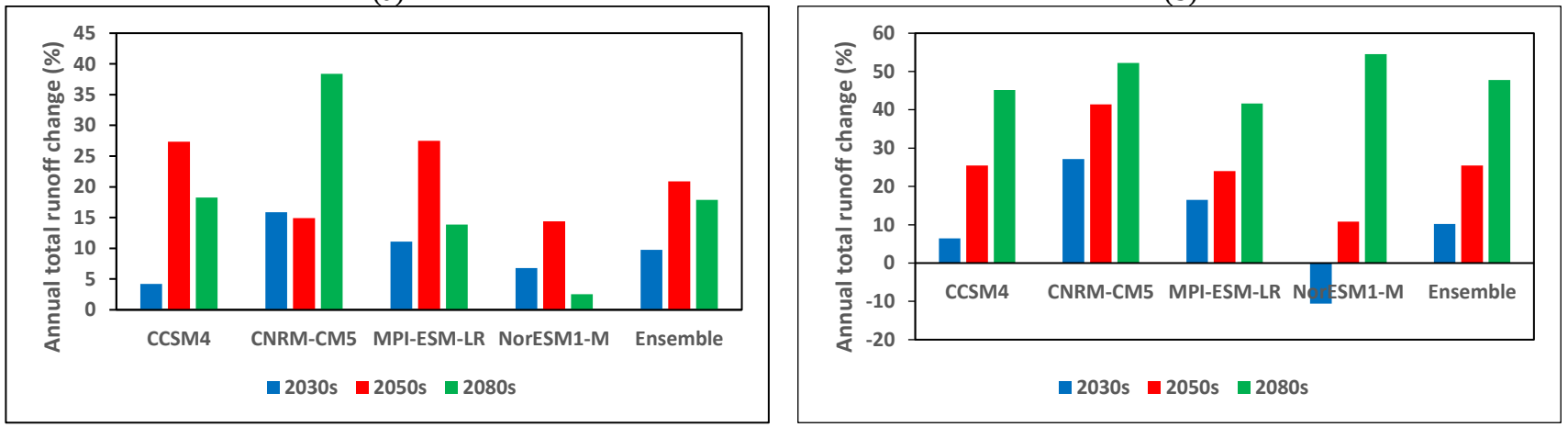

Fig. 4.18 Percentage change of mean annual total w.r.t. historical period for different climate models under (a) RCP 4.5 and (b) RCP 8.5

Analysis of the seasonal variation of discharges indicated that the majority of climatic scenarios predicted a peak discharge in July or August, similar to precipitation predictions. MPI-ESM-LR tends to simulate peak discharge later than the other models while NorESM1-M tends to simulate peak discharge earlier than the other models. Monsoon, pre-monsoon, and post-monsoon contributions grow as time progresses from near to far future, and are also anticipated to be larger under the RCP 8.5 scenario. Close examination of the graphs reveals that future streamflow will have more extreme events.

The relative change in SWAT projected daily average streamflow of all the four climate models and ensemble with respect to the daily average baseline discharge (CCSM4: 31.7 cumecs; CNRM-CM5: 34 cumecs; MPI-ESM-LR: 33.6 cumecs; NorESM1-M: 33.1 cumecs; and Ensemble: 33 cumecs) is shown in Table 4.17. All streamflow scenarios under RCP 4.5 projections as well as mid and far future periods under RCP 8.5 showed increased in daily average discharge in the watershed. In the 2030s under RCP 8.5, NorESM1-M model showed a reduction of 10.7 percent from 33.1 cumecs daily discharge. The maximum increment in daily streamflow is projected by NorESM1-M model in the 2080s under RCP 8.5 scenario to a change of 54.4 % more than its historical average of 33.1 cumecs. Under RCP 8.5, RHESSys projected higher daily average discharge in the 2080s as compared with the ‘50s and ‘30s.

Table 4.17 Relative percentage change in daily average discharge simulated by SWAT with respect to the baseline values for different climate models under RCP 4.5 and RCP 8.5 scenarios

RCP	Time slabs	CCSM4	CNRM-CM5	MPI-ESM-LR	NorESM1-M	Ensemble
RCP 4.5	**2030s**	4.1	15.7	11.0	6.6	9.6
	2050s	27.2	14.8	27.3	14.2	20.8
	2080s	18.1	38.2	13.7	2.4	17.8
RCP 8.5	**2030s**	6.3	27.0	16.3	-10.7	10.1
	2050s	25.3	41.2	23.8	10.7	25.3
	2080s	45.0	52.1	41.5	54.4	47.6

All units in %

Tables 4.18 (near future period), 4.19 (mid future period), and 4.20 (far future period) show the percentage changes in seasonal (monthly variation in a year) w.r.t. historical era. According to the ensemble model, streamflow is anticipated to increase by 7.2, 7.7, 23.4, and 0.9 percent in the 2030s under RCP 4.5 during the monsoon months of June, July, August, and September, compared

to their historical counterparts. During the same time period, in the RCP 8.5 scenario, streamflow increased by 13.4, 2.7, 15.6, and 7.6 percent, respectively. In the 2050s under RCP 4.5, the ensemble model predicts increases of 30.3, 18.5, 21.8, and 13 percent over historical streamflow during the months of June, July, August, and September, respectively. Under RCP 8.5, the increments were 34.6, 21.8, 34.5, and 14 percent, respectively, for the same time period. The similar pattern was seen in the 2080s, but with a greater scale of change for RCP 8.5. These findings are consistent with the results obtained for the watershed's precipitation regime. In general, positive changes i.e., increase in discharge were observed during monsoon and negative changes i.e., decrease in discharge were observed during low flow seasons particularly during pre-monsoon season. This implied that the watershed is expected to produce more extreme runoff.

Table 4.18 Percentage change in monthly discharge in Pare watershed during near future period

Units in %	RCP 4.5					RCP 8.5				
Month	**CCSM4**	**CNRM-CM5**	**MPI-ESM-LR**	**NorESM1-M**	**Ensemble**	**CCSM4**	**CNRM-CM5**	**MPI-ESM-LR**	**NorESM1-M**	**Ensemble**
Jan	33.0	32.9	-4.3	1.2	**15.0**	15.9	24.7	3.6	-7.6	**15.8**
Feb	4.0	21.9	-35.0	-22.9	**5.9**	21.2	35.1	10.0	-19.8	**16.4**
Mar	-13.9	53.3	-53.7	-56.7	**-22.4**	-1.3	-4.8	-17.0	-42.6	**-18.3**
Apr	16.8	26.1	-34.1	-34.1	**-20.9**	-11.5	26.0	-21.0	-41.7	**-19.2**
May	-14.2	2.1	-9.0	67.3	**9.1**	-8.8	51.2	4.8	4.9	**8.4**
Jun	8.6	9.4	20.5	-11.0	**7.2**	-8.9	28.0	37.2	-0.7	**13.4**
Jul	0.6	7.8	38.2	-0.7	**7.7**	0.8	9.6	33.6	-27.7	**2.7**
Aug	13.1	13.6	19.1	42.1	**23.4**	12.4	22.0	17.4	3.6	**15.6**
Sep	-0.6	15.8	-14.3	-5.0	**0.9**	36.1	28.7	-3.8	-16.8	**7.6**
Oct	7.7	47.5	21.7	7.8	**14.9**	27.3	50.7	20.7	9.7	**24.4**
Nov	15.0	51.5	19.1	1.1	**20.1**	21.5	48.5	8.9	1.8	**22.2**
Dec	7.5	39.5	2.4	2.0	**14.0**	17.4	35.2	2.7	0.6	**17.2**

Table 4.19 Percentage change in monthly discharge in Pare watershed during mid future period

Units in %	RCP 4.5					RCP 8.5				
Month	**CCSM4**	**CNRM-CM5**	**MPI-ESM-LR**	**NorESM1-M**	**Ensemble**	**CCSM4**	**CNRM-CM5**	**MPI-ESM-LR**	**NorESM1-M**	**Ensemble**
Jan	9.5	30.2	29.9	0.2	18.8	7.6	60.7	1.7	-3.6	23.6
Feb	79.1	73.7	-6.2	16.8	29.1	31.6	130.2	-20.6	-25.2	19.6
Mar	100.9	93.0	-16.8	-8.1	27.8	29.2	78.9	-60.8	-2.4	6.4
Apr	41.8	66.3	21.0	-4.5	41.0	28.4	68.9	-44.6	-4.3	15.0
May	4.2	43.9	-18.5	31.0	15.3	36.3	38.5	-4.3	-7.5	18.1
Jun	38.0	1.7	43.1	41.7	30.3	50.7	28.8	40.6	29.8	34.6
Jul	50.3	11.3	27.8	-2.2	18.5	20.1	31.7	27.9	22.1	21.8
Aug	16.1	-3.7	44.1	18.1	21.8	9.2	40.0	63.2	6.4	34.5
Sep	12.1	10.4	22.4	-4.3	13.0	33.2	28.9	-2.9	-5.9	14.0
Oct	-1.2	19.6	40.3	29.4	18.4	-0.9	88.0	42.7	20.5	33.6
Nov	1.5	46.6	20.8	-0.9	18.2	2.5	72.8	1.9	-5.9	21.7
Dec	2.9	23.2	25.4	1.9	16.3	3.8	54.0	7.7	-2.2	20.7

Table 4.20 Percentage change in monthly discharge in Pare watershed during far future period

Units in %	RCP 4.5					RCP 8.5				
Month	**CCSM4**	**CNRM-CM5**	**MPI-ESM-LR**	**NorESM1-M**	**Ensemble**	**CCSM4**	**CNRM-CM5**	**MPI-ESM-LR**	**NorESM1-M**	**Ensemble**
Jan	1.1	62.0	-1.0	-0.5	**17.4**	28.1	53.2	13.9	20.9	**31.4**
Feb	16.5	104.7	-31.1	31.9	**18.9**	81.2	173.7	-27.0	54.5	**41.6**
Mar	24.4	2.9	-41.8	-27.1	**-23.0**	201.5	154.8	-52.3	89.3	**112.7**
Apr	45.1	86.8	41.3	32.1	**58.3**	-16.1	66.3	-23.7	45.7	**30.3**
May	31.8	73.7	7.7	70.6	**48.3**	34.3	110.5	-43.0	115.6	**52.8**
Jun	50.2	14.4	36.6	-6.0	**24.3**	88.0	52.1	45.5	58.3	**57.2**
Jul	19.8	31.1	16.1	-13.4	**12.6**	54.8	40.9	65.7	71.7	**56.0**
Aug	-3.9	16.1	13.3	-3.6	**6.4**	45.6	27.5	76.3	52.4	**53.2**
Sep	0.8	32.8	1.3	-13.4	**4.6**	18.5	40.3	62.0	-4.2	**31.0**
Oct	-10.4	93.1	9.4	15.8	**21.8**	-6.1	47.4	23.2	48.5	**29.7**
Nov	-6.5	80.4	6.7	-10.7	**18.0**	-1.9	91.5	28.3	7.6	**33.0**
Dec	-7.8	61.6	3.8	-5.5	**16.0**	3.6	58.6	20.2	14.4	**27.6**

4.3.9 Other components of streamflow in SWAT Model

4.3.9.1 SURQ, LATQ and GWQ during calibration and validation period

Monthly time series plot of surface runoff (SURQ), lateral runoff (LATQ) and groundwater runoff (GWQ) during calibration period (1991-1997) is shown in Fig. 4.19 and for the validation period (2003-2005), it is shown in Fig. 4.20. It can be seen in the graphs that surface runoff was found quite prominent in SWAT simulations. Table 4.21 shows these components of streamflow for the combined period of calibration and validation.

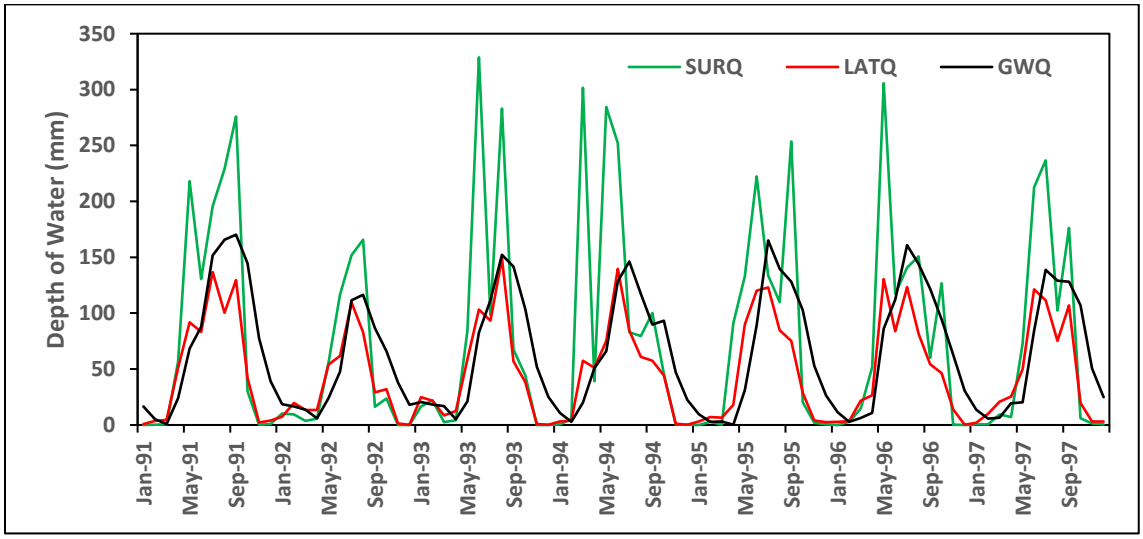

Fig. 4.19 SURQ, LATQ and GWQ during calibration at monthly time step

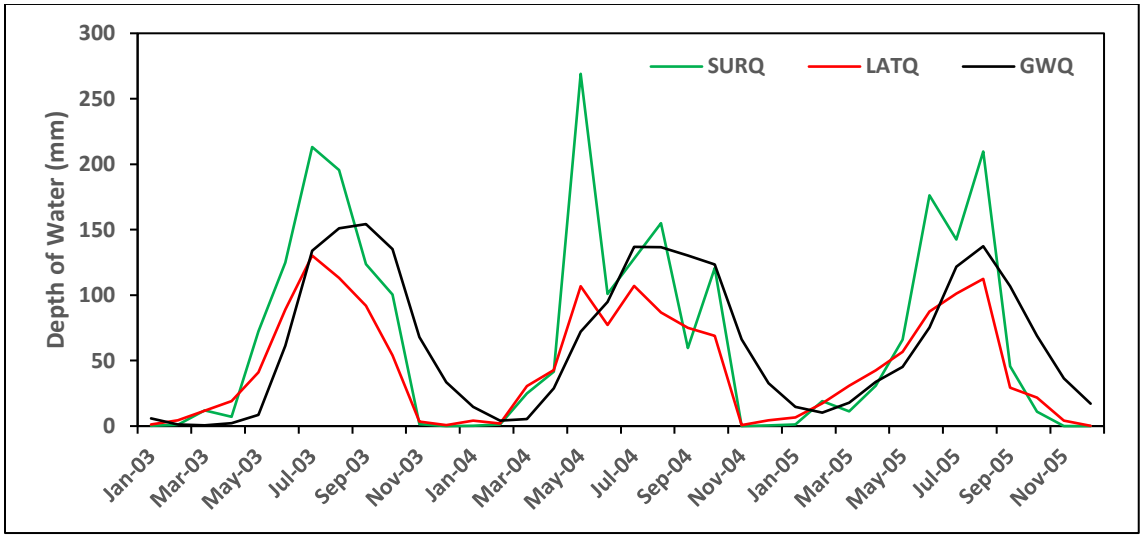

Fig. 4.20 SURQ, LATQ and GWQ during validation at monthly time step

Table 4.21 SURQ, LATQ and GWQ in Pare watershed generated by SWAT model during combine calibration and validation period

Month	SURQ (mm)	LATQ (mm)	GWQ (mm)
Jan	3.0	5.6	13.6
Feb	6.4	9.4	7.0
Mar	38.1	20.6	9.1
Apr	33.5	30.2	18.1
May	156.1	75.5	44.3
Jun	178.3	96.7	86.4
Jul	152.4	112.0	137.9
Aug	168.1	94.7	139.0
Sep	117.9	70.6	125.8
Oct	52.9	39.6	103.9
Nov	0.6	3.5	55.2
Dec	0.3	1.6	27.0
Annual	907.4	560.1	767.3

Ground water component usually recedes after the post-monsoon season till the end of March and start gaining from April when pre-monsoon rainfall occurred. Surface flow and lateral flow were found negligible from November till February. SURQ peaked in the month of June and from May to September, SURQ is above 100 mm in the watershed. The share of SURQ, LATQ and GWQ to the annual streamflow were observed as 40.6 percent, 25.1 percent, and 34.3 percent, respectively. It can be noted that the contribution of SURQ during pre-monsoon and monsoon combine (March to September) to the total annual streamflow in the watershed was about 37.8 percent, indicating very less contribution in the other seasons. The contribution of SURQ, LATQ and GWQ during monsoon months were found as 67.9 %, 66.8 %, and 63.7 %, respectively of their annual total. In the period of negligible rainfall in the watershed, i.e., from November to March, the GWQ share to the streamflow is about 55.7 percent, indicating high sub-surface water storage. Another observation from the Table 4.21 is that, SURQ, LATQ and GWQ peaked in successive months of June, July and August, which explain the nature of the flow perfectly in the watershed.

4.3.9.2 SURQ, LATQ and GWQ during baseline/historical period (1976-2005)

In Fig. 4.21, an ensemble model plot containing monthly SURQ, LATQ, and GWQ of the historical era is shown. According to the ensemble model, in the historical period, SWAT has simulated the monthly average SURQ in the Pare watershed to be about 23.7 mm/month, LATQ

as 35.3 mm/month and GWQ as 50.4 mm/month. Among the four climate models, CNRM-CM5 was found to have the largest monthly average SURQ (38.6 mm/month) while NorESM1-M model was found to have the largest monthly average LATQ and GWQ. According to the ensemble model, the peak of SURQ and LATQ occurred in July 1987 with a magnitude of 221.11 and 133.02 mm, respectively, while for GWQ, the peak occurred in July 1999 with magnitude of 161.86 mm.

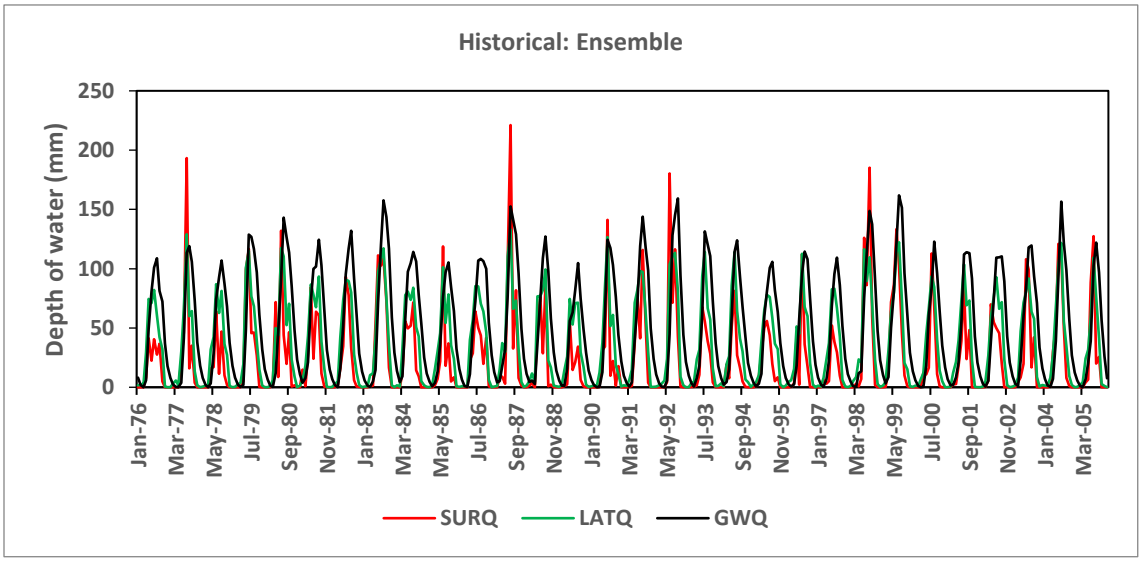

Fig. 4.21 SURQ, LATQ and GWQ in the Pare watershed during historical period

Seasonal break-up of these three streamflow components, along with mean annual values, during the historical era is illustrated in Table 4.22. As seen in the table, the GWQ component has dominated the streamflow for ensemble model while SURQ dominated in the four individual models. As seen in the calibration and validation period, the pattern of rising and recession of these components remain similar. The ensemble model has indicated that in the study area, during this period, GWQ contributes 605.3 mm annually towards the streamflow while SURQ and GWQ annually contribute 284.9 mm and 423.9 mm, respectively. Among the four climate models, CNRM-CM4 has the largest SURQ contribution, while NorESM1-M has the largest LATQ and GWQ contribution. According to the ensemble model, SURQ and LATQ peaked in July while GWQ peaked a month later in August, which is quite obvious to the nature of GWQ being delayed from SURQ and LATQ. Climate models CCSM4, CNRM-CM5 and MPI-ESM-LR also followed the same patter, however, for NorESM1-M model, SURQ, LATQ and GWQ peaked in successive months of June, July and August. According to the ensemble model, SURQ, LATQ, and GWQ

account for roughly 22, 32, and 46 percent of total streamflow, respectively.

4.3.9.3 SURQ, LATQ and GWQ during future period

Monthly SURQ, LATQ and GWQ of the three future eras (near, mid and far) resulted from ensemble of four climate models under RCP 4.5 projection scenario are plotted and shown in Figs. 4.22 (a), (b) and (c). For the projections under RCP 8.5 scenario, they are shown in Figs. 4.23 (a), (b) and (c). As per the ensemble model, monthly average SURQ for near, mid and far future periods were found as 28.9, 32.5, and 31.3 mm/month under RCP 4.5 and 28.6, 36.5 and 49.4 mm/month under RCP 8.5, respectively. In case of LATQ, these monthly average values were respectively 37.5, 40.8 and 40.2 mm/month under RCP 4.5 and 37.9, 41.3, and 45.9 mm/month under RCP 8.5. And, for GWQ, these values were found as 53.9, 59.2 and 57.8 mm/month under RCP 4.5 and 54.3, 59.8 and 67 mm/month under RCP 8.5, respectively. SURQ, LATQ, and GWQ were thus anticipated to be higher in the RCP 8.5 scenario than in the RCP 4.5 scenario, and they were also projected to grow as time slices moved from near to far future eras.

Table 4.23 shows the seasonal break-up of these streamflow components, as well as mean annual values, for the three future eras under RCPs 4.5 and 8.5 based on an ensemble of the four climate models. As seen in the table, in all RCP scenarios, GWQ outperforms SURQ and LATQ. These components grew in magnitudes as years progress from the near to the far future. Close analysis of Table 4.23 reveals that in the near future period, the monsoonal percentage contribution of the SURQ, LATQ and GWQ either remains constant or slightly decreased in the RCP 8.5 than in RCP 4.5 scenarios. However, in the other periods, these components increased in the RCP 8.5 scenarios. It is also observed that their monsoonal contribution to the annual total increased in future periods than in the historical era.

Table 4.22 Seasonal variation of SURQ, LATQ and GWQ in Pare watershed during historical period

Month	CCSM4			CNRM-CM5			MPI-ESM-LR			NorESM1-M			Ensemble		
	SURQ	LATQ	GWQ	SURQ	LATQ	GWQ	SURQ	LATQ	GWQ	SURQ	LATQ	GWQ	SURQ	LATQ	GWQ
Jan	0.1	1.5	3.9	0.5	2.0	5.1	0.3	1.0	6.0	0.4	1.3	4.8	0.0	0.9	7.9
Feb	3.5	3.0	0.7	0.6	2.0	1.0	6.0	2.6	1.3	1.6	3.6	1.2	0.6	2.2	2.3
Mar	18.8	11.2	2.2	10.1	6.8	1.2	10.9	10.0	3.9	19.2	14.6	3.1	3.1	9.5	1.9
Apr	46.0	22.9	9.5	31.2	20.2	4.7	32.2	20.8	9.3	43.8	32.3	16.6	14.1	28.4	11.5
May	90.0	41.1	19.5	89.8	38.6	19.1	74.5	42.3	19.7	54.7	43.1	32.6	36.0	55.9	38.5
Jun	138.8	56.5	40.5	154.9	59.5	40.5	122.5	56.1	40.4	157.0	71.7	55.0	76.0	86.5	77.0
Jul	150.1	66.8	66.8	170.6	67.3	66.6	132.7	63.3	64.0	129.6	76.5	86.2	76.5	94.9	115.1
Aug	97.0	50.9	73.5	127.6	59.4	80.5	132.2	60.2	79.8	59.6	48.9	86.3	48.1	73.7	121.4
Sep	46.8	33.9	62.6	62.9	36.3	69.8	85.5	44.2	72.4	59.2	38.7	71.6	25.9	50.1	102.3
Oct	17.2	14.8	45.4	16.7	18.8	51.9	20.5	19.6	55.9	5.9	14.7	49.7	3.8	19.1	72.7
Nov	0.8	1.5	22.7	3.3	3.4	27.3	5.7	4.2	31.0	1.2	1.7	25.5	0.8	2.4	37.0
Dec	0.5	0.5	10.5	0.1	0.3	12.7	0.3	0.5	14.5	0.0	0.3	12.0	0.0	0.2	17.6
Annual	**609.9**	**304.5**	**357.7**	**668.2**	**314.6**	**380.4**	**623.3**	**324.9**	**398.3**	**532.3**	**347.4**	**444.4**	**284.9**	**423.9**	**605.3**

All units in mm

(a)

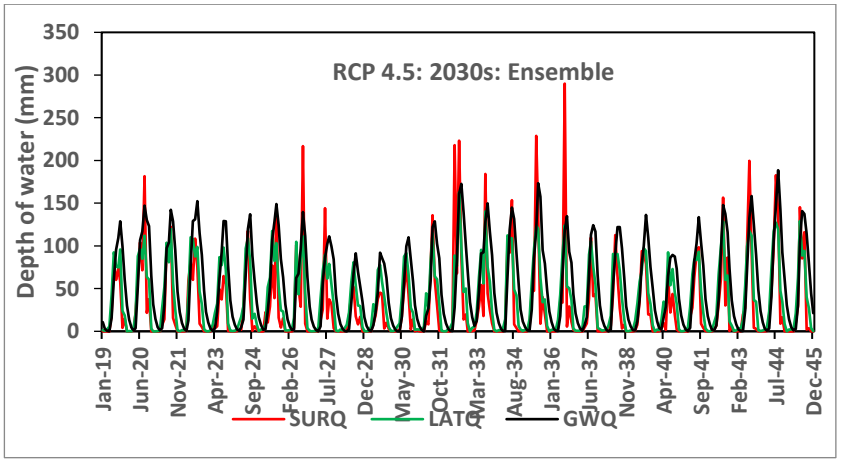

(b)

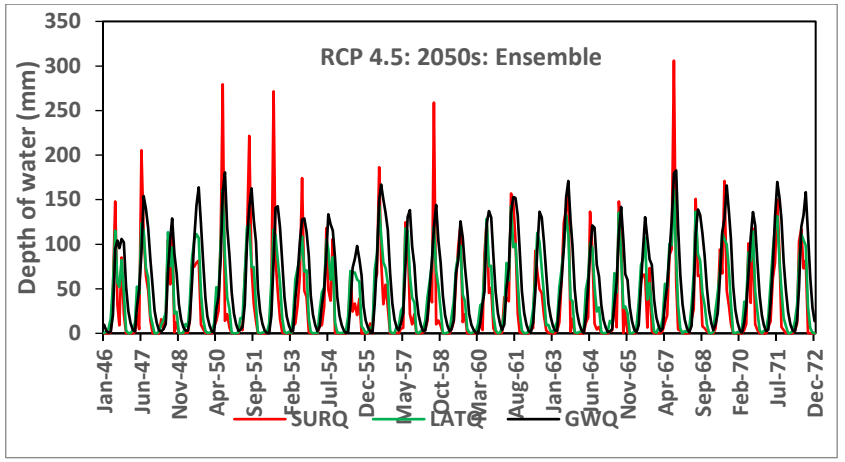

(c)

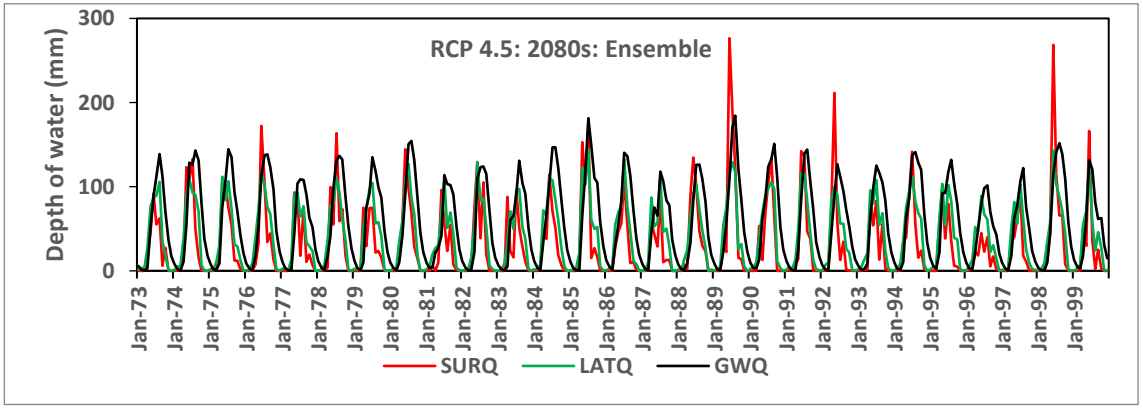

Fig. 4.22 SURQ, LATQ and GWQ in the Pare watershed during under RCP 4.5 projection for (a) near (b) mid, and (c) far future periods

(a)

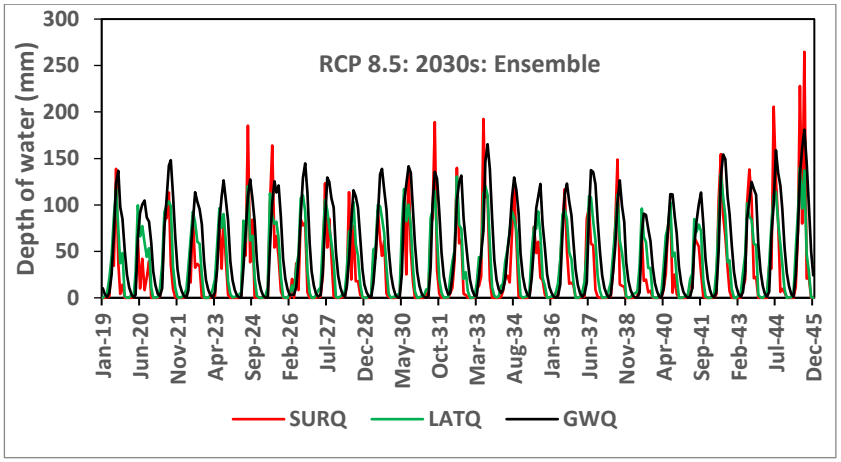

(b)

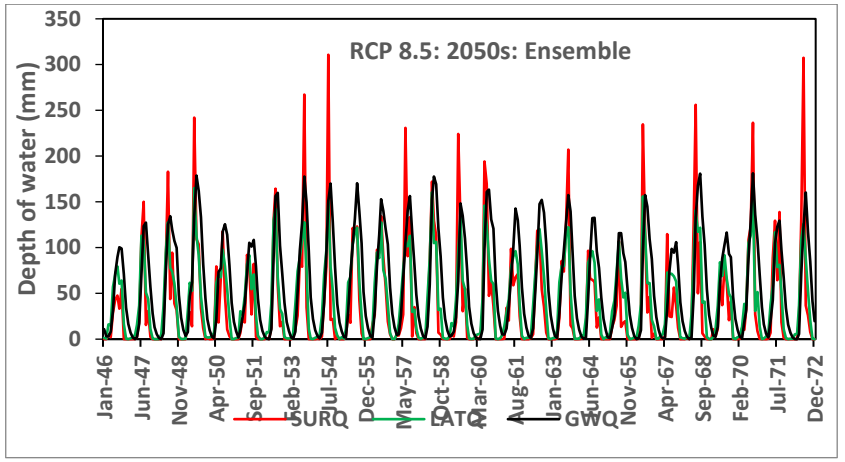

(c)

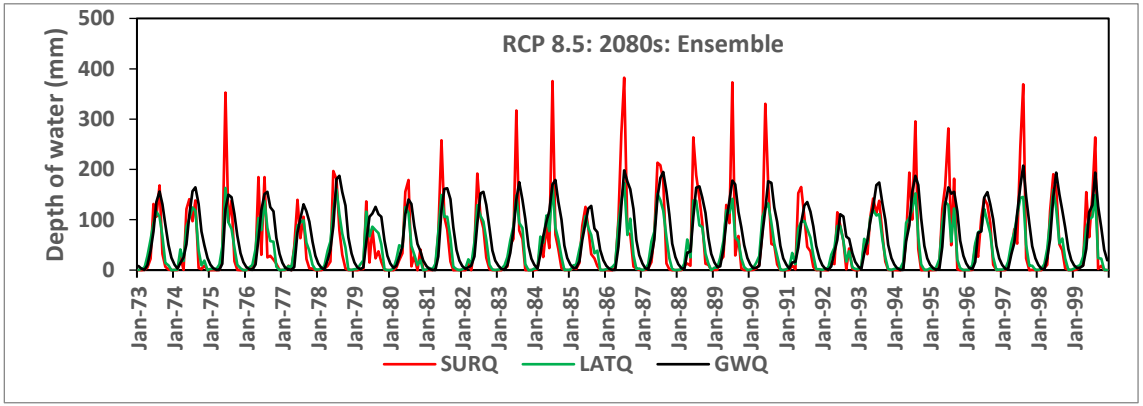

Fig. 4.23 SURQ, LATQ and GWQ in the Pare watershed during under RCP 8.5 projection for (a) near (b) mid, and (c) far future periods

Table 4.23 Seasonal variation of SURQ, LATQ and GWQ in Pare watershed during future periods (all units in mm)

Month	RCP 4.5: 2030s			RCP 4.5: 2050s			RCP 4.5: 2080s		
	SURQ	LATQ	GWQ	SURQ	LATQ	GWQ	SURQ	LATQ	GWQ
Jan	0.0	1.1	9.4	0.0	1.1	9.9	0.0	1.1	9.5
Feb	0.1	1.5	2.8	0.6	3.1	3.0	0.1	2.8	2.9
Mar	2.2	6.5	1.2	4.9	12.1	2.8	1.2	7.6	1.1
Apr	12.3	26.4	7.9	14.1	38.4	18.6	28.8	41.3	15.4
May	42.1	61.9	39.1	45.1	61.2	47.2	62.6	74.5	56.2
Jun	80.7	91.1	82.2	108.4	104.1	93.7	103.3	93.3	95.5
Jul	106.4	98.5	118.0	113.0	106.5	132.2	91.7	101.2	128.8
Aug	71.9	83.5	133.6	66.0	81.1	140.2	49.9	75.9	129.6
Sep	21.1	48.6	108.9	29.2	53.8	113.7	26.6	51.4	107.7
Oct	8.4	26.0	78.8	8.4	24.4	83.1	10.5	28.2	81.4
Nov	1.6	4.8	43.5	0.3	3.8	44.3	0.5	4.1	44.1
Dec	0.1	0.2	21.0	0.0	0.2	21.5	0.0	0.4	21.5
Annual	**346.8**	**450.0**	**646.4**	**389.9**	**489.9**	**710.5**	**375.2**	**481.8**	**693.6**
Month	**RCP 8.5: 2030s**			**RCP 8.5: 2050s**			**RCP 8.5: 2080s**		
	SURQ	LATQ	GWQ	SURQ	LATQ	GWQ	SURQ	LATQ	GWQ
Jan	0.0	0.6	9.8	0.0	0.8	10.2	0.0	1.4	10.7
Feb	0.1	2.3	3.2	0.8	2.2	3.1	0.7	3.4	3.4
Mar	2.4	6.9	1.3	3.1	9.6	2.0	9.1	16.5	5.4
Apr	10.4	25.7	8.1	14.8	32.7	13.1	12.9	32.5	17.8
May	47.1	61.0	37.9	48.7	63.1	43.4	79.8	77.4	51.3
Jun	91.9	93.5	82.9	125.4	105.0	93.8	155.9	112.8	107.1
Jul	82.1	95.5	119.1	115.1	108.1	134.0	173.6	122.4	153.2
Aug	70.3	82.0	128.3	84.3	87.4	143.9	107.6	93.2	160.7
Sep	29.7	54.0	109.7	32.7	53.2	117.1	42.9	60.9	128.2
Oct	7.9	28.7	84.2	12.5	29.5	88.1	7.1	25.0	93.9
Nov	0.8	4.0	45.5	0.8	3.3	46.5	3.1	4.5	48.9
Dec	0.0	0.1	22.0	0.0	0.3	22.6	0.0	0.4	24.0
Annual	**342.6**	**454.5**	**652.1**	**438.3**	**495.2**	**717.8**	**592.8**	**550.4**	**804.5**

Table 4.24 shows the percentage change in seasonal and annual mean SURQ, LATQ, and GWQ in future years as a result of the ensemble of the four climate models compared to the historical period. All three of these components are predicted to increase in the majority of the

months. In general, changes are found to be larger for RCP 8.5 than RCP 4.5, and also greater in the far future, especially during monsoon season. Under RCP 4.5, changes in the SURQ, LATQ, and GWQ during monsoon season were observed to be positive in the mid (2050s) and far (2080s), implying increasing magnitudes than in the historical period. All monsoon months except September during near future period under RCP 4.5 are also found increasing in magnitude. Under the RCP 8.5 scenario, no monsoon and post monsoon months are observed to have decreasing SURQ, LATQ, or GWQ at all time periods. Negative values in Table 4.24, indicating decrease in magnitude of corresponding streamflow components were observed mostly in winter months (December to February) as well as in pre monsoon months to some extent. These observations are indications that future hydrological scenario in the Pare watershed will be accompanied by intense flooding (high runoff peaks) associated with longer dry spells leading to conservation needs.

According to the RCP 4.5 scenario, the mean annual SURQ is expected to rise by 21.7 percent, 36.8 percent, and 31.7 percent in the 2030s, 2050s, and 2080s, respectively, over the historical period. LATQ is predicted to rise by 6.2 percent, 15.6 percent, and 13.7 percent over its historical period, whereas GWQ is expected to rise by 6.8 percent, 17.4 percent, and 14.6 percent in the 2030s, 2050s, and 2080s, respectively. These changes were exaggerated in the RCP 8.5 scenario, particularly for the SURQ component in which it is expected to increase by a whopping 108.1 percent over its annual historical surface runoff.

Table 4.24 Percentage change in long-term monthly averaged SURQ, LATQ and GWQ in Pare watershed during future periods w.r.t. historical period (all units in percentage)

Month	RCP 4.5: 2030s			RCP 4.5: 2050s			RCP 4.5: 2080s		
	SURQ	LATQ	GWQ	SURQ	LATQ	GWQ	SURQ	LATQ	GWQ
Jan	91.4	22.2	18.1	177.8	24.0	24.4	103.7	16.6	19.6
Feb	-88.6	-30.7	25.2	-3.9	39.4	33.9	-83.4	25.7	26.1
Mar	-30.7	-31.9	-38.4	56.7	26.7	46.9	-61.0	-19.9	-43.0
Apr	-13.1	-7.0	-31.3	-0.3	35.3	62.7	103.9	45.4	34.3
May	17.0	10.7	1.6	25.3	9.5	22.8	73.9	33.3	46.0
Jun	6.2	5.3	6.7	42.6	20.4	21.7	35.9	7.9	24.0
Jul	39.1	3.8	2.5	47.7	12.2	14.8	19.9	6.7	11.9
Aug	49.3	13.3	10.0	37.1	10.2	15.5	3.6	3.1	6.7
Sep	-18.5	-3.1	6.4	12.6	7.3	11.1	2.5	2.5	5.2
Oct	122.1	35.6	8.4	120.4	27.6	14.4	177.1	47.2	12.1
Nov	111.2	99.1	17.5	-57.4	58.8	19.8	-30.5	69.7	19.1
Dec	1083.0	-0.1	19.0	-93.5	-36.2	22.1	30.7	46.1	22.2
Annual	21.7	6.2	6.8	36.8	15.6	17.4	31.7	13.7	14.6
Month	**RCP 8.5: 2030s**			**RCP 8.5: 2050s**			**RCP 8.5: 2080s**		
	SURQ	LATQ	GWQ	SURQ	LATQ	GWQ	SURQ	LATQ	GWQ
Jan	-44.4	-38.6	23.6	-25.9	-8.8	28.9	196.3	50.1	34.6
Feb	-87.4	4.5	41.5	37.7	1.5	35.6	12.0	53.4	48.5
Mar	-22.8	-27.0	-33.3	0.7	0.7	2.1	194.3	73.4	181.7
Apr	-26.8	-9.4	-29.2	4.4	15.1	14.5	-8.5	14.5	55.2
May	30.9	9.2	-1.4	35.4	12.8	12.8	121.9	38.5	33.4
Jun	20.9	8.1	7.6	65.0	21.4	21.8	105.1	30.3	39.0
Jul	7.4	0.6	3.4	50.4	13.9	16.4	127.0	29.1	33.1
Aug	45.9	11.3	5.7	75.2	18.6	18.5	123.6	26.5	32.3
Sep	14.7	7.8	7.2	26.2	6.1	14.5	65.5	21.5	25.3
Oct	107.1	50.1	15.8	229.8	54.4	21.2	87.0	30.6	29.3
Nov	5.9	67.2	23.0	6.8	36.3	25.6	307.8	86.8	32.1
Dec	-100.0	-55.3	25.0	730.1	12.6	28.2	226.8	75.4	35.8
Annual	20.2	7.2	7.7	53.8	16.8	18.6	108.1	29.8	32.9

4.4 Hydrological Modelling of SWAT Model in Dudhnai Watershed

4.4.1 Precipitation regime during calibration and validation periods in Dudhnai

The yearly rainfall variation in Dudhnai watershed from 2005 to 2019 is shown in Fig. 4.24. The mean rainfall in the study area was observed as 2362 mm. In the years of 2005, 2008, 2010 2014, 2015, 2017 and 2019, the annual rainfall was above average while in the years- 2006, 2007, 2009, 2011, 2012, 2013, 2016 and 2018, the annual rainfall was below average. The maximum rainfall of 3432 mm was occurred in the year 2015 which accounted an excess rainfall of 1070 mm over the annual average rainfall in the Dudhnai watershed. While the least rainfall amount is observed in the year- 2006 in which the annual rainfall is 1662 mm accounting a deficit of 700 mm. This signifies that the rainfall variation in the study area is huge.

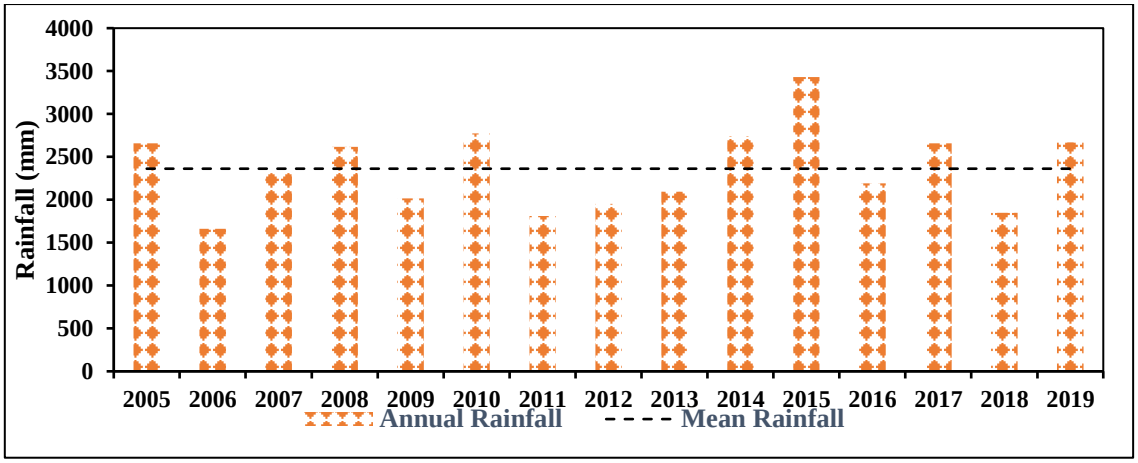

Fig. 4.24 Yearly rainfall variation in Dudhnai watershed

The monsoon rainfall variation in Dudhnai watershed from 2005 to 2019 is shown in Fig. 4.25. In the present study, the months of June, July, August and September were considered as monsoon season. The mean monsoon rainfall in the study area was observed as 1552 mm which was 66 percent of the annual average rainfall. Fig. 4.25 also shows the percentage contribution of monsoon to annual rainfall in each year from 2005 to 2019. The contribution of monsoon to the annual rainfall ranged from 49.32 percent in 2010 to 76.23 percent in 2015. In the years-2012 and 2014, the contribution of monsoon rainfall to annual rainfall is found over 70 percent.

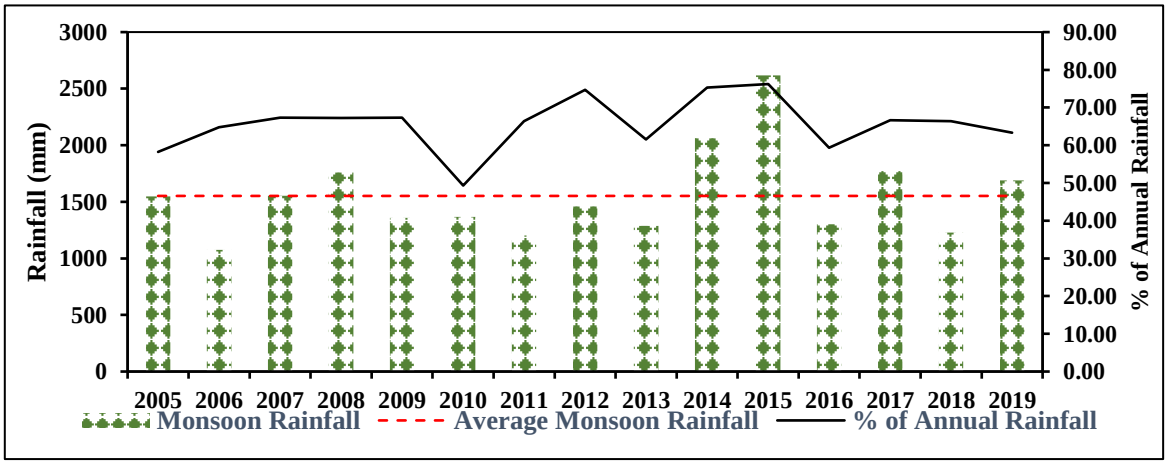

Fig. 4.25 Monsoon rainfall variation in Dudhnai watershed

Monthly variation of rainfall in Dudhnai watershed is shown in Fig. 4.26. It was observed that rainfall regime in the study area was dominated by Indian summer monsoon which occurred during June to September. It is also observed that, there were considerable amount of rainfall in the pre-monsoon season (March-May). It is interesting to mention that the combine rainfall during pre-monsoon and monsoon season i.e., from March to September, contributed more

than 90 percent of the total annual rainfall amount in the study area. In the other two seasons, other than the month of October, there were very low rainfall.

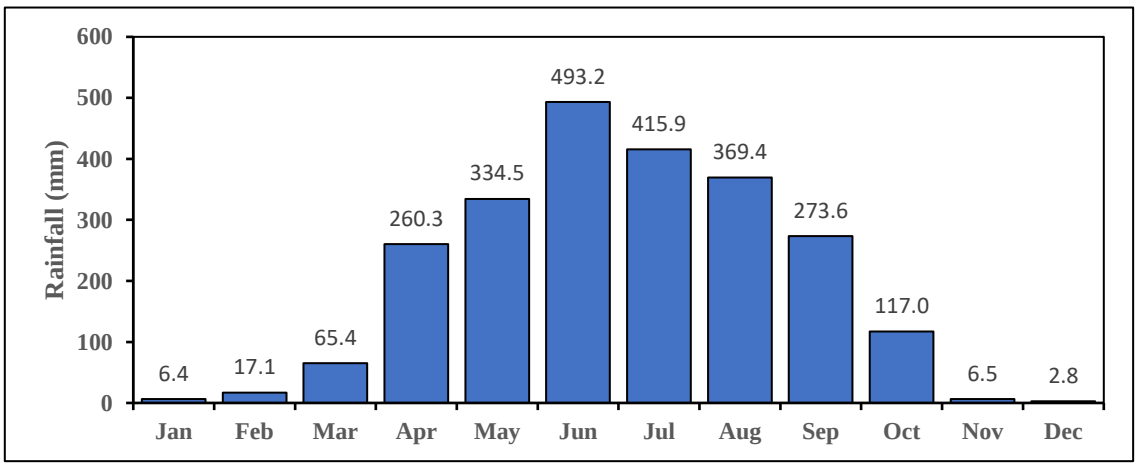

Fig. 4.26 Monthly variation of precipitation in Dudhnai watershed during 2005-2019

The percent departure of annual rainfall from the normal in the Dudhnai watershed is shown in Fig. 4.27. The analysis revealed that 2005, 2008, 2010, 2014, 2015, 2017 and 2019 are rainfall surplus years while in the remaining years the rainfall was deficit. The wettest year was found as 2015 in which there was a surplus rainfall of more than 45 percent of normal while the driest year is found as the year 2006 that has a deficit rainfall of more than 29 percent. It can be seen that during calibration period (2005-2014), the rainfall regime in the study area is dominated by deficit years while during validation period (2015-2019), it is dominated by surplus years.

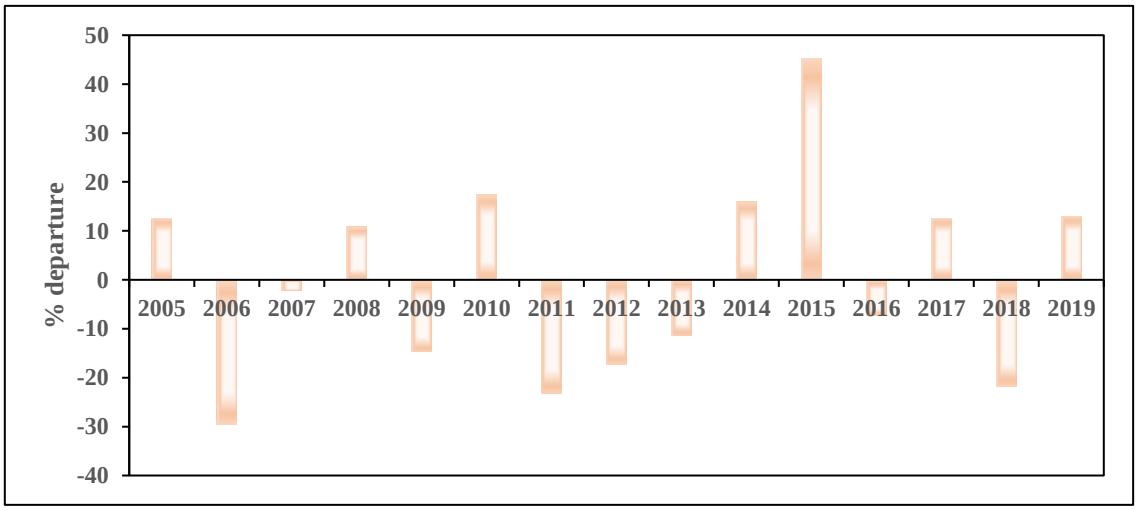

Fig. 4.27 Percent departure of annual rainfall from normal in Dudhnai watershed

4.4.2 Precipitation regime in Dudhnai watershed according to NEX-GDDP

The mean annual rainfall of each of the models and their ensembles during baseline and three

different future periods under RCPs 4.5 and 8.5 are illustrated in Table 4.25. Also, the percentage changes of the climate models in future periods w.r.t. baseline (1976-2005) are also illustrated in Table 4.25. There was a clear indication that, the general trend of annual rainfall in the study area was projected to increase in the future. Also, the projections were projected higher under RCP 8.5 scenarios as compared to RCP4.5 scenarios. The mean annual rainfall given by CCSM4, CNRM-CM5, MPI-ESM-LR, NorESM1-M and their ensemble during the baseline era were found as 3083.1 mm, 3050.5 mm, 3115.9 mm, 3060.7 mm, and 3077.5 mm, respectively. Of all the future scenarios, near future period of the climate model CNRM-CM5 under RCP 4.5 was seen to have lesser mean annual rainfall than its baseline period. In this particular scenario, it was projected to decrease in mean annual rainfall to the amount of just 0.5 percent lesser than the baseline. The ensemble climate model under RCP 4.5 were projected to be 4.9, 9.0, and 13.8, percent higher than the baseline mean during 2030s (near future), 2050s (mid future) and 2080s (far future), respectively. While under RCP 8.5, it projected to be 6.4, 10, and 23, percent higher than the historical mean during 2030s, 2050s and 2080s, respectively. Analyzing the percentage changes in rainfall in each month of the year w.r.t. the baseline period suggested that significant amount of rainfall increase was observed during monsoon as well as pre-monsoon season. On the other hand, decrease in rainfall was generally observed during months of November-March. These observations suggested that, the precipitation pattern in the watershed would witness shrinking of rainy days with higher intensity rainfall during monsoon and pre-monsoon seasons. The above observations can be interpreted from the percentage changes in future periods w.r.t. historical period in seasonal rainfall in the Dudhnai watershed, as illustrated in Table 4.26 (near future period), Table 4.27 (mid future period), and Table 4.28 (far future period).

Table 4.25 Mean annual rainfall of climate models in Dudhnai watershed and their percentage change w.r.t. baseline period

		CCSM4	% Change	CNRM-CM5	% Change	MPI-ESM-LR	% Change	NorESM1-M	% Change	Ensemble	% Change
Historical		3083.1	-	3050.5	-	3115.9	-	3060.7	-	3077.5	-
RCP 4.5	Near	3237.0	5.0	3036.1	-0.5	3345.0	7.4	3300.5	7.8	3229.7	4.9
	Mid	3478.0	12.8	3270.3	7.2	3244.1	4.1	3425.1	11.9	3354.4	9.0
	Far	3522.8	14.3	3887.9	27.5	3187.8	2.3	3408.5	11.4	3501.7	13.8
RCP 8.5	Near	3343.5	8.4	3156.8	3.5	3526.1	13.2	3070.1	0.3	3274.1	6.4
	Mid	3449.4	11.9	3575.3	17.2	3175.7	1.9	3339.9	9.1	3385.1	10.0
	Far	3936.5	27.7	3523.1	15.5	3620.7	16.2	4065.2	32.8	3786.4	23.0

Table 4.26 Percentage change in mean monthly rainfall of climate models in Dudhnai watershed w.r.t. baseline period during near future period

	RCP 4.5					RCP 8.5				
Month	**Ensemble**	**CCSM4**	**CNRM-CM5**	**MPI-ESM-LR**	**Nor-ESM1-M**	**Ensemble**	**CCSM4**	**CNRM-CM5**	**MPI-ESM-LR**	**Nor-ESM1-M**
Jan	41.0	72.6	33.3	7.1	37.0	-18.5	-1.1	-16.2	-18.6	-34.9
Feb	-17.7	-6.2	75.4	-21.1	-58.4	-38.1	-14.5	-43.3	-21.0	-57.3
Mar	-20.6	-25.2	22.5	-18.4	-35.0	-26.5	-14.7	-51.5	0.0	-37.5
Apr	-17.6	2.3	-17.3	-41.2	-17.0	-22.3	-23.9	-12.2	-23.7	-26.8
May	-0.4	-23.5	-4.9	-18.8	58.9	11.1	19.9	-2.3	0.3	28.9
Jun	9.9	13.0	-11.4	40.0	1.4	6.5	4.7	-9.0	24.5	7.2
Jul	8.5	24.6	-6.7	16.3	1.0	-1.1	3.6	-3.6	10.3	-15.2
Aug	10.4	4.8	-3.1	5.9	41.2	20.2	25.7	11.0	28.7	14.4
Sep	8.5	17.6	25.0	5.1	-9.9	30.5	36.5	57.5	19.7	14.3
Oct	22.3	-3.4	63.3	16.1	4.6	12.3	-25.2	41.9	23.0	-1.4
Nov	-15.2	8.2	-42.1	13.3	-23.4	-20.7	64.2	-39.6	-25.8	-24.0
Dec	-35.1	-67.8	-40.8	-49.6	-7.7	-56.8	-73.5	-69.4	-55.4	-38.9

Table 4.27 Percentage change in mean monthly rainfall of climate models in Dudhnai watershed w.r.t. baseline period during mid future period

	RCP 4.5					RCP 8.5				
Month	Ensemble	CCSM4	CNRM-CM5	MPI-ESM-LR	Nor-ESM1-M	Ensemble	CCSM4	CNRM-CM5	MPI-ESM-LR	Nor-ESM1-M
Jan	28.8	34.1	40.6	-18.6	43.9	-4.7	-23.5	90.3	-31.3	-30.9
Feb	0.9	28.4	15.6	-33.7	-5.0	-8.7	44.9	-2.4	-29.7	-32.7
Mar	5.1	44.2	-4.0	-14.4	-16.6	-10.1	11.6	-1.5	-40.8	-19.3
Apr	0.4	-0.3	18.0	-25.3	9.2	0.5	30.2	12.7	-41.2	-1.7
May	0.9	-17.0	-5.3	-21.2	60.1	2.9	-6.5	-11.1	-13.6	52.6
Jun	9.2	22.2	-10.4	-1.2	23.5	10.2	12.4	8.0	6.0	13.6
Jul	21.1	54.0	15.9	20.2	-5.0	11.1	23.0	21.1	-2.2	2.0
Aug	7.9	-12.0	7.7	25.9	7.4	19.6	6.0	24.8	35.0	7.9
Sep	11.0	20.1	35.2	1.9	-7.2	13.7	33.7	38.4	-10.1	1.6
Oct	7.8	-30.2	32.6	24.5	-7.0	24.2	-30.3	59.0	54.4	-5.1
Nov	-25.6	-47.5	-39.9	1.6	-30.0	-10.1	-37.0	47.8	-44.5	-57.9
Dec	11.9	101.6	36.9	49.3	-67.8	50.8	-75.9	312.3	155.5	8.0

Table 4.28 Percentage change in mean monthly rainfall of climate models in Dudhnai watershed w.r.t. baseline period during far future period

	RCP 4.5					RCP 8.5				
Month	Ensemble	CCSM4	CNRM-CM5	MPI-ESM-LR	Nor-ESM1-M	Ensemble	CCSM4	CNRM-CM5	MPI-ESM-LR	Nor-ESM1-M
Jan	38.6	13.6	26.7	-71.3	129.9	51.6	85.6	43.5	-49.3	83.6
Feb	46.6	152.5	89.9	-57.2	15.4	43.3	102.3	83.1	-65.4	42.9
Mar	-13.8	16.7	-26.7	8.2	-43.9	39.1	45.9	24.3	-4.4	57.4
Apr	40.1	70.6	36.6	-2.7	49.5	3.1	18.5	14.8	-50.9	24.2
May	24.9	21.5	36.1	-22.4	75.2	19.8	7.9	38.8	-26.1	70.9
Jun	6.6	18.9	-5.3	8.5	4.4	22.0	47.6	-16.5	9.6	43.4
Jul	15.8	17.5	37.7	4.7	1.5	27.2	54.6	7.4	20.5	29.4
Aug	5.5	-0.4	11.8	7.9	1.1	33.8	25.0	28.6	46.2	34.7
Sep	0.9	-32.9	50.2	7.8	-17.9	24.4	-3.3	48.4	76.8	-29.8
Oct	34.6	-26.2	120.5	24.2	1.6	7.8	-40.1	7.1	30.7	29.0
Nov	-18.7	-54.8	9.9	-20.6	-55.5	-5.8	-65.1	33.1	7.0	-77.9
Dec	58.4	42.8	51.7	29.6	75.3	22.2	48.1	136.9	-72.7	-43.4

4.4.3 Sensitivity analysis in SWAT in Dudhnai watershed

Sensitivity analysis were performed on these 15 SWAT model parameters during the calibration process in SWAT-CUP. After assigning initial ranges of the 15 model parameters, an iteration of 300 simulations were performed. The rankings of the 15 model parameters are displayed in Table 4.29. The results revealed that curve number (CN2) as the most sensitive parameter in simulating streamflow in Dudhnai River. Based on p-value and t-stat, curve number (CN2), channel hydraulic conductivity (CH_K2), and recession constant of bank (ALPHA_BNK) were the three most sensitive parameters. CN2 and CH_K2 are two model parameters which strongly influence the peaks of hydrograph. CN2 is a dimensionless quantity that is linked to the permeability of soil, land usage, and previous moisture conditions. Reduced surface runoff and increased infiltration were the results of a low CN value. Other sensitive variables like ALPHA_BNK, GWQMN, GW_REVAP, and REVAPMN have a big impact on the hydrograph's low flows (baseflow components).

4.4.4 Calibration of streamflow in SWAT model

Prior to calibration, SWAT was unable to simulate discharge satisfactorily with very low Nash Sutcliffe Efficiency (NSE) as the peak discharge and baseflow are highly overestimated particularly during the monsoon season. SWAT model was calibrated using observed streamflow at the outlet of the Dudhnai watershed for a period of ten years (2005-2014). The parameter range (minimum and maximum) and the method of parameter modification are illustrated in Table 4.30. Two modification methods viz. replace and relative, were employed in the calibration. Fifteen model parameters were modified in the calibration process. Best fit set of parameters was selected out of the three iterations of 300 sets of parameters based on the best Nash-Sutcliffe values. The best-fitted values (calibrated model parameters) of the 15 SWAT model parameters are shown in Table 4.30.

Table 4.29 Sensitivity ranks of the SWAT model parameters in Dudhnai watershed

Parameter	p-value	t-stat	Rank
CN2.mgt	0.000	-19.66	**1**
CH_K2.rte	0.000	18.22	**2**
ALPHA_BNK.rte	0.000	-6.71	**3**
CH_N2.rte	0.071	-1.81	**4**
SLSOIL.hru	0.120	1.56	**5**
REVAPMN.gw	0.202	-1.28	**6**
GW_REVAP.gw	0.207	-1.26	**7**
GW_DELAY.gw	0.229	1.21	**8**
SURLAG.bsn	0.305	-1.03	**9**
SOL_AWC(..).sol	0.355	0.93	**10**
SOL_K(..).sol	0.545	0.61	**11**
ESCO.hru	0.749	-0.32	**12**
OV_N.hru	0.858	0.18	**13**
GWQMN.gw	0.871	0.16	**14**
ALPHA_BF.gw	0.920	0.10	**15**

Table 4.30 Parameter range, parameter change method and fitted model parameter values in SWAT-CUP

Sl. No.	Parameter	Minimum	Maximum	Fitted Value	Method
1.	CN2.mgt	-0.3891	0.0038	-0.2915	Relative
2.	ALPHA_BF.gw	0.3340	1.0000	0.8590	Replace
3.	GW_DELAY.gw	0.0000	270.9827	86.2628	Replace
4.	GWQMN.gw	771.2238	2315.4429	830.4188	Replace
5.	ESCO.hru	0.6006	0.8603	0.6487	Replace
6.	SOL_AWC(..).sol	-0.0118	0.3651	0.0065	Relative
7.	SOL_K(..).sol	-0.0566	0.4306	0.0303	Relative
8.	CH_N2.rte	0.1489	0.3000	0.1824	Replace
9.	CH_K2.rte	29.5850	109.9150	105.2290	Replace
10.	GW_REVAP.gw	0.0681	0.1645	0.1258	Replace
11.	REVAPMN.gw	126.9777	381.3557	255.4386	Replace
12.	ALPHA_BNK.rte	0.4006	1.0000	0.9870	Replace
13.	OV_N.hru	0.1296	0.3689	0.2584	Replace
14.	SLSOIL.hru	22.0922	107.4078	88.7806	Replace
15.	SURLAG.bsn	0.0500	2.7200	0.7308	Replace

Fig. 4.28 depicts daily time series plots of observed and simulated runoffs in the SWAT model for the calibration period (2005-2014). Fig. 4.29 depicts the monthly fluctuation of observed and simulated runoffs throughout the same time period. The model reflects the runoff changes reasonably well, according to a qualitative comparison of observed and simulated daily and monthly runoff. In this watershed also, the model's simulated discharge matches the rainfall pattern

better than the measured runoff. Although the peaks of the simulated and actual runoffs differ somewhat, their volumes are nearly identical. Table 4.31 shows the model performance indicators for the constructed SWAT model in the Dudhnai watershed during calibration period.

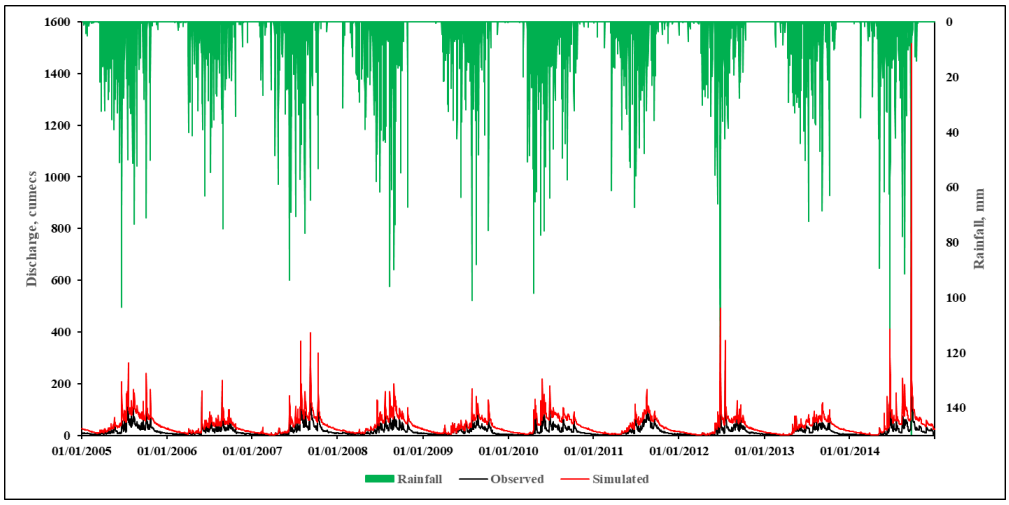

Fig. 4.28 Daily variation of observed and simulated discharge in SWAT model for Dudhnai River during calibration period

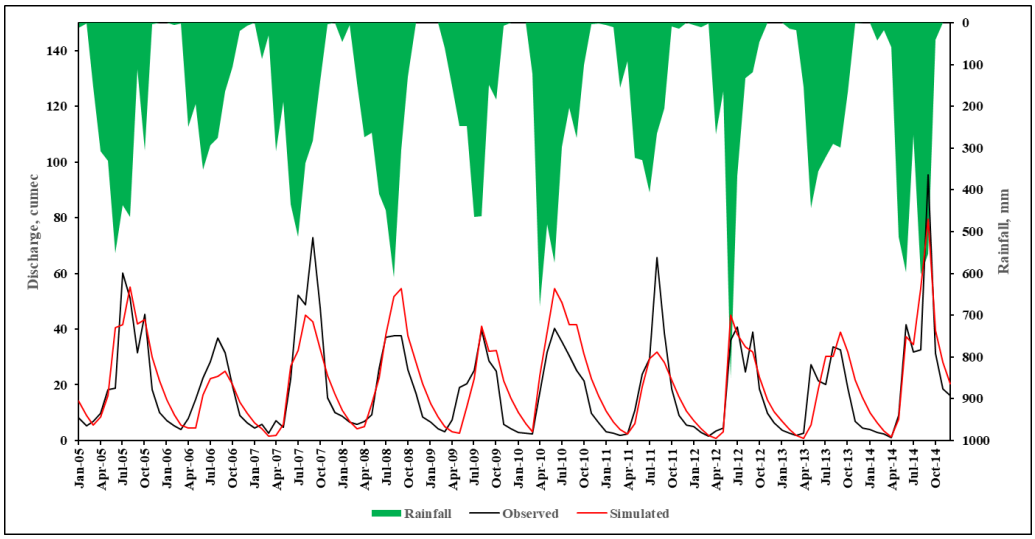

Fig. 4.29 Monthly variation of observed and simulated discharge in SWAT model for Dudhnai River during calibration period

Scatter plot between the observed and simulated runoff is shown in Fig. 4.30 along with the 1:1 line. The plot shows R^2 value of 0.55 which is reasonably good for mountainous watersheds. It

implies that the constructed SWAT model for the Dudhnai watershed was able to explain almost 55% of the actual runoff variation. Comparing the data points with the 1:1 line revealed good model performance, however, some dispersions of points were also observed. As mentioned earlier, a hydrological model be considered suitable if the NSE is greater than 0.50, the PBIAS is less than 25%, and R^2 values greater than 0.50. Based on these, the SWAT model developed in the Dudhnai watershed functioned satisfactorily on daily and monthly timesteps. The SWAT model was found to be 54 percent and 70 percent efficient at daily and monthly timesteps, respectively. The SWAT model's PBIAS was calculated to be -9.7 and -10 for daily and monthly timesteps, respectively, showing that the discharge was overestimated by the SWAT model. At daily and monthly timesteps, the standard error of estimates (SEE) was calculated to be 20.31 cumecs and 9.33 cumecs, respectively. For daily and monthly timesteps, the coefficient of determination (R^2) values was estimated to be 0.55 and 0.72, respectively, demonstrating moderately good model prediction.

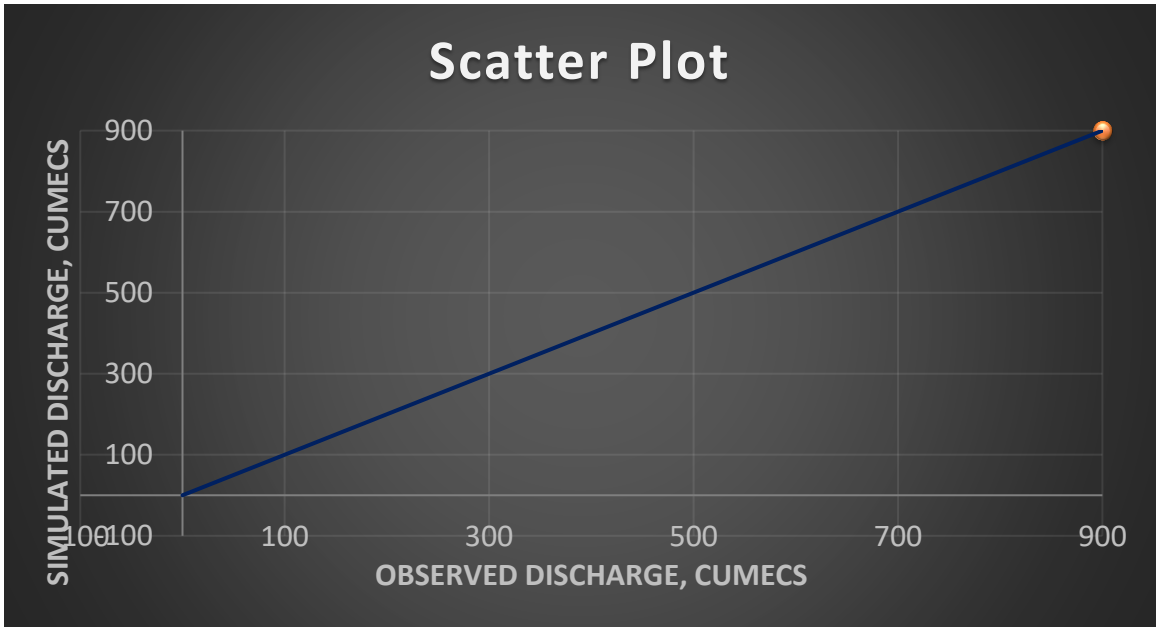

Fig. 4.30 Scatter plot between daily observed and simulated discharge during calibration period in SWAT model

Table 4.31 SWAT model performance indices for daily and monthly timesteps during calibration in Dudhnai watershed

Performance Indicators	Timestep	
	Daily	Monthly
NSE	0.54	0.70
R^2	0.55	0.72
PBIAS	-9.7	-10.0
SEE	20.31	9.33

4.4.5 Validation of streamflow in SWAT model

The setup SWAT model was validated for five years, from 2015 to 2019, using the calibrated model parameters in Table 4.30. The measured versus simulated discharge for daily and monthly timescales during validation phase are shown in Figs. 4.31 and 4.32, respectively. The plots revealed that SWAT model overestimated the measured discharge data in the Dudhnai watershed. Fig. 4.33 shows a scatter plot of observed and modelled runoff, as well as the 1:1 line. The figure indicates an R^2 of 0.46, which is fairly good indication.

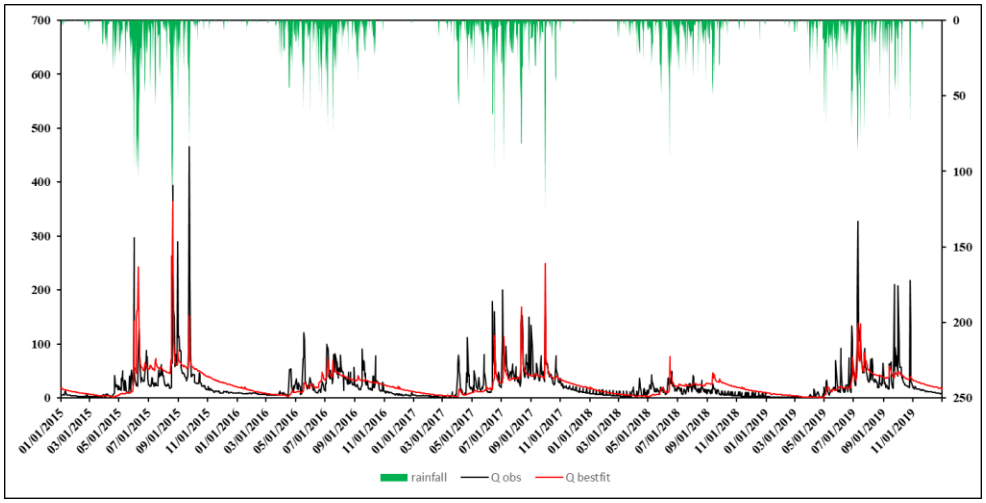

Fig. 4.31 Daily variation of observed vs simulated discharge in SWAT model for Dudhnai River during validation period

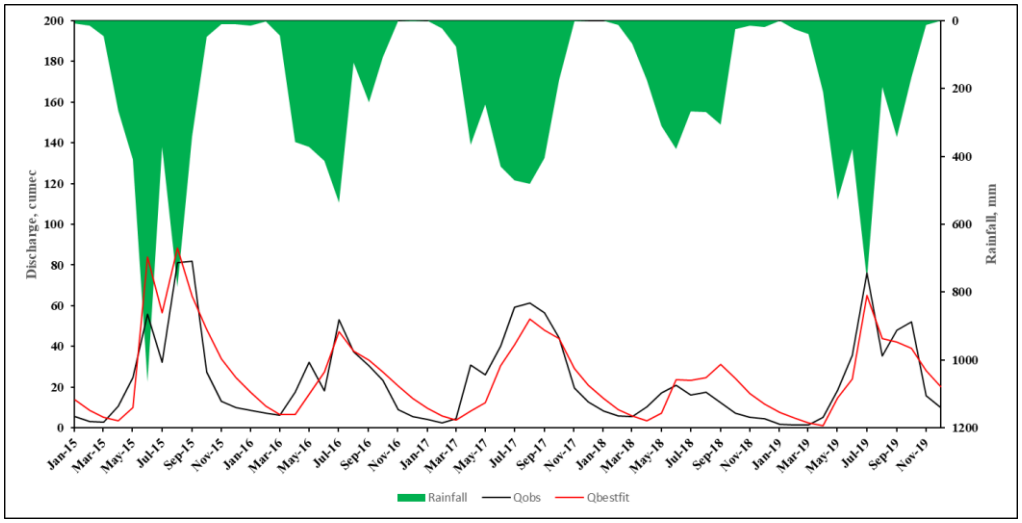

Fig. 4.32 Monthly variation of observed vs simulated discharge in SWAT model for Dudhnai River during validation period

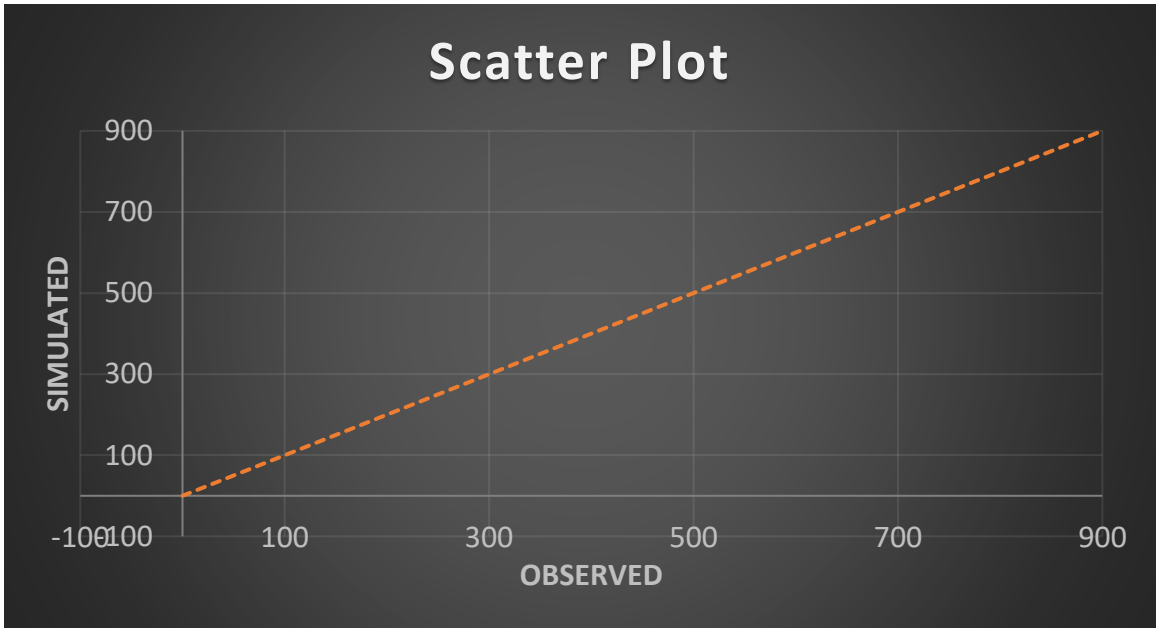

Fig. 4.33 Scatter plot between daily observed and SWAT simulated discharge during validation period

Table 4.32 shows the model performance indicators, which show that the SWAT model performs satisfactorily. On monthly timesteps, the SWAT model constructed in the Dudhnai watershed functioned admirably. The SWAT model's efficiencies were determined to be 44% and 72%, respectively, at daily and monthly timesteps. For daily and monthly timesteps, the SWAT model's

PBIAS was predicted to be -8 percent, indicating that the model overestimated discharge. For daily and monthly timesteps, the standard error of estimates (SEE) was calculated to be 24.34 cumecs and 11.15 cumecs, respectively. During the validation period, the SWAT model's coefficient of determination (R^2) values was estimated to be 0.46 and 0.74 for daily and monthly timesteps, respectively. All of the performance measures indicated that the model was capable to represent the watershed's hydrologic response and simulate the water yield while taking into account streamflow variability.

Table 4.32 SWAT model performance indices for daily and monthly timesteps during validation in Dudhnai watershed

Performance Indicators	Timestep	
	Daily	Monthly
NSE	0.44	0.72
R^2	0.46	0.74
PBIAS	-8.04	-8.0
SEE	24.34	11.15

4.4.6 Uncertainties in SWAT model's prediction of streamflow in Dudhnai watershed

Uncertainty analysis was carried out for the calibration and validation periods in SWAT-CUP. The measures of uncertainties in the prediction were determined from p-factor and r-factor of the 95PPU. The values of these factors achieved during calibration and validation of daily discharge data are illustrated in Table 4.33. Observed discharge, best fit simulated discharge, rainfall and 95PPU uncertainty band of the calibration and validation periods were plotted and shown in Figs. 4.34 and 4.35, respectively.

Table 4.33 Measures of model uncertainties during calibration and validation in Dudhnai

Performance Indicators	Periods	
	Calibration	Validation
p-factor	0.87	0.83
r-factor	0.84	0.89

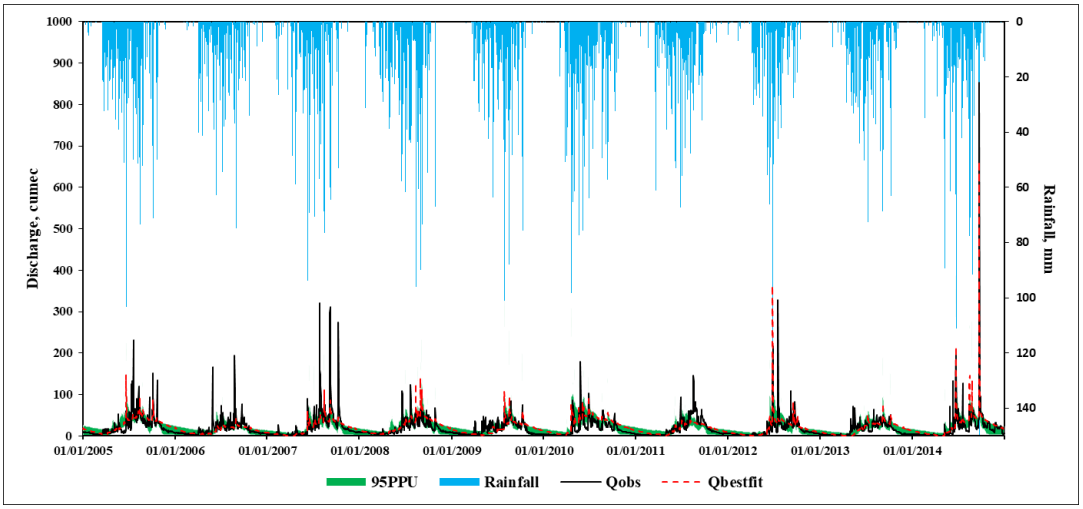

Fig. 4.34 95PPU, rainfall, measured and best fit predicted discharge during calibration in SWAT for Dudhnai watershed

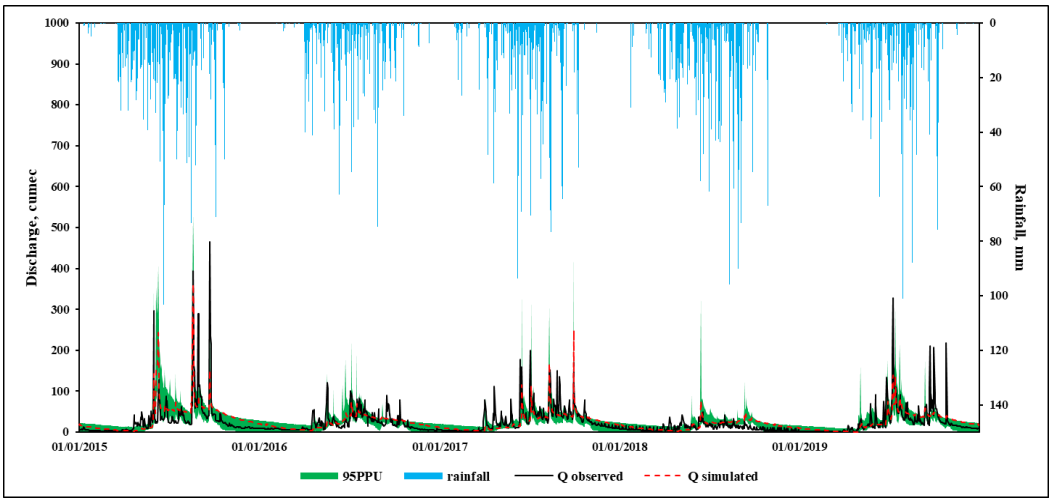

Fig. 4.35 95ppu, rainfall, measured and best fit predicted discharge during validation in SWAT for Dudhnai watershed

The p- factors of the SWAT model during calibration and validation periods were found as 0.87 and 0.83, respectively. It indicates that 87 percent of the measured data was bracketed within the 95ppu band during model calibration and 83 percent during model validation. The average measure of thickness of the 95ppu bands (r-factors) during model training and validation were found as 0.84 and 0.89, respectively. Based on these values, the SWAT model developed for the Dudhnai watershed could be considered satisfactory. Considering studies from Singh et al. (2007), Das *et al.* (2019), Bhattacharya *et al.* (2019), and Singh and Goyal (2017); presence of orographic

effects of precipitation; inadequate rainfall gauging networks; and uncertainties expected from single measurement gauging station data, the results obtained are quite satisfactory.

4.4.7 Projection of future streamflow using SWAT in Dudhnai

Figures 4.36 (a) and (b) show the yearly total runoff in the Dudhnai watershed simulated using five climate models including an ensemble model in SWAT from 1976 to 2005 and from 2019 to 2099 under RCPs 4.5 and 8.5. In comparison to the baseline/historical period, the predicted yearly runoff in the Dudhnai watershed is expected to increase under both RCP 4.5 and RCP 8.5. The amount of projected streamflow increase was found to be greater under RCP 8.5 than under RCP 4.5. Figures 4.37 (a) and (b) demonstrate the relative percentage change in mean annual total runoff simulated by SWAT with respect to historical era under RCPs 4.5 and 8.5. Climate models-CCSM4, CNRM-CM5, MPI-ESM-LR, NorESM1-M, and their ensemble had baseline average annual runoff of 1288.9, 1381.1, 1365.4, 1345.3, and 1343.7 mm, respectively. The highest growth was shown by the NorESM1-M model during the 2080s (far future era) under the RCP 8.5 projection scenarios, with a 42.4 percent increase over its historical period. The reduction in streamflow scenario was seen for the NorESM1-M model (with a reduction of about -1.1 percent over its historical period during near future period under RCP 8.5) and CNRM-CM5 model (with a reduction of about -2.3 percent over its historical period during near future period under RCP 4.5). The percentage change in ensemble discharge revealed a rising trend in streamflow for both RCPs and also increased further as time slice shifts from near to far future periods under RCP 8.5 projection scenarios, indicating a generic rising situation. To ease in understanding the change, the percentage changes in annual runoff for various climate models were illustrated in Table 4.34.

(a) (b)

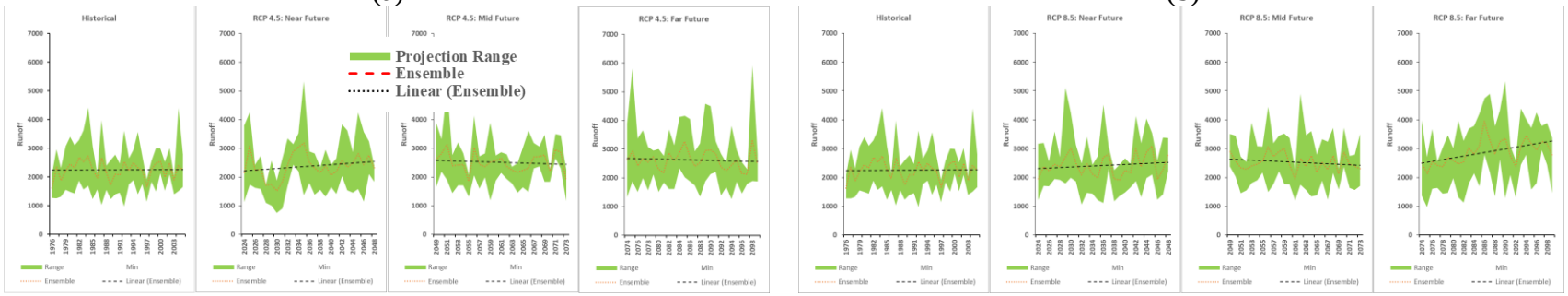

Fig. 4.36 Average yearly discharge projections by ensemble climate in the Dudhnai watershed during (a) RCP 4.5 and (b) RCP 8.5

(a) (b)

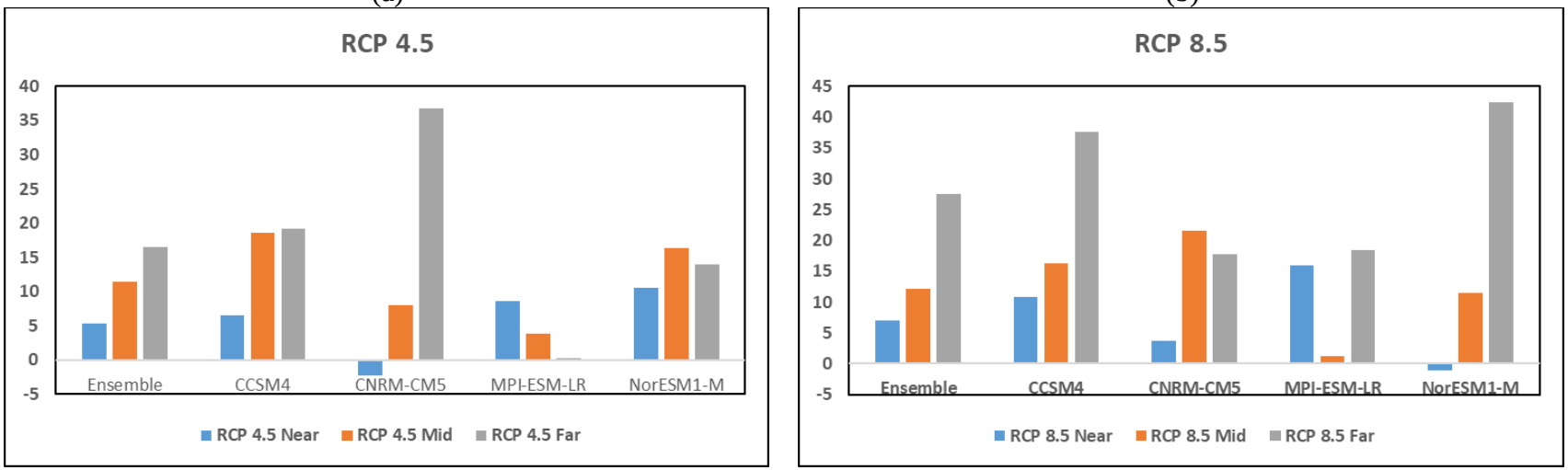

Fig. 4.37 Percentage change of mean annual total w.r.t. historical period for different climate models under (a) RCP 4.5 and (b) RCP 8.5

Table 4.34 Percentage change in annual average runoff simulated by SWAT w.r.t. historical for different climate models in Dudhnai watershed

RCP	Time slabs	CCSM4	CNRM-CM5	MPI-ESM-LR	NorESM1-M	Ensemble
RCP 4.5	**2030s (near)**	6.5	-2.3	8.7	10.5	5.4
	2050s (mid)	18.6	8.0	3.8	16.4	11.4
	2080s (far	19.1	36.8	0.3	14.0	16.6
RCP 8.5	**2030s (near)**	10.8	3.7	16.0	-1.1	7.1
	2050s (mid)	16.3	21.6	1.2	11.5	12.2
	2080s (far)	37.6	17.8	18.4	42.4	27.5

All units in %

Tables 4.35 (near future period), 4.36 (mid future period), and 4.37 (far future period) show the percentage changes in seasonal (monthly variation in a year) w.r.t. historical era. According to the ensemble model, streamflow is anticipated to increase by 13.9, 5.8, 11.2, and 5.5 percent in the near future period under RCP 4.5 during the monsoon months of June, July, August, and September, compared to their historical counterparts. During the same time period, in the RCP 8.5 scenario, streamflow increased by 11.7, 1.1, 18.4, and 12.2 percent, respectively. In the mid future period under RCP 4.5, the ensemble model predicted increases of 8.3, 23.6, 18.7, and 10.1 percent over historical streamflow during the months of June, July, August, and September, respectively. Under RCP 8.5, the increments were 18, 13.7, 22.5, and 10.9 percent, respectively, for the same time period. The similar pattern was seen in the 2080s, but with a greater scale of change for RCP 8.5. These findings are consistent with the results obtained for the watershed's precipitation regime. In general, positive changes i.e., increase in discharge were observed during monsoon and negative changes i.e., decrease in discharge were observed during low flow seasons particularly during pre-monsoon season. This implied that this watershed, like Pare watershed, is expected to produce more extreme runoff.

Table 4.35 Percentage change in monthly discharge in Dudhnai watershed during near future period

Units in %	RCP 4.5					RCP 8.5				
Month	**CCSM4**	**CNRM-CM5**	**MPI-ESM-LR**	**NorESM1-M**	**Ensemble**	**CCSM4**	**CNRM-CM5**	**MPI-ESM-LR**	**NorESM1-M**	**Ensemble**
Jan	3.6	-3.4	-0.3	-2.9	**1.6**	5.6	-4.6	2.3	-7.7	**3.2**
Feb	3.8	-1.7	-0.6	-6.3	**0.1**	6.1	-4.8	1.6	-11.0	**0.8**
Mar	-13.9	-3.9	-9.8	-20.7	**-1.4**	-10.8	-20.4	-7.4	-25.5	**-1.8**
Apr	-4.7	-24.1	-45.5	-15.6	**-6.4**	-31.9	-31.6	-38.3	-37.5	**-8.9**
May	-25.0	5.9	-42.2	51.4	**-8.2**	13.5	6.6	-5.3	5.4	**-9.1**
Jun	6.1	-5.1	46.8	11.4	**13.9**	-0.8	-2.6	30.6	17.2	**11.7**
Jul	22.7	-13.3	28.4	2.9	**5.8**	9.3	-11.7	18.4	-8.7	**1.1**
Aug	10.1	-8.6	15.7	33.0	**11.2**	28.5	11.9	43.7	0.0	**18.4**
Sep	17.5	0.2	1.2	3.4	**5.5**	31.3	26.4	12.6	-0.1	**12.2**
Oct	13.8	26.1	4.7	11.0	**6.1**	11.1	21.6	17.6	9.0	**10.8**
Nov	1.3	14.6	9.0	0.6	**8.5**	15.4	18.3	13.2	-5.1	**13.3**
Dec	3.3	4.5	2.7	-3.1	**7.2**	8.1	-1.4	10.1	-6.6	**8.9**

Table 4.36 Percentage change in monthly discharge in Dudhnai watershed during mid future period

Units in %	RCP 4.5					RCP 8.5				
Month	**CCSM4**	**CNRM-CM5**	**MPI-ESM-LR**	**NorESM1-M**	**Ensemble**	**CCSM4**	**CNRM-CM5**	**MPI-ESM-LR**	**NorESM1-M**	**Ensemble**
Jan	10.9	6.9	-5.3	6.9	**6.3**	6.5	10.9	-10.5	3.7	**7.8**
Feb	11.2	5.9	-6.7	3.7	**5.0**	6.6	9.3	-11.6	-0.8	**5.7**
Mar	13.7	-4.9	-12.9	-3.2	**4.3**	-4.2	-2.1	-23.0	-13.3	**4.5**
Apr	10.6	0.8	-41.9	5.3	**3.6**	29.9	3.8	-55.8	-1.6	**2.7**
May	-18.4	8.4	-30.4	51.0	**-2.5**	-5.7	0.5	-23.7	29.9	**-4.5**
Jun	18.2	-8.0	-8.1	41.9	**8.3**	15.0	14.3	8.8	28.3	**18.0**
Jul	59.1	2.7	33.9	5.1	**23.6**	34.1	25.2	0.4	4.1	**13.7**
Aug	12.0	14.6	30.6	9.1	**18.7**	22.4	28.1	42.9	11.6	**22.5**
Sep	26.0	16.3	1.9	2.1	**10.1**	24.2	22.5	-8.0	9.5	**10.9**
Oct	10.6	30.0	3.2	15.5	**10.9**	8.1	35.0	13.0	8.2	**13.0**
Nov	1.0	16.7	1.1	6.4	**13.3**	-0.7	60.6	-5.4	4.2	**15.3**
Dec	8.9	10.2	-3.5	5.1	**10.2**	3.3	23.2	-10.9	2.8	**12.8**

Table 4.37 Percentage change in monthly discharge in Dudhnai watershed during far future period

Units in %	RCP 4.5					RCP 8.5				
Month	**CCSM4**	**CNRM-CM5**	**MPI-ESM-LR**	**NorESM1-M**	**Ensemble**	**CCSM4**	**CNRM-CM5**	**MPI-ESM-LR**	**NorESM1-M**	**Ensemble**
Jan	0.7	31.8	-7.7	4.5	**11.5**	6.5	8.6	-6.0	8.3	**14.4**
Feb	1.9	32.2	-8.7	2.7	**8.5**	7.6	9.2	-8.6	11.9	**10.1**
Mar	11.2	14.0	-14.0	-13.0	**7.2**	43.5	4.3	-13.4	52.1	**12.2**
Apr	93.5	35.8	-17.5	51.3	**23.4**	25.9	-1.5	-42.5	37.2	**14.0**
May	34.3	70.0	-27.0	89.1	**26.3**	16.8	56.4	-52.1	76.4	**12.4**
Jun	33.8	3.3	4.1	24.1	**29.4**	57.5	-1.2	12.1	89.7	**47.7**
Jul	27.8	42.9	10.2	-4.6	**19.4**	79.8	5.9	21.4	53.4	**41.5**
Aug	19.2	19.9	14.0	0.6	**14.4**	48.3	30.1	61.8	30.9	**41.2**
Sep	-13.8	35.2	-1.7	-4.5	**6.7**	23.6	27.5	61.6	1.4	**22.5**
Oct	-14.3	73.3	5.6	9.1	**11.2**	-6.7	14.8	26.2	16.4	**16.6**
Nov	-10.7	75.6	-0.7	2.4	**15.9**	-7.9	42.5	22.1	13.3	**22.6**
Dec	0.8	55.7	-3.1	3.9	**18.4**	3.9	13.2	1.6	9.6	**20.7**

4.4.8 Other components of streamflow in SWAT Model in Dudhnai

4.4.8.1 SURQ, LATQ and GWQ during baseline/historical period (1976-2005)

In Fig. 4.38, an ensemble model plot containing monthly SURQ, LATQ, and GWQ of the historical era is shown. According to the ensemble model, in the historical period, SWAT has simulated the monthly average SURQ in the Dudhnai watershed to be about 76.4 mm/month, LATQ as 1.3 mm/month and GWQ as 100.7 mm/month. Comparing the two watersheds (Pare and Dudhnai), SURQ was found mor prominent in Dudhnai. Also, in Dudhnai watershed, the lateral flow contribution to the streamflow was found very less (negligible). This may be attributed to its small size watershed in which lateral flow or prompt interflow reaches the streams very quickly. Very similar to the results obtained in Pare watersheds, although the SURQ was found lesser than GWQ in ensemble model, the scenario was interchanged in the individual climate models. Among the four climate models, CCSM4 was found to have the largest monthly average SURQ (123.8 mm/month) closely followed by CNRM-CM5 with an average monthly SURQ of 121 mm. While NorESM1-M model was found to have the largest monthly average GWQ. The pattern of GWQ also suggested that, unlike Pare River, Dudhnai River is very dependable with constant supply of water from springs or GWQ throughout the year.

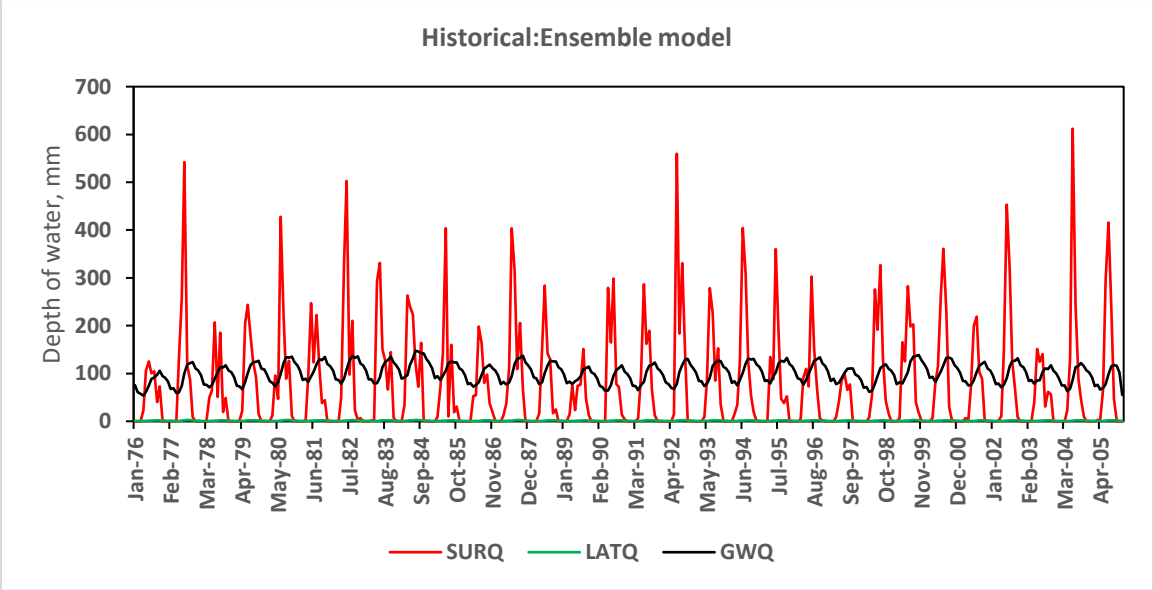

Fig. 4.38 SURQ, LATQ and GWQ in the Dudhnai watershed during historical period

Seasonal break-up of these three streamflow components, during the historical era is illustrated in Table 4.38. As seen in the table, the GWQ component has dominated the streamflow for ensemble model while SURQ dominated in the four individual models. The ensemble model has indicated that in the study area, during this period, GWQ contributes 1208.1 mm annually towards the streamflow while SURQ and GWQ annually contribute 916.5 mm and 15.7 mm, respectively. Among the four climate models, CCSM4 has shown the largest SURQ contribution, while NorESM1-M has the largest LATQ and GWQ contribution. According to the ensemble model, SURQ, LATQ and GWQ peaked in June, August and October, respectively.

4.4.8.2 SURQ, LATQ and GWQ during future period

Monthly SURQ, LATQ and GWQ of the three future eras (near, mid and far) resulted from ensemble of four climate models under RCP 4.5 projection scenario are plotted and shown in Figs. 4.39 (a), (b) and (c). For the projections under RCP 8.5 scenario, they are shown in Figs. 4.40 (a), (b) and (c). As per the ensemble model, monthly average SURQ for near, mid and far future periods were found as 87, 92.1, and 96.9 mm/month under RCP 4.5 and 89.4, 93.6 and 116.1 mm/month under RCP 8.5, respectively. In case of LATQ, these monthly average values were respectively 1.3, 1.4 and 1.4 mm/month under RCP 4.5 and 1.3, 1.4, and 1.5 mm/month under RCP 8.5. And, for GWQ, these values were found as 100.3, 105.8 and 110.3 mm/month under RCP 4.5 and 100.9, 105.7 and 111.2 mm/month under RCP 8.5, respectively. SURQ, LATQ, and GWQ were thus anticipated to be higher in the RCP 8.5 scenario than in the RCP 4.5 scenario, and they were also projected to grow as time slices moved from near to far future eras. Table 4.39 shows the seasonal break-up of these streamflow components for the three future eras under RCPs 4.5 and 8.5 based on ensemble climate model. As seen in the table, in all RCP scenarios, GWQ outperforms SURQ and LATQ. It is also observed that their monsoonal contribution to the annual total increased in future periods than in the historical era.

Table 4.38 Seasonal variation of SURQ, LATQ and GWQ in Dudhnai watershed during historical period

Month	CCSM4			CNRM-CM5			MPI-ESM-LR			NorESM1-M			Ensemble		
	SURQ	LATQ	GWQ	SURQ	LATQ	GWQ	SURQ	LATQ	GWQ	SURQ	LATQ	GWQ	SURQ	LATQ	GWQ
Jan	0.0	0.5	47.1	0.0	0.6	53.0	0.0	0.7	61.3	0.0	0.6	61.7	0.0	0.9	98.3
Feb	0.2	0.4	34.5	1.4	0.4	39.6	0.7	0.5	46.7	2.4	0.5	48.4	0.0	0.6	80.7
Mar	27.1	0.4	32.1	11.2	0.4	35.0	14.0	0.4	43.6	43.3	0.4	46.6	4.3	0.6	81.3
Apr	108.7	0.4	24.6	64.0	0.4	28.9	82.2	0.4	37.6	103.2	0.5	42.7	48.9	0.6	73.6
May	250.9	0.6	31.7	189.2	0.6	36.0	211.8	0.6	43.3	144.1	0.8	48.0	128.5	0.9	80.5
Jun	398.5	0.9	42.9	387.2	0.9	46.6	332.7	0.9	53.2	430.4	1.1	59.2	284.1	1.4	92.5
Jul	294.4	1.3	53.4	347.5	1.3	59.2	297.1	1.3	66.4	268.2	1.5	73.0	208.3	1.9	111.0
Aug	220.6	1.4	57.9	263.7	1.5	65.1	247.7	1.6	73.2	158.0	1.6	77.7	139.5	2.2	121.3
Sep	132.4	1.4	57.1	112.7	1.4	64.4	152.6	1.5	74.9	133.1	1.5	77.4	74.1	2.1	122.8
Oct	52.4	1.2	58.1	65.0	1.3	64.5	69.8	1.5	75.7	34.9	1.4	77.2	26.8	2.0	125.8
Nov	0.4	0.9	53.9	12.6	1.0	60.0	7.9	1.1	69.8	2.8	1.1	70.2	1.9	1.5	113.3
Dec	0.0	0.7	54.0	0.0	0.8	59.4	0.0	0.9	67.9	0.0	0.8	69.0	0.0	1.2	107.1
Annual	**1485.6**	**10.2**	**547.3**	**1454.5**	**10.5**	**611.8**	**1416.5**	**11.4**	**713.7**	**1320.4**	**11.8**	**751.2**	**916.5**	**15.7**	**1208.1**

All units in mm

(a)

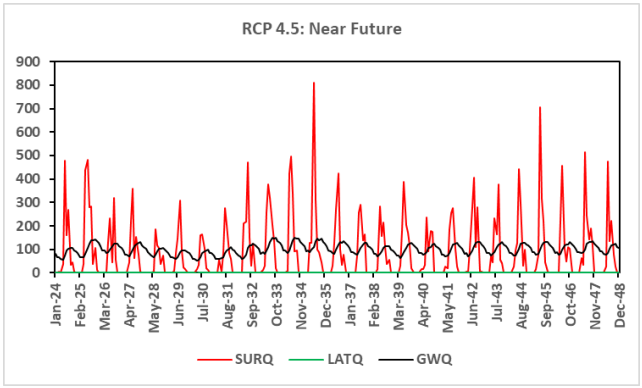

(b)

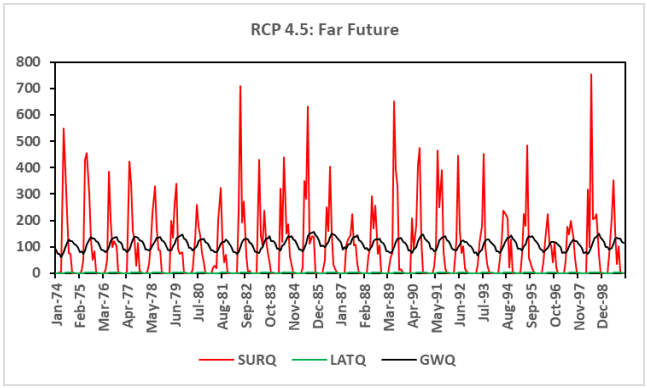

(c)

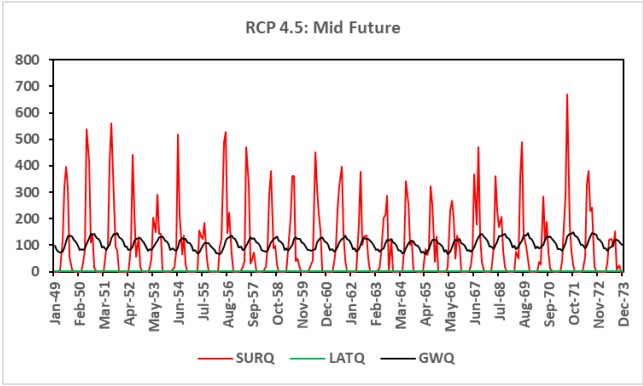

Fig. 4.39 SURQ, LATQ and GWQ in the Dudhnai watershed during under RCP 4.5 projection for (a) near (b) mid, and (c) far future periods

(a)

(b)

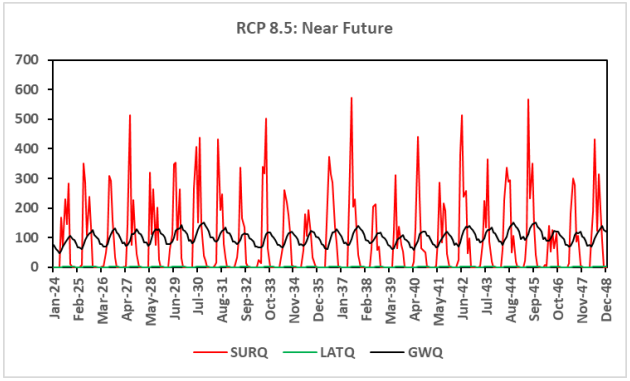

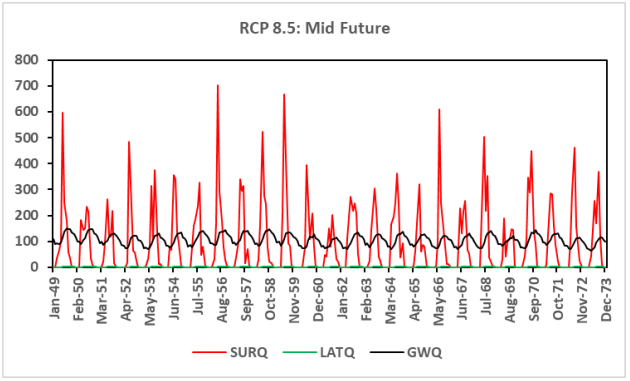

(c)

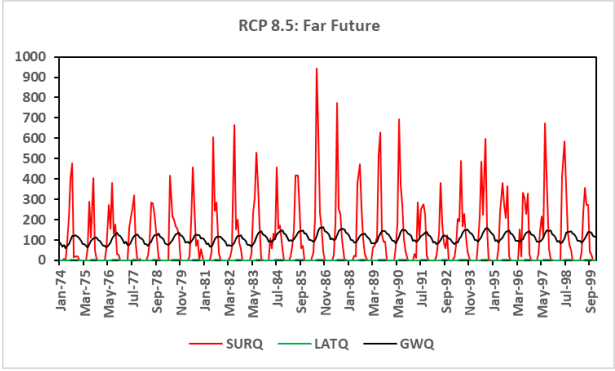

Fig. 4.40 SURQ, LATQ and GWQ in the Dudhnai watershed during under RCP 8.5 projection for (a) near (b) mid, and (c) far future periods

Table 4.39 Seasonal variation of SURQ, LATQ and GWQ in Dudhnai watershed during future periods (all units in mm)

Month	RCP 4.5: near future			RCP 4.5: mid future			RCP 4.5: far future		
	SURQ	LATQ	GWQ	SURQ	LATQ	GWQ	SURQ	LATQ	GWQ
Jan	0.0	0.9	98.7	0.0	0.9	103.4	0.0	0.9	106.8
Feb	0.1	0.6	80.4	0.0	0.6	84.3	0.0	0.6	87.4
Mar	1.8	0.6	81.0	2.2	0.6	86.2	2.1	0.6	88.1
Apr	25.2	0.6	72.9	38.6	0.6	77.7	93.0	0.7	80.9
May	131.7	0.8	77.4	127.8	1.0	85.0	191.1	1.1	91.3
Jun	332.2	1.3	90.3	325.0	1.4	97.1	315.1	1.6	103.8
Jul	245.1	1.9	109.4	300.0	2.0	117.0	270.5	2.1	122.6
Aug	178.5	2.2	120.9	178.7	2.3	128.3	165.9	2.3	132.7
Sep	85.4	2.2	122.8	95.2	2.2	128.7	71.8	2.2	133.0
Oct	43.0	2.0	126.1	37.4	2.0	130.9	51.9	2.1	135.9
Nov	0.9	1.6	114.4	0.2	1.5	117.8	1.9	1.6	122.6
Dec	0.0	1.2	109.1	0.0	1.2	113.1	0.0	1.3	118.2
Annual	1043.8	15.8	1203.4	1105.1	16.5	1269.7	1163.3	17.1	1323.4
Month	**RCP 8.5: near future**			**RCP 8.5: mid future**			**RCP 8.5: far future**		
	SURQ	LATQ	GWQ	SURQ	LATQ	GWQ	SURQ	LATQ	GWQ
Jan	0.0	0.9	99.2	0.0	0.9	104.2	0.0	0.9	104.2
Feb	0.0	0.6	80.7	0.0	0.6	85.0	0.0	0.6	85.0
Mar	0.7	0.6	81.2	2.1	0.6	86.4	2.1	0.6	86.4
Apr	19.4	0.6	72.7	42.3	0.6	77.5	42.3	0.6	77.5
May	157.2	0.8	78.0	129.1	0.9	84.0	129.1	0.9	84.0
Jun	317.3	1.3	91.5	340.2	1.4	96.2	340.2	1.4	96.2
Jul	204.6	1.9	109.8	256.5	2.0	115.9	256.5	2.0	115.9
Aug	216.3	2.1	120.2	213.1	2.2	127.0	213.1	2.2	127.0
Sep	120.7	2.2	123.6	94.7	2.2	128.2	94.7	2.2	128.2
Oct	35.2	2.1	128.3	41.6	2.1	131.8	41.6	2.1	131.8
Nov	1.8	1.6	115.4	3.1	1.6	118.6	3.1	1.6	118.6
Dec	0.0	1.2	110.5	0.0	1.2	113.9	0.0	1.2	113.9
Annual	1073.3	16.0	1211.0	1122.7	16.5	1268.7	1122.7	16.5	1268.7

Tables 4.40-4.42 show the percentage change in seasonal and annual mean SURQ, LATQ, and GWQ in three future time slices under RCP 4.5 climate projections. The corresponding plots for RCP 8.5 climate projections are shown in Tables 4.43-4.45. In general, changes were found to be larger for RCP 8.5 than RCP 4.5, and also greater in the far future, especially during monsoon season. As shown in the tables, majority of the changes were positive, projecting increase in values in the future. The changes in LATQ component of the streamflow were found insignificant in the future, suggesting that it is expected to remain more or less the same. Different climate models showed mixed results for GWQ component in which it either project positive or negative changes in the future, however, ensemble model projected it to increase in the future periods. In the earlier sections, discharge in the Dudhnai watershed was projected to increase in the future. And in this section, we observed minor changes for LATQ and GWQ with very high changes in SURQ. This implied that, this watershed, like Pare watershed, would be vulnerable to direct surface runoff which has the capacity to cause flash floods, soil erosions and impart huge damages to the people living in both highlands and lowlands areas. As for the ensemble climate model, decrease in SURQ was observed in low flow periods (Nov-Mar) in some of the climate scenarios and significant increase in SURQ was observed especially during monsoon season. This is one of the indications that the watershed would witness more extreme events in the future.

Table 4.40 Percentage change in SURQ, LATQ & GWQ in Dudhnai watershed during near future period under RCP 4.5

	Ensemble			CCSM4			CNRM-CM5			MPI-ESM-LR			NorESM1-M		
Month	**SURQ**	**LATQ**	**GWQ**	**SURQ**	**LATQ**	**GWQ**	**SURQ**	**LATQ**	**GWQ**	**SURQ**	**LATQ**	**GWQ**	**SURQ**	**LATQ**	**GWQ**
Jan	0	0	0.4	0	20	4.5	0	0	-4.9	0	0	0	0	0	-2.9
Feb	0	0	-0.4	50	0	5.5	200	0	-5.8	-100.0	0	-0.4	-95.8	-20	-6.6
Mar	-58.1	0	-0.4	-41.0	0	0.9	10.7	0	-4.0	-55.0	0	-3.2	-69.7	0	-9.0
Apr	-48.5	0	-1.0	-9.1	0	16.7	-48.4	0	-0.3	-70.0	0	-12.0	-19.0	0	-11.2
May	2.5	-11.1	-3.9	-34.1	16.7	2.2	1.2	0	-6.9	-41.7	-16.7	-7.2	107.4	-12.5	-6.0
Jun	16.9	-7.1	-2.4	11.4	0	4.0	-10.0	-11.1	-11.6	62.5	0	-2.8	2.7	0	-1.2
Jul	17.7	0	-1.4	41.3	0	1.9	-11.3	-7.7	-8.8	31.4	0	-0.8	3.4	0	-2.2
Aug	28.0	0	-0.3	8.4	7.1	4.8	-2.2	-13.3	-11.1	13.3	0	0.1	85.4	0	0.5
Sep	15.2	4.8	0	24.8	0	6.1	31.3	0	-7.6	3.3	6.7	0.1	-11.0	0	-2.2
Oct	60.4	0	0.2	-4.0	8.3	3.6	119.1	0	-7.1	22.5	0	0.4	36.7	0	-2.6
Nov	-52.6	6.7	1.0	0	11.1	4.5	-59.5	10	-4.8	2.5	9.1	1.4	-85.7	0	-3.0
Dec	0	0	1.9	0	14.3	5	0	0	-2.9	0	0	2.1	0	0	-1.7
Annual	**13.9**	**0.6**	**-0.4**	**7.4**	**3.9**	**4.6**	**-0.2**	**-2.9**	**-6.7**	**14.2**	**1.8**	**-1.2**	**19.2**	**-1.7**	**-3.5**

Table 4.41 Percentage change in SURQ, LATQ & GWQ in Dudhnai watershed during mid future period under RCP 4.5

	Ensemble			CCSM4			CNRM-CM5			MPI-ESM-LR			NorESM1-M		
Month	**SURQ**	**LATQ**	**GWQ**	**SURQ**	**LATQ**	**GWQ**	**SURQ**	**LATQ**	**GWQ**	**SURQ**	**LATQ**	**GWQ**	**SURQ**	**LATQ**	**GWQ**
Jan	0	0	5.2	0	20	12.5	0	16.7	7.5	0	0	-6.0	0	0	7.8
Feb	0	0	4.5	450	0	13.0	-92.9	25	7.8	-100	0	-7.7	-45.8	0	5.0
Mar	-48.8	0	6.0	62.0	0	21.5	-55.4	0	10.6	-45.7	0	-11.5	-39.3	0	8.4
Apr	-21.1	0	5.6	-19.2	50	35.4	-0.5	0	19.0	-60.1	0	-17.8	13.2	0	5.4
May	-0.5	11.1	5.6	-27.1	16.7	24.9	-0.5	16.7	10.6	-32.1	0	-14.3	87.4	12.5	15.6
Jun	14.4	0	5.0	26.3	11.1	17.9	-11.1	-11.1	0.4	0.9	-11.1	-14.1	34.3	18.2	15.9
Jul	44.0	5.3	5.4	84.8	7.7	18.2	16.0	0	5.2	45.5	-7.7	-11.7	-8.2	6.7	12.5
Aug	28.1	4.5	5.8	-11.8	14.3	16.4	15.2	0	5.5	48.7	-6.25	-9.2	18.0	6.2	11.1
Sep	28.5	4.8	4.8	37.8	7.1	14.4	50.0	7.1	6.2	2.3	0	-9.6	-7.3	6.7	8.9
Oct	39.6	0	4.1	-20.0	8.3	10.5	50.0	7.7	7.6	29.2	0	-7.1	39.5	0	6.3
Nov	-89.5	0	4.0	-75	11.1	10.6	-60.3	10	6.3	-39.2	0	-6.0	-78.6	0	6.4
Dec	0	0	5.6	0	14.3	12.2	0	12.5	7.9	0	0	-5.0	0	0	7.5
Annual	**20.6**	**5.1**	**5.1**	**20.0**	**9.8**	**16.0**	**8.6**	**4.8**	**7.2**	**11.0**	**-3.5**	**-9.4**	**21.0**	**5.9**	**9.3**

Table 4.42 Percentage change in SURQ, LATQ & GWQ in Dudhnai watershed during far future period under RCP 4.5

	Ensemble			CCSM4			CNRM-CM5			MPI-ESM-LR			NorESM1-M		
Month	**SURQ**	**LATQ**	**GWQ**	**SURQ**	**LATQ**	**GWQ**	**SURQ**	**LATQ**	**GWQ**	**SURQ**	**LATQ**	**GWQ**	**SURQ**	**LATQ**	**GWQ**
Jan	0	0	8.6	0	0	0.4	0	33.3	32.6	0	0	-8.2	0	0	4.9
Feb	0	0	8.3	1200	0	0	14.3	25	37.1	-85.7	0	-10.9	4.2	0	3.3
Mar	-51.2	0	8.4	43.9	0	6.5	-81.3	25	41.1	-1.4	0	-14.2	-79.2	0	3.4
Apr	90.2	16.7	9.9	108.2	25	22.4	38.1	25	49.5	-22.1	25	-13.0	99.9	0	1.6
May	48.7	22.2	13.4	28.4	50	29.3	65.5	33.3	49.7	-32.2	0	-12.5	127.8	12.5	14.4
Jun	10.9	14.3	12.2	26.0	33.3	20.5	-8.4	11.1	30.7	13.7	0	-11.1	7.3	18.2	14.4
Jul	29.9	10.5	10.5	30.3	7.7	15.4	54.0	15.4	28.2	12.5	0	-9.0	-4.4	6.7	8.8
Aug	18.9	4.5	9.4	11.2	7.1	10.4	18.0	13.3	26.7	21.6	-6.3	-11.2	1.1	6.2	8.4
Sep	-3.1	4.8	8.3	-43.1	0	5.1	78.0	14.3	28.1	6.6	0	-8.5	-29.8	6.7	5.4
Oct	93.7	5	8.0	-26.5	0	1.9	202.8	23.1	31.9	28.4	-6.7	-6.6	42.7	0	4.4
Nov	0	6.7	8.2	-25	0	2.4	21.4	30	32.8	-12.7	0	-6.7	-96.4	0	4.6
Dec	0	8.3	10.4	0	0	4.3	0	25	32.3	0	0	-5.4	0	0	6.5
Annual	**26.9**	**8.9**	**9.5**	**23.5**	**6.9**	**8.7**	**38.8**	**21.9**	**33.4**	**5.5**	**-1.8**	**-9.3**	**18.7**	**5.9**	**6.7**

Table 4.43 Percentage change in SURQ, LATQ & GWQ in Dudhnai watershed during near future period under RCP 8.5

	Ensemble			CCSM4			CNRM-CM5			MPI-ESM-LR			NorESM1-M		
Month	**SURQ**	**LATQ**	**GWQ**	**SURQ**	**LATQ**	**GWQ**	**SURQ**	**LATQ**	**GWQ**	**SURQ**	**LATQ**	**GWQ**	**SURQ**	**LATQ**	**GWQ**
Jan	0	0	0.9	0	20	6.4	0	0	-4.7	0	0	2.1	0	0	-8.4
Feb	0	0	0	-50	0	7.8	-100	0	-6.1	-57.1	0	1.7	-100	-20	-11.4
Mar	-83.7	0	-0.1	-29.2	0	4.0	-97.3	0	-10.6	-35.7	0	0	-75.8	0	-12.0
Apr	-60.3	0	-1.2	-50.7	0	12.6	-45.6	0	-4.2	-60.8	0	-4.5	-42.1	-20	-20.1
May	22.3	-11.1	-3.1	23.8	16.7	6.9	5.2	-16.7	-10.8	0.8	0	-0.7	41.0	-12.5	-14.6
Jun	11.7	-7.1	-1.1	-0.5	11.1	9.3	-4.0	-11.1	-15.9	36.9	11.1	2.3	13.0	0	-7.9
Jul	-1.8	0	-1.1	7.9	0	6.9	-7.3	-15.4	-12.7	20.6	0	0.2	-20.1	-6.7	-8.2
Aug	55.1	-4.5	-0.9	44.1	7.1	5.7	22.4	-13.3	-11.5	57.6	0	1.1	23.0	-6.3	-7.9
Sep	62.9	4.8	0.7	62.2	7.1	8.9	100.8	0	-8.5	27.9	6.7	1.2	20.3	0	-6.6
Oct	31.3	5	2.0	-35.3	8.3	6.7	60.2	0	-5.1	39.7	6.7	4.0	17.2	0	-6.5
Nov	-5.3	6.7	1.9	1475	11.1	7.2	-51.6	10	-4.8	-41.8	9.1	3.7	-42.9	0	-7.5
Dec	0	0	3.2	0	14.3	7.6	0	0	-3.4	0	0	5.0	0	0	-5.7
Annual	**17.1**	**1.9**	**0.2**	**12.5**	**5.9**	**7.3**	**9.1**	**-3.8**	**-8.1**	**24.0**	**3.5**	**1.7**	**3.9**	**-4.2**	**-9.0**

Table 4.44 Percentage change in SURQ, LATQ & GWQ in Dudhnai watershed during mid future period under RCP 8.5

	Ensemble			CCSM4			CNRM-CM5			MPI-ESM-LR			NorESM1-M		
Month	**SURQ**	**LATQ**	**GWQ**	**SURQ**	**LATQ**	**GWQ**	**SURQ**	**LATQ**	**GWQ**	**SURQ**	**LATQ**	**GWQ**	**SURQ**	**LATQ**	**GWQ**
Jan	0	0	6.0	0	20	7.4	0	16.7	10.6	0	0	-11.6	0	16.7	3.6
Feb	0	0	5.3	750	0	6.1	-85.7	25	11.6	-14.3	0	-15.2	-87.5	-20	0.2
Mar	-51.2	0	6.3	-6.6	0	8.4	-48.2	0	13.7	-81.4	0	-20.2	-52.9	0	2.6
Apr	-13.5	0	5.3	32.3	25	26.0	-1.6	0	17.6	-76.8	0	-28.5	-4.7	0	1.4
May	0.5	0	4.3	-15.0	33.3	22.4	-10.7	0	9.7	-21.3	-16.7	-23.1	71.5	0	8.1
Jun	19.7	0	4	17.7	11.1	10.7	16.2	-11.1	2.1	15.2	-11.1	-19.0	20.5	9.1	9.8
Jul	23.1	5.3	4.4	40.1	7.7	11.4	36.0	0	3.7	6.3	-15.4	-18.5	0.3	6.7	8.6
Aug	52.8	0	4.7	19.9	7.1	7.8	39.2	0	5.5	71.7	-12.5	-16.3	20.8	6.2	7.3
Sep	27.8	4.8	4.4	51.7	0	8.2	56.3	7.1	7.1	-18.0	-6.7	-17.5	8.6	6.7	4.3
Oct	55.2	5	4.8	-22.9	8.3	5.0	89.7	15.4	9.3	82.7	-6.7	-13.6	9.2	0	3.6
Nov	63.2	6.7	4.7	125	11.1	4.5	138.9	20	9.7	-75.9	0	-12.9	-96.4	0	2.6
Dec	0	0	6.3	0	0	6.3	0	12.5	10.8	0	0	-11.5	0	0	4.8
Annual	**22.5**	**5.1**	**5.0**	**19.3**	**6.9**	**9.2**	**27.7**	**7.6**	**8.7**	**10.7**	**-7.0**	**-16.6**	**15.7**	**4.2**	**4.9**

Table 4.45 Percentage change in SURQ, LATQ & GWQ in Dudhnai watershed during far future period under RCP 8.5

	Ensemble			CCSM4			CNRM-CM5			MPI-ESM-LR			NorESM1-M		
Month	**SURQ**	**LATQ**	**GWQ**	**SURQ**	**LATQ**	**GWQ**	**SURQ**	**LATQ**	**GWQ**	**SURQ**	**LATQ**	**GWQ**	**SURQ**	**LATQ**	**GWQ**
Jan	0	11.1	9.7	0	20	6.6	0	16.7	9.1	0	0	-7.2	0	16.7	8.6
Feb	0	16.7	8.8	1100	0	5.2	-7.1	25	9.6	-71.4	0	-10.7	345.8	0	5.6
Mar	209.3	0	10.9	110.3	0	14.6	5.4	0	12.9	-10	0	-14.4	86.8	25	13.3
Apr	-0.8	16.7	11.0	22.6	25	22.0	-8.1	25	16.3	-72.7	0	-29.5	46.3	40	14.8
May	36.3	11.1	11.4	11.4	33.3	19.2	65.6	16.7	21.7	-48.5	-16.7	-21.2	113.9	25	22.9
Jun	41.8	14.3	11.4	63.6	22.2	17.9	-18.5	11.1	12.0	21.0	-11.1	-20.3	70.9	27.3	20.8
Jul	61.2	10.5	10.3	94.2	15.4	15.7	11.4	0	7.4	40.7	-7.7	-17.2	58.3	13.3	16.2
Aug	82.8	9.1	11.0	50.3	14.3	15.5	48.5	0	7.1	87.7	-6.3	-12.4	62.1	12.5	16.9
Sep	65.2	9.5	10.7	10.7	7.1	10.5	72.9	7.1	9.8	140.0	6.7	-8.0	-35.8	13.3	11.1
Oct	32.8	10	9.7	-44.1	0	5.2	2.6	7.7	10.1	42.8	6.7	-5.7	96.8	7.1	10.1
Nov	131.6	6.7	9.2	-100	0	5.8	96.8	10	9.2	69.6	9.1	-5.7	-92.9	0	9.4
Dec	0	8.3	11.5	0	0	8.0	0	12.5	10.4	0	11.1	-4.0	0	12.5	11.3
Annual	**52.0**	**10.8**	**10.5**	**48.3**	**9.8**	**11.4**	**21.4**	**9.5**	**10.6**	**34.8**	**0.0**	**-11.8**	**60.7**	**12.7**	**13.2**

4.5 Return Flood Analysis

To determine the return flood in the Dudhnai watershed annual maximum series of the observed discharge (1989-2019), simulated discharge of the future periods (2024-2099) under RCP 4.5 and 8.5 were determined (ensemble discharge projections were used). They are plotted in order to visualize as shown in Fig. 4.41.

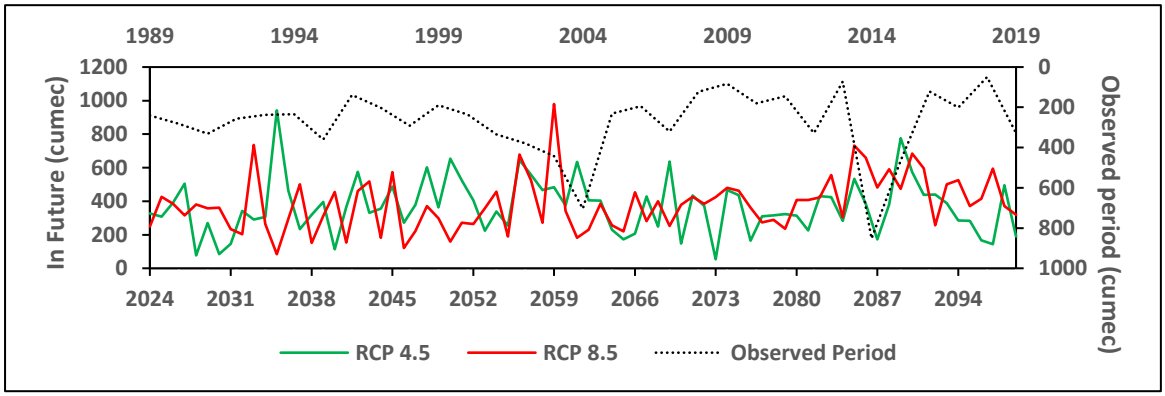

Fig. 4.41 Annual maximum series of discharge data in the Dudhnai watershed

For the measured discharge period from 1989 to 2019, the maximum daily discharge of 852 cumecs was observed in 2014. This was followed by 704, 466, 442 and 379 cumecs in the year-2004, 2015, 2003 and 2002, respectively. Under RCP 4.5 discharge projection, the top five in order of flood magnitude were found as 942 (year:2035), 776 (year:2089), 654 (year:2050), 646 (year:2056) and 636 (year:2069), cumecs. In case of RCP 8.5 discharge projection. The top five flood magnitude in order of magnitude were found as 979 (year:2059), 735 (year:2033), 732 (year:2085), 685 (year:2090), and 679 (year:2056), cumecs. This is also one of the indicators that in future, more extreme events are likely to occur. Based on these annual maximum series, return flood of 25-, 50-, 100-, and 200-years return period were determined. Table 4.46 shows the various return flood (in cumecs) for various return periods under scenarios from measured discharge and simulated discharge. Interestingly, the return floods were smaller for RCP 8.5 scenarios as compared to both measure and RCP 4.5 scenarios. The return floods as resulted from RCP 4.5 scenarios were found greater than return flood generated from observed discharges. The period used for determining return floods for measured discharge scenarios were very less (31 years only) as compared to the RCP scenarios which used 76 years of data.

Table 4.46 Return floods in Dudhnai watershed based on Gumbel Method

Return Period (Years)	From Observed Discharge (Cumecs)	Under RCP 4.5 Scenarios (Cumecs)	Under RCP 8.5 Scenarios (Cumecs)
25	681.5518	731.4681	648.7245
50	788.7308	828.4834	734.5464
100	895.1184	924.7823	819.7346
200	1001.118	1020.73	904.6119

4.5.1 1-D hydrodynamic modelling in HEC-RAS

HEC-RAS was attempted to perform 1-d hydrodynamic modelling in the Dudhnai River taking outlet of Dudhnai watershed as the upstream point and confluence with Dudhnai River as the downstream point. Using RAS-Mapper in HEC-RAS, cross-sections from 8 sections were attempted to extract from DEM. Location map of the river section and cross-sections points were shown in Fig. 4.42.

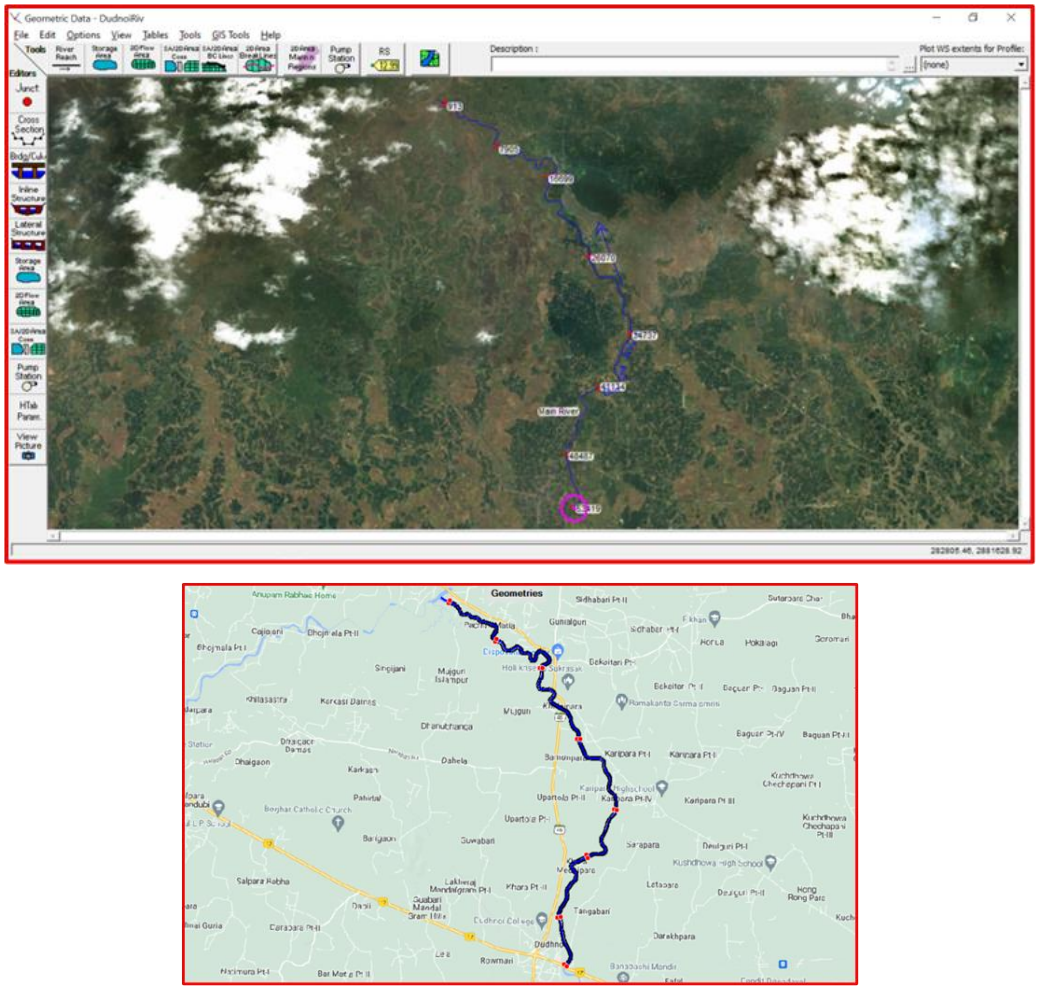

Fig. 4.42 Dudhnai River up to the confluence with Krishnai River

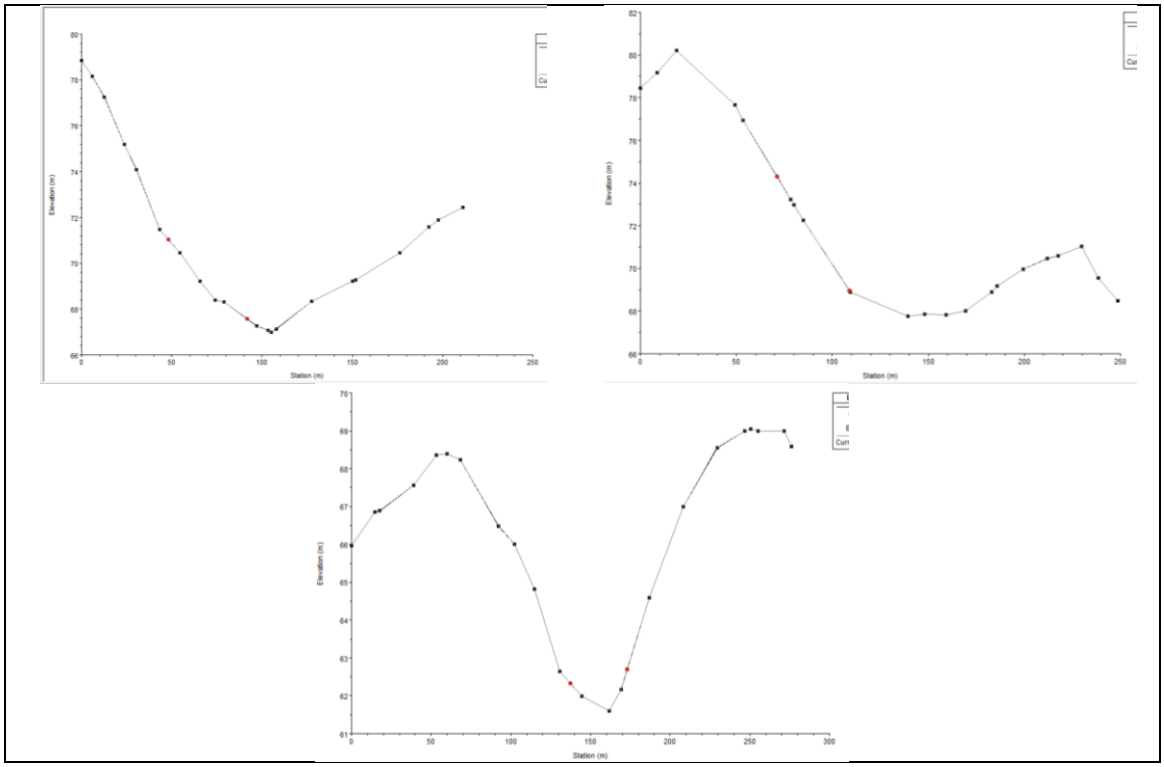

Fig. 4.43 Cross-sections extracted from DEM

The figure suggests that, there might be some error present in the source DEM since it was not able to extract the profile of the river properly. Many other DEMs from different sources such as SRTM, ALOS, ASTER and CARTOSAT were employed to improve the results but in vain. On examining, the river extracted from DEMs, using 'Hydrology tool' in ArcGIS, is not following the actual course of the Dudhnai River, as illustrated in Fig. 4.44. This may be due to inability of the DEM (coarse resolution) to capture small change in elevation/slope. In the figure, the areas to the north of 'change point' are very flat land, in which, stream extracted from DEM divert towards left of the change point. The objective is to showcase the suitability of open source DEMs for hydrodynamic modelling, however, it cannot be achieved, thus requiring cross-sections data for this study area. With no cross-section data, the steady and unsteady states modelling was carried out by assuming trapezoidal sections of depth- 5 to 8 m and side slope (H:V)- 3:1 to 5:1. The width of the river was determined from google earth image. Table 4.47 shows the results of steady state modelling on assumed cross-section data, in terms of overtopping of the banks in 8 cross-sections of the Dudhnai River. Floods of the years- 2014 and 2004, and return floods of 25-50-, 100-, and 200-years return period were analyzed and presented in the table. The results and difficulties faced were presented in the 17th Meeting of Regional Coordination Committee of North Eastern Regional Centre, Guwahati,

National Institute of Hydrology. Water Resources Department of Meghalaya is going to conduct bathymetry in various sections of the Dudhnai River in near future. Based on the discussion held in the meet, this objective has to be taken as new study in the future.

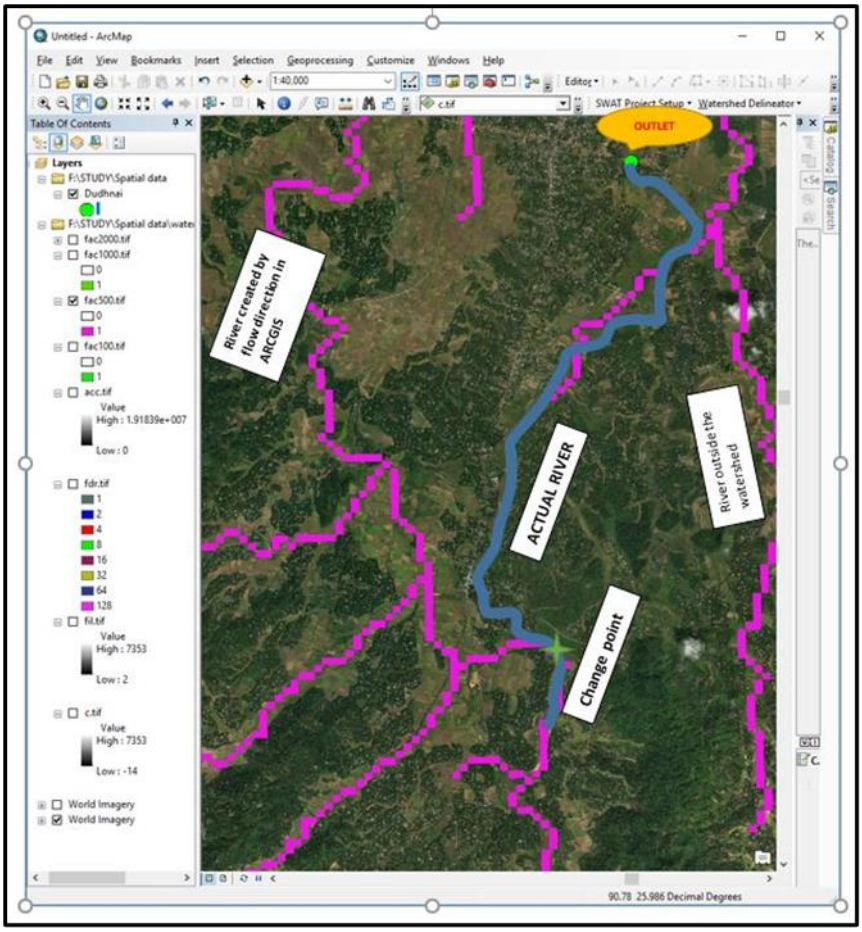

Fig. 4.44 Difference between actual course of river and river extracted from DEM

Table 4.47 Over topping of banks under steady state condition in Dudhnai River

Flood	Number of sections overtopped	Sections
Flood of 2014 (852 cumec)		
Flood of 2004 (704 cumec)		
25-year return flood (682 cumec)	5 out of 8	48487, 34737, 26070, 16699, & 913
50-year return flood (789 cumec)		
100-year return flood (895 cumec)		
200-year return flood (1001 cumec)	5 out of 8	48487, 41134, 34737, 26070, 16699, 7905, & 913

CHAPTER V
SUMMARY AND CONCLUSIONS

5.1 Summary

The aim of the present study was to determine the impact of climate change on discharge in two-midsized watersheds situated in mountainous region of the north eastern part of India. Pare watershed in Papumpare district of Arunachal and Dudhnai watershed sharing boundary with two states- Assam and Meghalaya were selected. Meteorological and spatial data employed in this study were from open source. The discharge data were acquired from NEEPCO and CWC for Pare and Dudhnai watersheds, respectively. Since, the watersheds are prone to soil erosion, watershed prioritization were carried out using the morphometric parameters. A hydrological model- SWAT was selected to represent the hydrological behaviors of the two watersheds. Measured daily discharge data were utilized to calibrate and validate the SWAT model. Once the model was calibrated for respective watersheds, the SWAT model was then simulated for historical period (1976-2005), near future period (2019-2045), mid future period (2046-2072) and far future period (2073-2099) in the Pare watershed. Similarly, the calibrated SWAT model in Dudhnai watershed was simulated for historical period (1976-2005), near future period (2024-2048), mid future period (2049-2073) and far future period (2074-2099). The resulting discharge and its components were analyzed during these periods. Projected future streamflow scenarios were presented and analyze in terms of percentage change from those in the historical/baseline period. The Dudhnai watershed has flood plains in the northern part of the watershed for which return floods of various return periods were determined. Results were presented in figures and tables and were discussed in the Results and Discussion chapter.

5.2 Conclusions

The following major conclusions were drawn from the present study:

1. In the last two decades, days and nights were getting warmer with decrease in rainfall. However, it was associated with increasing rainfall intensity and consecutive dry days and decreasing consecutive wet days.
2. According to morphometric analysis, Chil sub-watershed (Dudhnai) and SW25 (Pare) are the most vulnerable sub watersheds to soil erosion, which required interventions to soil and water conservation measures on priority basis.
3. In Pare watershed, of all the climate scenarios, only a scenario of RCP 8.5 in near future period for the climate model NorESM1-M had projected decrease in average annual

precipitation in the study area by about 7.5 percent from historical period. While in Dudhnai watershed, of all the climate scenarios, only a scenario of RCP 4.5 in near future period for the climate model CNRM-CM5 had projected decrease in average annual precipitation in the study area by just 0.5 percent from historical period.

4. In general, both precipitation and temperature were projected to increase towards the end of the century and they were also projected greater under RCP 8.5 scenario as compare to RCP 4.5 scenario. There was shrinking of wet episodes in the study areas with increase in precipitation amount that suggested more extreme events to occur in the future.
5. Considering the uncertainties that may be associated in mountainous regions and from sparse hydro-meteorological networks, SWAT model was able to satisfactorily represent the Pare and Dudhnai watersheds. Comparing the two watersheds, SWAT model performed slightly better in Pare watershed.
6. The developed SWAT model underestimated the actual discharge in Pare watershed while it had slightly overestimated the actual discharge in Dudhnai watershed. The indicators to measure the uncertainties of SWAT predicted discharge (p-factor and r-factor) were within the recommended permissible limits for prediction of discharge, and therefore concluded the SWAT model constructed in both the watersheds was suitable for its application.
7. In both the watersheds, channel hydraulic conductivity, curve number for antecedent moisture condition II, and bank storage's recession constant were the most sensitive parameter affecting stream discharge.
8. In Pare watershed, only NorESM1-M had projected decreasing streamflow conditions in the near future period under RCP 8.5 projection scenarios with a decrease of roughly 10.7 percent. While in Dudhnai watershed, only CNRM-CM5 and NorESM1-M models in near future period under RCP 4.5 and RCP 8.5 scenarios, respectively had shown decrease in discharge with magnitudes of -2.3 percent and -1.1 percent, respectively.
9. In the future projections, significant positive changes in discharge were observed during the monsoon months in both the watersheds. While majority of the negative changes were occurred during Nov-Mar months. This implied that the nature of flow will be amplified in the future, i.e., high flow would become more high and low flow would become leaner.
10. Among the streamflow components, percentage increment in surface runoff were projected to occur at higher pace than the lateral and baseflow components. This could cause serious flooding in the low-lying areas downstream and heavy soil loss from the upstream of the watershed.

11. Comparing the return floods from three different scenarios- observed maximum series, RCP 4.5 maximum series and RCCP 8.5 maximum series, it was concluded that the return floods are not going to change significantly in the future in Dudhnai watershed.
12. Although both precipitation and streamflow were projected to increase in the future, their pattern is important. In both the watersheds, despite increasing precipitation and streamflow, the watersheds were expected to witness long spell of dry period with intense flooding potential within short span of rainy days.
13. Reports from various news outlet of losing springs in both the watersheds aided by the results obtained in this study, we concluded that the state of the watersheds is quite vulnerable to extreme events in the future. Therefore, we recommend stakeholders such as Water Resource Departments, Agriculture Departments and Irrigation Departments to collectively approach watershed management in scientific manner, creation of water harvesting structures in suitable sites and also promote afforestation.

Scope for future work

Cross-section data of the Dudhnai which is soon to be determined by the WRD, Meghalaya would be used as new study in future. Because orographic effects of precipitation are likely to exist in mountainous watersheds such as these watersheds of Pare and Dudhnai. The confidentially of hydrological simulations would be increased by using sufficient rainfall gauging networks, as well as high resolution soil and land use data.

REFERENCES

Abbaspour, K. C. 2011. SWAT-CUP2: SWAT Calibration and Uncertainty Programs Manual Version 2, Department of Systems Analysis, Integrated Assessment and Modelling (SIAM), Eawag. Swiss Federal Institute of Aquatic Science and Technology, Duebendorf, Switzerland, 106.

Abbaspour, K. C. 2015. SWAT-CUP: SWAT calibration and uncertainty programs—a user manual. Eawag, Swiss Federal Institute of Aquatic Science and Technology.

Abbaspour, K. C., Vaghefi, S. A., and Srinivasan, T. 2018. A guideline for successful calibration and uncertainty analysis for Soil and Water Assessment: A review paper from the 2016 international SWAT conference. Water, 10(6). Doi:10.3390/w10010006.

Abbaspour, K.C., Johnson, C.A., and Van Genuchten, M.T. 2004. Estimating uncertain flow and transport parameters using a sequential uncertainty fitting procedure. Vadose Zone Journal, 3(4): 1340–1352.

Afshar, A. A., Hasanzadeh, Y., Besalatpour, A. A., and PourrezaBilondi, M. 2017. Climate change forecasting in a mountainous data scarce watershed using CMIP5 models under representative concentration pathways. Theor. Appl. Climatol., 129: 683–699.

Agyekum, J., Annor, T., Lamptey, B., Quansah, E., and Agyeman, R. Y. K. 2018. Evaluation of CMIP5 global climate models over the Volta Basin: precipitation. Adv. Meteorol., 2018, 1–24.

Ahmed SA, Chandrashekarappa KN, Raj SK, Nischitha V, Kavitha G (2010) Evaluation of Morphometric Parameters Derived from ASTER and SRTM DEM – A Study on Bandihole Sub Watershed Basin in Karnataka. J Indian Soc Remote Sens. pp 207–218

Ahmed, K., Sachindra, D. A., Shahid, S., Demirel, M. C., and Chung, E. S. 2018. Selection of multi-model ensemble of GCMs for the simulation of precipitation based on spatial assessment metrics. Hydrol. Earth Syst. Sci. Discuss., 23: 4803–4824.

Ahmed, K., Shahid, S., Sachindra, D. A., Nawaz, N., and Chung, E. S. 2019. Fidelity assessment of general circulation model simulated precipitation and temperature over Pakistan using a feature selection method. J. Hydrol., 573: 281–298.

Allen, R.G. 1986. A Penman for all seasons. J. Irrig. and Drain Engg., ASCE, 112(4): 348-368.

Allen, R.G., Jensen, M.E., Wright, J.L., and Burman, R.D. 1989. Operational estimates of evapotranspiration. Agron. J., 81:650-662.

Altaf F, Meraj G, Romshoo SA (2013) Morphometric analysis to infer hydrological behaviour of Lidder Watershed. Western Himalaya, India Geograph J. https://doi.org/10.1155/2013/178021.

Arnold, J. G., Srinivasan, R., Muttiah, R. S., and Williams, J. R. 1998. Large-area hydrologic modeling and assessment: Part I. Model development. Journal of American Water Resource Association, 34(1): 73–89

Arp, P. A., and Yin, X. 1992. Predicting water fluxes through forests from monthly precipitation and mean monthly air temperature records. Canadian Journal of Forest Research, 22:864–877.

Band, L. E., Patterson, P., Nemani, R., and Running, S.W. 1993. Forest Ecosystem Processes at the Watershed Scale-Incorporating Hillslope Hydrology. Agric For Meteorol., 63, 93–126.

Band, L. E., Peterson, D. L., Running, S. W., Coughlan, J., Lammers, R., Dungan, J., and Nemani, R. 1991. Forest ecosystem processes at the watershed scale: basis for distributed simulation. Ecological Modelling, 56: 171-196.

Bannister, D., Herzog, M., Graf, H. F., Hosking, J. S., and Short, C. A. 2017. An assessment of recent and future temperature change over the Sichuan Basin, China, using CMIP5 climate models. J. Climate, 30: 6701–6722.

Basheer, A. K., Haishen, L., Omer, A., Ali, A. B., and Abdelgader, M. S. A. 2015. Impacts of climate change under CMIP5 RCP scenarios on the streamflow in the Dinder River and ecosystem habitats in Dinder National Park, Sudan. Hydrol. Earth Syst. Sci., 20:1331–1353.

Beg AAF (2015) Morphometric toolbox: a new technique in basin morphometric analysis using ArcGIS. Global J Earth Sci Eng 2:21–30

Bhagawati K, Bhagawati R, Sen A, Shukla KK, Alone RA (2016) Rainfall trend and variability analysis of subtropical hills of Arunachal Pradesh in Northeastern Himalayan Region of India. Curr World Environ 11(2):631–636.

Bhagawati R, Bhagawati K, Jini D, Alone RA, Singh R, Chandra A, Makdoh B, Sen A, Shukla KK (2017) Review on climate change and its impact on agriculture of Arunachal Pradesh in the Northeastern Himalayan Region of India. Nat Environ Pollut Technol, 16(2):535–539.

Bhatta, B., Shrestha, S., Shrestha, P. K., and Talchabhadel, R. 2019. Evaluationand application of a SWAT model to assess the climate change impact on thehydrology of the Himalayan River Basin. Catena, 181: 104082.

Bhattacharya, T., Khare, D., and Arora, M. 2019. A case study for the assessment of the suitability of gridded reanalysis weather data for hydrological simulation in Beas River basin of North Western Himalaya. Applied Water Science, 9:110. https://doi.org/10.1007/s13201-019-0993-x

Bicknell, B. R., Imhoff, J. C., Kittle Jr. J. L., Jobes, T. H., and Donigian Jr, A. S. 2001. Hydrological Simulation Program–Fortran (HSPF). User's Manual for Release 12. U.S. EPA National Exposure Research Laboratory, Athens, GA, in cooperation with U.S. Geological Survey, Water Resources Division, Reston, VA.

Borah H, Deka S (2020) Morphometric analysis for prioritization of Sub-Watersheds of Jamuna River Watershed, Assam, India using remote sensing and GIS technique. Int J Control Autom, 13(2):18–26.

Brakensiek, D.L. 1967. Kinematic flood routing. Transactions of the ASAE, 10(3):340-343.

Brocca, L., Melone, F., and Moramarco, T. 2008. On the estimation of antecedent wetness conditions in rainfall-runoff modeling. Hydrological Processes, 22: 629–642.

Chandniha SK, Kansal ML (2014) Prioritization of sub-watersheds based on morphometric analysis using geospatial technique in Piperiya watershed. Appl. Water Sci, India. https://doi.org/10.1007/s13201-014-0248-9

Chopra R, Dhiman RD, Sharma PK (2005) Morphometric analysis of subwatersheds in Gurdaspur District Punjab using remote sensing and GIS techniques. J Indian Soc Remote Sens, 33:531–539.

Clarke JI (1966) Morphometry from maps. Essays in geomorphology. Elsevier Publ, Co, New York.

Doni, T., and Gajurel, P. R. 2020. Diversity of wild edible plants traditionally used by the Galo tribe of Indian Eastern Himalayan state of Arunachal Pradesh. Plant Science Today, 7(4): 523–533. https://doi.org/10.14719/pst.2020.7.4.855

Eze EB, Efiong J (2010) Morphometric parameters of the Calabar river basin: implication for hydrologic processes. J Geograph Geol 2(1):18–26

Faniran A (1968) The index of drainage intensity-A provisional new drainage factor. Aust J Sci 31:328–330

Gassman, P. W., Reyes, M. R., Green, C. H., and Arnold, J. G. 2007. The soil and water

assessment tool: historical development, applications, and future research directions. American Society of Agricultural and Biological Engineers, 50(4):1211–1250.
Green, W.H., and Ampt, G.A. 1911. Studies on soil physics, 1. The flow of air and water through soils. Journal of Agricultural Sciences, 4:11-24.
Grose, M. R., Brown, J. N., Narsey, S., Brown, J. R., Murphy, B. F., Langlais, C., Gupta, A. S., Moise, A. F., and Irving, D. B. 2014. Assessment of the CMIP5 global climate model simulations of the western tropical Pacific climate system and comparison to CMIP3. Int. J. Climatol., 34: 3382–3399.
Gumbel, E.J. (1941) The return period of flood flows. The Annals of Mathematical Statistics, 12, 163-190.
Guug, S.S., Abdul-Ganiyu, S., and Kasei, R.A. 2020. Application of SWAT hydrological model for assessing water availability at the Sherigu catchment of Ghana and Southern Burkina Faso, HydroResearch. https://doi.org/10.1016/j.hydres.2020.10.002
Habte, K., Mamo, M., and Jain, M. K. 2013. Runoff and sediment modeling using SWAT in Gumera Catchment, Ethiopia. Open Journal of Modern Hydrology,3: 196–205.
Hack JT (1957) Studies of longitudinal stream profiles in Virginia and Maryland. Geological Survey Professional Paper 294- B. United States Government Printing Office, Washington
Hargreaves, G.L., Hargreaves, G.H. and J.P. Riley. 1985. Agricultural benefits for Senegal River Basin. J. Irrig. and Drain. Engg., 111(2):113-124.
Homsi, R., Shiru, M. S., Shahid, S., Ismail, T., Harun, S. B., AlAnsari, N., Chau, K. W., and Yaseen, Z. M. 2020. Precipitation projection using a CMIP5 GCM ensemble model: a regional investigation of Syria. Eng. Appl. Comput. Fluid. Mech., 14: 90–106.
Horton RE (1932) Drainage-basin characteristics. Trans Am Geophys Union 13:350–361. https://doi.org/10.1029/TR013i001p00350
Horton RE (1945) Erosional development of streams and their drainage basins; hydrophysical approach to quantitative morphology. Geol Soc Am Bull 56:275
Houghton, J. T., Ding, Y., and Griggs, D. J. 2001. Climate Change 2001: The Scientific Basis. Intergovernmental Panel on Climate Change (IPCC). Cambridge University Press, Cambridge, 881.
IPCC (Intergovernmental Panel on Climate Change) (2013). Climate Change 2013 – the physical science basis, working group I contribution to the IPCC fifth assessment report (WGI AR5) of the intergovernmental panel on climate change. Cambridge University Press, 422-808.
Jacques PD, Salvador ED, Machado R, Grohmann CH, Nummer AR (2014) Application of morphometry in neotectonic studies at the eastern edge of the Parana Basin Santa Catarina State Brazil. Geomorphology 213:13–23.
Jain, S. K., Tyagi, J., and Singh, V. 2010. Simulation of runoff and sediment yield for a Himalayan Watershed using SWAT model. Journal of Water Resource and Protection, 2: 267–281.
Jena RK, Dandabat AK (2019) Estimation of morphometric study on Shetrunji river using remote sensing and GIS. ISH - Hydro 2019. International Conference- Osmania University.
Jena, P., Azad, S., and Rajeevan, M. N. 2016. CMIP5 projected changes in the annual cycle of Indian monsoon rainfall. Climate, 4, 14.
Jensen, M.E., R.D. Burman, and R.G. Allen (ed). 1990. Evapotranspiration and irrigation water requirements. ASCE Manuals and Reports on Engineering Practice No. 70, ASCE, N.Y.
Jha, M., Arnold, J. G., Gassman, P. W., Giorgi, F., and Gu, R. R. 2006. Climate change sensitivity assessment on upper Mississippi river basin streamflows using SWAT.

Journal of the American Water Resources Association, American Water Resources Association, August: 997-1015.
Kale VS, Gupta A (2001) Introduction to Geomorphology. Orient Longman Ltd, India.
Kale VS, Shejwalkar N (2007) Western Ghat escarpment evolution in the Deccan basalt province: geomorphic observations based on DEM analysis. J Geol Soc India 70:459–473.
Karcher, S. C., VanBriesen, J. M., and Nietch, C. T. (2013). Alternative land-use method for spatially informed watershed management decision making usingSWAT. Journal of Environmental Engineering, 139(12).
Kimmins, J. P., Mailly, D., and Seely, B. 1999. Modelling forest ecosystem net primary production: the hybrid simulation approach used in FORECAST. Ecological Model, 122:195–224.
King, K. W., Arnold, J. G., and Bingner, R. L. 1999. Comparison of Green-Ampt and curve number methods on Goodwin creek watershed using SWAT. Transactions of the American Society of Agricultural Engineers, 42(4): 919– 925.
Korup O, Schmidt J, McSavaney MJ (2005) Regional relief characteristics and denudation pattern of the western Southern Alps New Zealand. Geomorphology 71:402–423.
Krause, P., Boyle, D.P., and Bäse, F. 2005. Comparison of different efficiency criteria for hydrological model assessment. Adv Geosci., 5: 89–97. https://doi.org/10.5194/adgeo-5-89-2005
Krysanova, V., Hattermann, F., and Wechsung, F. 2005. Development of the ecohydrological model SWIM for regional impact studies and vulnerability assessment. Hydrological Processes, 19: 763–783.
Laio, F., Porporato, A., Fernandez-Illescas, C., and Rodriguez-Iturbe, I. 2001. Plants in water controlled ecosystems: active role in hydrological processes and response to water stress II. Probabilistic soil moisture dynamics. Advances in Water Research, 24: 707–723.
Latif, M., Hannachi, A., and Syed, F. 2018. Analysis of rainfall trends over Indo-Pakistan summer monsoon and related dynamics based on CMIP5 climate model simulations. Int. J. Climatol., 38 (S1), e577–e595.
Le, T., and Bae, D. H. 2013. Evaluating the utility of IPCC AR4 GCMs for hydrological application in South Korea. Water Res. Manage., 27: 3227–3246.
Leavesley, G. H., Lichty, R.W., Troutman, B. M., and Saindon, L. G. 1983. Precipitation-Runoff Modeling System: User's Manual. U.S. Geological Survey Water-Resources Investigations Report, 83-4238:207.
Liang, X., Lettenmaier, D.P., Wood, E.F., and Burges, S.J. 1994. A simple hydrologically based model of land surface water and energy fluxes for general circulation models. Journal of geophysical research, 99(D7): 415-428.
Lindsay JB, Evans MG (2008) The influence of elevation error on the morphometrics of channel networks extracted from DEMs and the implications for hydrological modelling. Hydrol Process, 22(11):1588–1603.
Luo, Y., Arnold, J., Allen, P., and Chen, X. 2012. Baseflow simulation using SWAT model in an inland river basin in Tianshan Mountains, Northwest China. Hydrological Earth System Science, 16(4): 1259–1267.
Magesh N, Jitheshlal K, Chandrasekar N, Jini K (2013) Geographical information system-based morphometric analysis of Bharathapuzha river basin, Kerala. India Appl Water Sci 3:467–477
Marahatta, S., Devkota, L. P., and Aryal, D. 2021. Application of SWAT in Hydrological Simulation of Complex Mountainous River Basin (Part I: Model Development). Water, 13: 1546. https://doi.org/10.3390/w13111546

Melton MA (1957) An analysis of the relations among elements of climate, surface properties, and geomorphology, in, DTIC Document.
Melton MA (1965) The geomorphic and paleoclimatic significance of alluvial deposits in southern Arizona. J Geol. https://doi.org/10.1086/627044
Miller VC (1953) A Quantitative geomorphic study of drainage basin characteristics in the Clinch Mountain area Virginia and tennessee. J Geol 65(1):112–113.
Monteith, J. 1965. Evaporation and the environment. Proceedings of the 19th Symposium of the Society for Experimental Biology, Cambridge University Press, 205–233.
Moriasi, D. N., Arnold, J. G., Van Liew, M. W., Binger, R. L., Harmel, R. D., and Veith, T. 2007. Model evaluation guidelines for systematic quantification of accuracy in watershed simulations. Transaction ASABE, 50(3): 885–900.
Moss, R. H., Edmonds, J. A., Hibbard, K. A., Manning, M. R., Rose, S. K., van Vuuren, D. P., Carter, T. R., Emori, S., Kainuma, M., Kram, T., Meehl, G. A., Mitchell, J. F., Nakicenovic, N., Riahi, K., Smith, S. J., Stouffer, R. J., Thomson, A. M., Weyant, J. P., and Wilbanks, T. J. 2010. The next generation of scenarios for climate change research and assessment. Nature, 463(7282): 747–56.
Nag SK (1998) Morphometric analysis using remote sensing techniques in the Chaka subbasin Purulia district, West Bengal. J Indian Soc Remote Sens 26(1):69–76
Nash, J. E., and Sutcliffe, J. V. 1970. River flow forecasting through conceptual models part I: A discussion of principles. Journal of Hydrology, 10: 282– 290.
Neitsch, S. L., Arnold, J. G., Kiniry, J. R., and Williams, J. R. 2001. Soil and Water Assessment Tool (SWAT) Theoretical Documentation, 781. Temple: Blackland Research Center, Texas Agricultural Experiment Station.
Neitsch, S.L., Arnold, J.G., Kiniry, J.R., and Williams, J.R. 2005. Soil and Water Assessment Tool Theoretical Documentation (p. 494). Temple: Blackland Research Center, Texas Agricultural Experiment Station.
Neves, G. L., Barbosa, M. A. G. A., Anjinho, P. de S., Guimarães, T. T., Filho, J. S. das V., and Mauad, F. F. 2020. Evaluation of the impacts of climate change on streamflow through hydrological simulation and under downscaling scenarios: case study in a watershed in southeastern Brazil. Environ Monit Assess, 192:707. https://doi.org/10.1007/s10661-020-08671-x
Ning, J., Gao, Z., and Lu, Q. 2015. Runoff simulation using a modified SWAT model with spatially continuous HRUs. Environment Earth Science, 74: 5895.
Nookaratnam K, Srivastava YK, Venkateswarao V, Amminedu E, Murthy KSR (2005) Check dam positioning by prioritization of microwatersheds using SYI model and morphometric analysis – Remote sensing and GIS perspective. J Indian Soc Remote Sens, 33(1)
Obeidat M, Awawdeh M, Al-Hantouli F (2021) Morphometric analysis and prioritisation of watersheds for flood risk management in Wadi Easal Basin (WEB), Jordan, using geospatial technologies. J Flood Risk Manag. https://doi.org/10.1111/jfr3.12711
Oja, T., Xiwei, Y. and Arp, P. A. 1995. The forest modelling series ForM-S: Applications to the Soiling spruce site. Ecological Modelling, 83:207–217.
Overton, D.E. 1966. Muskingum flood routing of upland streamflow. Journal of Hydrology, 4:185-200.
Pandey A, Chowdary VM, Mal BC (2007) Identification of critical erosion prone areas in the small agricultural watershed using USLE, GIS and remote sensing. Water Resour Manage 21(4):729–746

Pandey, B. K., Khare, D., Kawasaki, A., and Mishra, P. K. 2019. Climate change impact assessment on blue and green water by coupling of representative CMIP5 climate models with physical based hydrological model. Water Res. Manage., 33: 141–158.
Panjwani, S., Naresh Kumar, S., Ahuja, L., and Islam, A. 2019. Prioritization of global climate models using fuzzy analytic hierarchy process and reliability index. Theor. Appl. Climatol. 137: 2381–2392.
Parajuli, P. B. 2010. Assessing sensitivity of hydrologic responses to climate change from forested watershed in Mississippi. Hydrol. Process., 24(26): 3785–3797.
Pareta K, Pareta U (2011) Quantitative morphometric analysis of a watershed of Yamuna Basin, India using ASTER (DEM) data and GIS. Int J Geomat Geosci 2(1):248–269
Patel PP, Sarkar A (2010) Terrain characterization using SRTM data. J Indian Soc Remote Sens 38(1):11–24
Patle GT, Libang A, Ahuja S (2016) Analysis of rainfall and temperature variability and trend detection: a non parametric Mann Kendall test approach. In: 3rd international conference on computing for sustainable global development (INDIACom), New Delhi.
Penman, H.L. 1956. Evaporation: An introductory survey. Netherlands Journal of Agricultural Science, 4:7-29.
Phillip, J. 1957. The theory of infiltration: 4. Sorptivity and algebraic infiltration equation. Soil Sci., 84: 257–264.
Priestley, C.H.B., and Taylor, R. J. 1972. On the assessment of surface heat flux and evaporation using large-scale parameters. Mon. Weather. Rev., 100:81-92.
Puno GR, Puno RCC (2019) Watershed conservation prioritization using geomorphometric and land use-land cover parameters. Glob J Environ Sci Manag 5(3):279–294
Quansah, J. E., Naliaka, A. B., Fall, S., Ankumah, R., and Afandi, G. E. 2021. Assessing Future Impacts of Climate Change on Streamflow within the Alabama River Basin. Climate, 9: 55. https://doi.org/10.3390/cli9040055
Rahmati O, Samadi M, Shahabi H, Azareh A, Rafiei-Sardooi E, Alilou H, Melesse AM, Pradhan B, Chapi K, Shirzadi A (2019) SWPT: An automated GIS-based tool for prioritization of sub-watersheds based on morphometric and topo-hydrological factors. Geosci Front 10:2167–2175
Rallison, R.E., and Miller, N. 1981. Past, present and future SCS runoff procedure. p. 353-364. In V.P. Singh (ed.). Rainfall runoff relationship. Water Resources Publication, Littleton, CO8.
Rastogi RA, Sharma TC (1976) Quantitative analysis of drainage basin characteristics. Jour. Soil and water Conservation in India 26(1&4): 18–25
Rekha VB, George AV, Rita M (2011) Morphometric Analysis and Micro-watershed Prioritization of Peruvanthanam Sub-watershed, the Manimala River Basin, Kerala, South India. Environ Res Eng Manag 3(57):6–14
Richards, L.A. 1931. Capillary conduction of liquids through porous mediums. Physics, 1: 318–333.
Risbey, J. S., and Entekhabi, D.1996. Observed Sacramento basin streanflow response to precipitation and temperature changes and its relevance to climate change studied. Journal of Hydrology,184:209-223.
Ritchie, J. T., and Otter, S. 1985. Description and performance of CERES-Wheat: A user-oriented wheat yield model. ARS Wheat Yield Project, USDA Rep. ARS-38: 159–175.
Ritchie, J.T. 1972. Model for predicting evaporation from a row crop with incomplete cover. Water Resour. Res., 8:1204-1213.
Romshoo SA, Bhat SA, Rashid I (2012) Geoinformatics for assessing the morphometric control on hydrological response at watershed scale in the upper Indus basin. J Earth Syst

Sci 121(3):659–686
Rostamian, R., Jaleh, A., Afyuni, M., Mousavi, S. F., Heidarpour, M., Jalalian, A., and Abbaspour, K. C. 2008. Application of a SWAT model for estimating runoff and sediment in two mountainous basins in central Iran. Hydrological Science Journal, 53: 977–988.
Ruan, Y., Yao, Z., Wang, R., and Liu, Z. 2018. Ranking of CMIP5 GCM skills in simulating observed precipitation over the Lower Mekong Basin, using an improved score-based method. Water, 10, 1868.
Rudraiah M, Govindaiah S, Srinivas VS (2008) Morphometry using remote sensing and GIS techniques in the subbasins of Kagna river basin, Gulburga District, Karnataka. India J Indian Soc Remote Sens 36(4):351–360
Rupakumar, K., Pant, G. B., Parthasarthy, B., and Sonatak, N. A. 1992. Spatial and sub seasonal pattern of the long term trends of Indian summer monsoon rainfall. Int J Climatol., 12: 257–268.
Rupp, DE, Abatzoglou, JT, Hegewisch, KC, Mote, PW. (2013). Evaluation of CMIP5 20th century climate simulations for the pacific northwest USA. Journal of Geophysical Research: Atmospheres, 118(19): 10884–10906.
Said S, Siddique R, Shakeel M (2018) Morphometric analysis and subwatersheds prioritization of Nagmati River watershed, Kutch District, Gujarat using GIS based approach. J Water Land Develop. 39(X–XII), 131–139
Schumm SA (1956) Evolution of drainage systems and slopes in badlands at Perth Amboy. New Jersey, Geological society of America bulletin 67: 597–646.
Sharma, K. P., Vorosmarty, C. J., and MOORE III, B. 2000. Sensitivity of the Himalayan hydrology to land-use and climatic changes. Climatic Change,47: 117–139.
Singh, V. P., Jain, S. K., and Tyagi, A. 2007. Risk and reliability analysis: a handbook for civil and environmental engineers. ASCE Press, Reston.
Singh, V., and Goyal, M. K. 2017. Curve number modifications and parameterization sensitivity analysis for reducing model uncertainty in simulated and projected streamflows in a Himalayan catchment. Ecological Engineering, 108: 17–29. http://dx.doi.org/10.1016/j.ecoleng.2017.08.002
Singh, W. R., Barman, S., Sharma, S. K., Taggu, A., Bandyopadhyay, A., and Bhadra, A. 2021. Historical and projected precipitation extremes over Pare watershed in Arunachal Pradesh, India. Applied Water Science, 11:60. https://doi.org/10.1007/s13201-021-01382-9
Sreedevi PD, Owais S, Khan HH, Ahmed S (2009) Morphometric analysis of a watershed of south India using SRTM data and GIS. J Geol Soc India 73:543–552
Strahler AN (1952) Hypsometric (area-altitude) analysis of erosional topography. Geol Soc Am Bull 63:1117–1142
Strahler AN (1957) Quantitative analysis of watershed geomorphology. Trans Am Geophys Union 38:913–920
Strahler AN (1964) Quantitative geomorphology of drainage basins and channel networks in Handbook of Applied Hydrology, V. T. Chow, Ed., section 4–11, McGraw-Hill, New York, NY, USA, 1964
Subramanya, K. (2008) Engineering Hydrology. Tata McGraw-Hill Publishing Company Limited, New Delhi.
Syed NH, Rehman AA, Hussain D, Ishaq S, Khan AA (2017) Morphometric analysis to prioritize sub- watershed for flood risk assessment in Central Karakoram National Park using GIS / RS approach. Remote Sensing and Spatial Information Sciences, IV-4/W4, 2017, 4th International GeoAdvances Workshop, 14–15 October 2017, Safranbolu,

Karabuk, Turkey
Thornthwaite, C.W. 1948. An approach toward a rational classification of climate. Geographical Review, 38:55-94.
Thrasher, B., Maurer, E. P., McKellar, C., and Duffy, P. B. 2012. Technical Note: Bias correcting climate model simulated daily temperature extremes with quantile mapping. Hydrology and Earth System Sciences, 16(9): 3309-3314.
Tukura NG, Akalu MM, Hussein M, Befekadu A (2021) Morphometric analysis and sub-watershed prioritization of Welmal watershed, Ganale-Dawa River Basin, Ethiopia: implications for sediment erosion. J Sediment Environ. https://doi.org/10.1007/s43217-020-00039-y
Upadhyay, H., Mittal, H. K., Singh, M., and Hirapara, J. G. 2019. Application of SWAT Model for Estimation of Runoff in Pindwara Watershed and Assessment of its Feasibility. Int. J. Curr. Microbiol. App. Sci., 8(6): 3056-3065.
US Army Corps of Engineers. 2000. Hydrologic Modeling System HEC-HMS, technical reference manual, CPD-74B, Hydrologic Engineering Centre, Davis, CA.
USDA Soil Conservation Service. 1972. National Engineering Handbook Section 4 Hydrology, Chapters 4-10.
Vertenstein, M., Oleson, K., Levis, S., and Hoffman, F. 2004. Community Land Model Version 3.0 (CLM3.0) User's Guide. Community Climate System Model, National Center for Atmostpheric Research, Boulder, CO.
Wang D, Laffan SW, Liu Y, Wu L (2010) Morphometric characterisation of landform from DEMs. Int J Geogr Inf Sci 24(2):305–326
Wang, J., Yang, H., Li, L., Gourley, J. J., Khan, S. I., Yilmaz, K. K., Adler, R. F., Policelli, F. S., Habib, S., Irwn, D., Limaye, A. S., Korme, T., and Okello, L. 2011. The coupled routing and excess storage (CREST) distributed hydrological model. Hydrological Sciences Journal, 56(1). https://doi.org/10.1080/02626667.2010.543087
Wigmosta, M. S., Vail, L. W., and Lettenmaier, D. P. 1994. A distributed hydrology-vegetation model for complex terrain. Water Resources Research, 30(6):1665–1679.
Williams, J.R. 1969. Flood routing with variable travel time or variable storage coefficients. Trans. ASAE, 12(1):100-103.
Wood, A. W., Leung, L. R., Sridhar, V., and Lettenmaier, D. P. 2004. Hydrologic implications of dynamical and statistical approaches to downscaling climate model outputs. Climatic Change, 15: 189–216.
Wu, Y., Zhong, P., Xu, B., Zhu, F., and Fu, J. 2018. Evaluation of global climate model on performances of precipitation simulation and prediction in the Huaihe River basin. Theor. Appl. Climatol., 133: 191–204.
Yang, J., Reichert, P., Abbaspour, K. C., Xia, J., and Yang, H. 2008. Comparing uncertainty analysis techniques for a SWAT application to the Chaohe basin in China. Journal of Hydrology, 358(1-2): 14–23.
Yin, X., and Arp, P. A. 1993. Predicting forest soil temperatures from monthly air temperature and precipitation records. Canadian Journal of Forest Research, 23:2521–2536.
Zamani, R., and Berndtsson, R. 2019. Evaluation of CMIP5 models for west and southwest Iran using TOPSIS-based method. Theor. Appl. Climatol., 137: 533–543.
Zavoianu I (1985) Morphometry of drainage basins (Developments in Water Science). Elsevier, Amsterdam.
Zierl, B., and Bugmann, H. 2005. Global change impacts on hydrological processes in Alpine catchments. Water Resources Research, 41(2).